

ABSTRACT

Title of Document: In-Mold Assembly of Multi-Functional
Structures

Wojciech Bejgerowski,
Doctor of Philosophy, 2010

Directed By: Professor Satyandra K. Gupta
Department of Mechanical Engineering

Combining the recent advances in injection moldable polymer composites with the multi-material molding techniques enable fabrication of multi-functional structures to serve multiple functions (e.g., carry load, support motion, dissipate heat, store energy). Current in-mold assembly methods, however, cannot be simply scaled to create structures with miniature features, as the process conditions and the assembly failure modes change with the feature size. This dissertation identifies and addresses the issues associated with the in-mold assembly of multi-functional structures with miniature components. First, the functional capability of embedding actuators is developed. As a part of this effort, computational modeling methods are developed to assess the functionality of the structure with respect to the material properties, process parameters and the heat source. Using these models, the effective material thermal conductivity required to dissipate the heat generated by the embedded small scale

actuator is identified. Also, the influence of the fiber orientation on the heat dissipation performance is characterized. Finally, models for integrated product and process design are presented to ensure the miniature actuator survivability during embedding process. The second functional capability developed as a part of this dissertation is the in-mold assembly of multi-material structures capable of motion and load transfer, such as mechanisms with compliant hinges. The necessary hinge and link design features are identified. The shapes and orientations of these features are analyzed with respect to their functionality, mutual dependencies, and the process cost. The parametric model of the interface design is developed. This model is used to minimize both the final assembly weight and the mold complexity as the process cost measure. Also, to minimize the manufacturing waste and the risk of assembly failure due to unbalanced mold filling, the design optimization of runner systems used in multi-cavity molds for in-mold assembly is developed. The complete optimization model is characterized and formulated. The best method to solve the runner optimization problem is identified. To demonstrate the applicability of the tools developed in this dissertation towards the miniaturization of robotic devices, a case study of a novel miniature air vehicle drive mechanism is presented.

In-Mold Assembly of Multi-Functional Structures

By

Wojciech Bejgerowski

Dissertation submitted to the Faculty of the Graduate School of the
University of Maryland, College Park, in partial fulfillment
of the requirements for the degree of
Doctor of Philosophy
2010

Advisory Committee:

Professor Satyandra K. Gupta, Chairman/Advisor
Assistant Professor Sarah Bergbreiter
Professor Hugh A. Bruck
Professor Srinivasa Raghavan
Dr. Chandrasekhar Thamire

© Copyright by
Wojciech Bejgerowski
2010

Acknowledgements

First and foremost, I would like to express a sincere gratitude and appreciation to Professor Satyandra K. Gupta for all of his mentoring and guidance. His support, encouragement and advice through my time at the University of Maryland made this dissertation possible. He also gave me a valuable perspective at self-management on many levels. My sincere thanks also go to Professor Hugh Bruck for his valuable numerous advice and discussions not only about the research, but also about life in general. I wish to acknowledge Professor Sarah Bergbreiter, Professor Srinivasa Raghavan and Dr. Chandrasekhar Thamire for serving on my advisory committee.

This work was supported by the Army Research Office through MAV MURI Program (Grant No. ARMY W911NF0410176) and NSF grants DMI-0457058 and OCI-0636164. I am thankful to the University of Maryland, the Mechanical Engineering Department for the given opportunity and support.

I am fortunate to have a very supportive family; they encouraged and supported me every day of this journey of scholarship – thank you Bozena, Tony and Mom!

I owe special thanks to Alan, Arvind A., Arvind B. and Atul for their valuable every-day research insights and suggestions, often needed motivation, as well as distractions both in and out of the lab.

I would also like to thank all my colleagues and friends from the Advanced Manufacturing Laboratory and Mechanical Engineering Department – Arun, Dan, Dominik, John, Juan, Leicester and Tobias, who have provided me with friendly and motivating work environment. Guru and Patrick helped me to complete several tasks and experiments.

Finally, I would like to thank all of my friends I made during my stay in the U.S. who have helped me to expand my social and intellectual horizons and numerous manual capabilities. I am lucky that I had an opportunity to interact with you all.

Table of Contents

Acknowledgements.....	ii
Table of Contents.....	iv
Index of Figures.....	vii
Index of Tables.....	xii
1 Introduction.....	1
1.1 Background.....	1
1.2 Motivation and Challenges.....	6
1.3 Dissertation Goals and Scope.....	12
2 Literature Review.....	17
2.1 In-mold Assembly.....	17
2.1.1 Multi-Material Molding.....	18
2.1.2 Insert Molding and Over Molding.....	25
2.2 Manufacturing of Multi-Functional Structures.....	29
2.2.1 Embedded Actuators.....	31
2.2.2 Filled Polymers.....	35
2.2.3 Compliant Mechanisms.....	38
2.3 Molding Process Design.....	46
2.3.1 Gate Placement Optimization.....	48
2.3.2 Runner Optimization.....	55
2.4 Summary.....	61
3 Embedding Actuators in Multi - Functional Structures.....	64
3.1 Motivation and Challenges.....	65
3.2 Overview of the Design Process.....	67
3.3 Development of Thermal Model.....	70
3.3.1 Acquiring Experimental Data for Model Calibration.....	70
3.3.2 Thermal Model Description.....	74
3.3.3 Model Calibration.....	76
3.3.4 Modeling of Thermally Conductive Polymer Structures.....	78

3.3.5	Analysis of Thermal Conductivity for Filled Polymers.....	83
3.4	Incorporating In-mold Assembly Process Constraints during Optimization...	87
3.5	Summary.....	94
4	Design and Fabrication of Miniature Compliant Hinges for	
	Multi-Material Compliant Mechanisms	96
4.1	Motivation and Challenges	97
4.2	Overview of the Design Process	100
4.3	Shape Synthesis of Compliant Hinges.....	102
4.4	Modeling and Analysis of Compliant Hinges.....	110
4.5	In-mold Assembly of Compliant Hinges	118
4.5.1	Process Overview and Mold Design.....	119
4.5.2	Mold Cavity Design.....	121
4.5.3	Gate Design.....	124
4.5.4	Runner Design	126
4.6	Case Study	127
4.6.1	Overview of Design Process.....	128
4.6.2	Elaboration of Mechanism Shape	131
4.6.3	Wing Selection.....	135
4.6.4	Modeling and Optimization of Mechanism	138
4.6.5	Results.....	143
4.7	Summary.....	146
5	Runner Optimization for In-mold Assembly of Multi-Material	
	Compliant Mechanisms	148
5.1	Motivation and Challenges	149
5.2	Overview of the Approach.....	153
5.3	Development of Optimization Problem	154
5.3.1	General Formulation	154
5.3.2	Mathematical Formulation.....	155
5.4	Computational Experiment	160
5.4.1	Computational Framework	160
5.4.2	Case Study: Multi-Material MAV Drive Frame.....	161

5.4.3	Implementation of Design Optimization Approach.....	163
5.4.4	Development of Pressure Meta-Model	169
5.4.5	Development of Custom Mold Filling Simulation	171
5.5	Evaluation of Potential Solution Methods	181
5.5.1	Identification of Optimization Approaches	181
5.5.2	Performance Metrics Identification	188
5.5.3	Results and Discussion	197
5.6	Summary.....	204
6	Conclusions.....	207
6.1	Intellectual Contributions.....	207
6.1.1	Development of Methods for Embedding Actuators using In-Mold Assembly Process	207
6.1.2	Development of Design Solutions and Models for realizing Multi-Material Compliant Mechanisms with Miniature Hinges using In-Mold Assembly.....	208
6.1.3	Development of Methods to Optimize Runner Systems for Multi-Cavity Molds used in In-Mold Assembly.....	209
6.2	Anticipated Benefits.....	210
6.3	Future Directions	212
6.3.1	Modeling of Thermally Conductive Filled Polymer Structures with Embedded Actuators	212
6.3.2	Characterization of Design Features to Facilitate Other Classes of Miniature Compliant Joints	213
6.3.3	Multi-Material Interface Optimization	214
6.3.4	Runner System Layout Optimization.....	214
	Bibliography	216

Index of Figures

Figure 1.1	Macro-scale multi-functional structures manufactured using multi-material molding: (a) Black and Decker drill housing, and (b) automotive tail light.....	2
Figure 1.2	Babyplast [®] injection molding machine	3
Figure 1.3	Cavity transfer molding of a macro-scale compliant hinge [42].....	4
Figure 1.4	Morphing cavity methods for in-mold assembly: (a) moving a mold piece, (b) replacing a mold piece and (c) removing a partition [89]	5
Figure 1.5	DC motor disabled during in-mold assembly due to excessive deformation: (a) assembly and (b) deformed motor housing	8
Figure 1.6	Failure modes of multi-material interface due to excessive stress concentration: (a) compliant hinge interlocking feature, and (b), (c) link encapsulation	9
Figure 1.7	Failure modes of multi-material interface due to hinge displacement caused by unbalanced flow fields.....	11
Figure 2.1	Bond strength of two component test specimens [55].....	19
Figure 2.2	A compatibility matrix for various polymers [37]	19
Figure 2.3	Interlocking features for macro-scale heterogeneous structures: (a) rectangular and (b) circular [21]	20
Figure 2.4	3-DOF compliant joint with complex interlocking features [42].....	21
Figure 2.5	2-DOF movement of in-mold assembled gimbal [89]	22
Figure 2.6	Deformation of the mesoscale core versus radial support length for in-mold assembled revolute joints [7]	23
Figure 2.7	Various processing aspects of micro assembly injection molding [80] ..	24
Figure 2.8	Insert-molded parts molding simulation [23]	26

Figure 2.9 Load-bearing component manufactured using metal over-molding PMH technology with interlocking holes ensuring adhesion [44].....	27
Figure 2.10 Load-bearing component manufactured using metal over-molding PMH technology with a thermoplastic coating promoting the adhesion [44] ..	27
Figure 2.11 Definition of the linear four-node axi-symmetric interface element [45]	28
Figure 2.12 Schematics of two types of clinch-lock concepts [46]	29
Figure 2.13 2D micro-gripper with four silicon-polymer forward actuators [32]	32
Figure 2.14 Actuation sequences of ANTLA robot segment: (a) neutral state (b) upward actuation (c) downward actuation (d) asymmetrical actuation (turning) [64]	34
Figure 2.15 Multifunctional Structural Module with embedded electronic components: (a) solid model, (b) molded prototype [48].....	35
Figure 2.16 Flapping wing air vehicle compliant mechanism concept [106].....	40
Figure 2.17 Diagram of filleted V-shape hinge: 3D (a), 2D (b); and cycloidal hinge: 3D (c), 2D (d) [106].....	41
Figure 2.18 Compliant structures manufactured using multi-material molding: (a) compliant clip, (b) rotor system [42].....	42
Figure 2.19 Running robot leg design made using hard and soft viscoelastic materials for compliance and damping [28].....	43
Figure 2.20 Hierarchical compliance structure of a gecko-inspired robot [28].....	43
Figure 2.21 SDM process plan for creating multi-material parts with fibers traversing material boundaries [28].....	44
Figure 2.22 Prototypes of contact-aided revolute joints: (a) drive rotor and (b) gate rotor [22].....	45
Figure 2.23 Wire-form torsion-bar mechanism prototype hinge [87]	46
Figure 2.24 Flow Resistance Search Scheme flowchart [119]	51
Figure 2.25 Gate placement optimization approach to achieve balanced flows [118]	52

Figure 2.26 Gate placement optimization mGA algorithm [70].....	53
Figure 2.27 Algorithms for designing injection molding system: (a) gate type definition and (b) runner type selection and parameter calculation [94].	54
Figure 2.28 Two-stage flow balancing optimization methodology for a multi-gated cavity [120].....	57
Figure 2.29 Experimental investigation of filling stage in micro-molding [43].....	60
Figure 3.1 Minimally Invasive Neurosurgical Intracranial Robot (MINIR) [85].....	66
Figure 3.2 Flapping wing MAV mechanism [14].....	66
Figure 3.3 Parametric optimization of in-mold assembly using thermally conductive polymers.....	68
Figure 3.4 Embedded resistor: in-mold assembly.....	72
Figure 3.5 Resistor embedded in Grilamid L16 (PA 12).....	72
Figure 3.6 Resistor embedded in NJ-6000 TC (PA 12-F)	73
Figure 3.7 Schematic of temperature sampling points: (a) cross-section, and (b) side view	74
Figure 3.8 FEA model assembly: (a) leads (b) ceramic casing (c) polymer casing .	75
Figure 3.9 Surfaces for applying FEA boundary conditions (highlighted): (a) heat power, (b) convection to air.....	75
Figure 3.10 FEA model mesh	75
Figure 3.11 Temperature field FEA result for unfilled Nylon 12 sample	77
Figure 3.12 Cross-sectioning of the embedded resistor specimen.....	79
Figure 3.13 FEM model with voids	80
Figure 3.14 Mold flow simulation sample result: (a) side view and (b) isometric view of a segment	80
Figure 3.15 FEM model with orthotropic thermal conductivities assigned: (a) isometric view and (b) side view	82

Figure 3.16 Temperature field FEA result for PA12-F filled polymer composite	83
Figure 3.17 Modified FEA model: (a) assembly, (b) directional thermal conductivities.....	85
Figure 3.18 Temperature field FEA result for the most anisotropic case	85
Figure 3.19 Isotropic thermal conductivity influence on the temperature of embedded component	87
Figure 3.20 Embedded motor: (a) physical assembly exploded and (b) cross-section dimensions.....	89
Figure 3.21 ANSYS model: (a) key dimensions and boundary conditions, (b) mesh	90
Figure 3.22 ANSYS results for the total von Mises strain plot on motor housing	90
Figure 3.23 In-mold assembly setup for manufacturing the motor holder	91
Figure 3.24 In-mold assembled motor holders: (a) PA 12, (b) PA 12-F	92
Figure 3.25 FEA thermal analysis results: (a) PA 12, (b) PA 12-F	93
Figure 4.1 MAVs developed in AML: (a) 9.7 g “Small bird”, (b) 27.9 g “Big bird” and (c) 38 g “Jumbo bird”	100
Figure 4.2 Miniature hinge design optimization approach	102
Figure 4.3 Miniature hinge design shape synthesis	108
Figure 4.4 Hinge and link connection design shape synthesis (cross-section)	108
Figure 4.5 Hinge FEA boundary conditions	112
Figure 4.6 Specimen for tensile testing of the hinge	113
Figure 4.7 Tensile test specimen hinge FEA boundary conditions	114
Figure 4.8 Displacement magnitude result for the tensile test specimen.....	114
Figure 4.9 Von Mises stresses in the final LDPE hinge design.....	115
Figure 4.10 Von Mises stresses in the final HIPP hinge design	117
Figure 4.11 Overview of the developed in-mold assembly process	120

Figure 4.12 Gate designs used in the in-mold assembly process: (a) first-stage film gate, and (b) second-stage side gate layout	124
Figure 4.13 Initial runner design used in the in-mold assembly process	127
Figure 4.14 Schematic diagram of compliant mechanism for flapping wing action	129
Figure 4.15 MAV drive mechanism design	132
Figure 4.16 Constrained dimensions of the design	135
Figure 4.17 Final MAV wing design	137
Figure 4.18 Optimization process flowchart	139
Figure 4.19 Kinematic representation of the model	140
Figure 4.20 Model synthesis with input boundary conditions (BC) and estimated reaction forces	141
Figure 4.21 Multi-material molding of MAV drive frame	144
Figure 4.22 MAV assembly	145
Figure 5.1 Schematic of pressure exerted on the first stage component	151
Figure 5.2 Displaced in-mold assembled hinges in a multi-material mechanism (embedded hinge section lengths marked)	152
Figure 5.3 Runner system optimization approach	154
Figure 5.4 Molding system for In-mold assembly of MAV drive frame: (a) CAD model with marked nodes and (b) corresponding tree structure	162
Figure 5.5 Matrix representation of the molding system: (a) edge diameter in inches, (b) edge length in inches, and (c) nodal type	163
Figure 5.6 Case study design variables' assignment	165
Figure 5.7 Meta model building flowchart	171
Figure 5.8 Flowchart for estimation of nodal flow arrival times	172
Figure 5.9 Molding system of case study I: (a) tree representation with dimensions and (b) corresponding MoldFlow [®] 1D filling study	176

Figure 5.10 Molding system of case study II: (a) tree representation with dimensions and (b) corresponding MoldFlow [®] 1D filling study.....	177
Figure 5.11 Molding system for In-mold assembly of MAV drive frame: (a) CAD model with marked nodes and (b) corresponding tree structure	179
Figure 5.12 Constraint violation influence on optimization results.....	198
Figure 5.13 <i>MOGA</i> optimization result – Pareto sets from eight trials	200
Figure 5.14 MoldFlow [®] optimal solution validation: (a) mesh, (b) fill time plot	203

Index of Tables

Table 3.1 Properties of materials used in the experiment	71
Table 3.2 Embedded resistor sample dimensions	74
Table 3.3 Thermal properties used in FEA	77
Table 3.4 Process settings used in flow simulation	81
Table 3.5 Embedded resistor temperature [C] as a function of directional thermal conductivity.....	84
Table 3.6 In-mold assembly process parameters	91
Table 3.7 Results of the embedded motor experiment.....	93
Table 4.1 Hinge design parameters.....	109
Table 4.2 Hinge design constraints	109
Table 4.3 Material properties used in the FEA	112
Table 4.4 Key dimensions of the LDPE final hinge design.....	116
Table 4.5 Key modified dimensions of the final HIPP hinge design.....	118
Table 4.6 Processing parameters used to in-mold assembly the drive mechanism	121
Table 4.7 MAV wings characteristics.....	137

Table 4.8	FEA load components.....	142
Table 4.9	MAV test flight results.....	145
Table 5.1	Injection molding processing parameters used in the case study	164
Table 5.2	Case study design variables upper and lower boundaries (in inches).....	169
Table 5.3	Simulation parameters used for building the meta model	170
Table 5.4	Common MoldFlow® simulation parameters used in validation studies.....	175
Table 5.5	Case study I results comparison with MoldFlow® 1D simulation.....	176
Table 5.6	Case study II results comparison with MoldFlow® 1D simulation	178
Table 5.7	Case study III results comparison with MoldFlow® 3D simulation	180
Table 5.8	Notation for optimization methods' exploration.....	188
Table 5.9	Performance metrics of the optimization approaches	189
Table 5.10	Rank table of the optimization approaches	197
Table 5.11	Final parameters used in the investigated GA optimizations.....	200
Table 5.12	Final optimal solution	202
Table 5.13	Validation of flow arrival times obtained by the custom simulation.....	204

1 Introduction

1.1 *Background*

Recent advances in injection moldable polymer composites enable manufacturing of structures using materials with enhanced properties (e.g., heat dissipation, impact resistance, corrosion resistance). The use of different material composition in different portions of a structure enables it to perform multiple functions, such as carrying load, motion support, heat dissipation or energy storage. Hence, *multi-functional structures* have emerged as a very useful concept for realizing high performance solutions in highly demanding environments with many different requirements. Many of these concepts are based on biological entities that utilize the material-function compatibility within a continuum structure and therefore simultaneously serve multiple functional purposes. Thus, the ability to create multi-material, multi-functional polymer structures is highly desirable for many applications, especially in miniaturization of devices, such as bio-medical and miniature robots.

However, manufacturing such multi-functional assemblies becomes challenging with the feature size reduction from the macro-scale solutions. Traditional macro-scale assembly approaches impose restrictions on the size and geometric complexity of the multi-material interfaces. These approaches lead to suboptimal solutions. On the other hand, more complex multi-material geometries can be realized through self assembly; however this method is not cost-effective for the size scales beyond the

micro-scale. Hence scalable and cost effective automated assembly methods suitable to high volume production have to be explored.

Recent advances in in-mold assembly have enabled manufacturing of multi-functional structures with geometrically complex features at the macro-scale without performing assembly operations. These advances have fundamentally changed how packaging, tools, and many automotive components are currently designed and produced. Example parts manufactured using multi-material in-mold assembly are shown in Figure 1.1.



Figure 1.1 Macro-scale multi-functional structures manufactured using multi-material molding: (a) Black and Decker drill housing, and (b) automotive tail light

Injection molding (IM) is a method of processing thermoplastic polymers. IM is used to produce a wide variety of products with varying shapes and sizes [13, 12, 38, 75, 79]. In this process, the polymer is heated over its melting point and then injected into a mold cavity under high pressure. This melt solidifies to take the shape of the cavity. After the melt solidifies, the mold opens, the part is ejected from the mold, the mold closes and the process is repeated. After a mold is manufactured, a high

volume of molded products can be produced quickly and inexpensively. The IM machine used in the Advanced Manufacturing Laboratory (AML) at the University of Maryland is shown in Figure 1.2.



Figure 1.2 Babyplast[®] injection molding machine

In-mold assembly process is a molding process in which the assembly operation takes place inside the mold. This can include a subsequent injection of two or more polymers into a cavity to form a multi-material structure, or injecting a polymer into a mold pre-loaded with elements (such as actuators, electronic components or other functional parts) in order to assemble the components during the molding process. In-mold assembly eliminates post-molding assembly operations, which reduces manufacturing time and product costs. In addition, at the miniature scale, in-mold assembly not only eliminates tedious and time-consuming precision manual assembly

operation, but also can enable manufacturing assemblies otherwise impossible to achieve.

In-mold assembly of multi-material structures can be realized using two different methods. One of the options is the cavity transfer molding, which utilizes over-molding process. The first stage component is molded using traditional IM and manually or automatically moved to another mold cavity before injecting the next stage polymer. Essentially, the multi-material structure is produced using regular IM. The first stage part is referred to as the pre-molded component. The process steps for realizing in-mold assembled macro-scale compliant multi-material joint using the cavity transfer molding are shown in Figure 1.3.

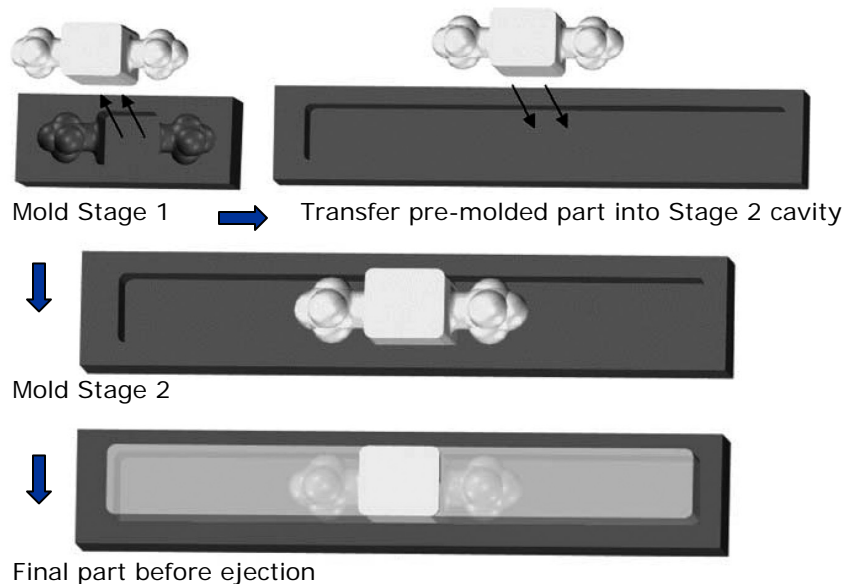


Figure 1.3 Cavity transfer molding of a macro-scale compliant hinge [42]

The second option is the morphing cavity method, which primarily differs from the cavity transfer method in that the first stage part does not leave the mold for the

second stage injection. Instead, mold pieces are moved to create room for the second stage injection. Methods of changing the cavity shape include: (1) realignment of one or more mold pieces after injection of the first stage component to change the cavity shape, (2) swapping one or more mold pieces in the initial cavity with a differently shaped mold piece, and (3) adding partitions or shut-off surfaces in the initial cavity to be removed during subsequent stages [89]. These methods are shown schematically in Figure 1.4. Because these methods must satisfy the general assembly and disassembly constraints imposed on the mold pieces, the shape complexity of the part significantly affects the complexity of the molds.

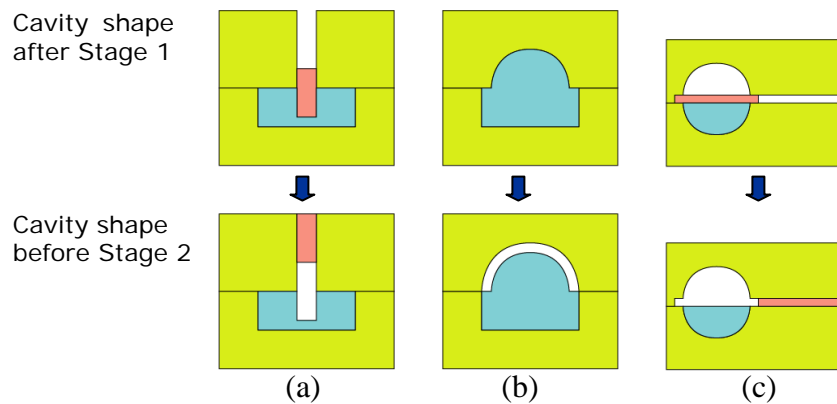


Figure 1.4 Morphing cavity methods for in-mold assembly: (a) moving a mold piece, (b) replacing a mold piece and (c) removing a partition [89]

Using injection moldable polymer composites with fillers enhancing the functionality has gained popularity over the last decade [9, 10, 15-17, 31, 33-35, 55, 54]. New methods have been developed to model and optimize the heat transfer within a thermally conductive polymer structure as a function of the functional filler

orientation [1, 9, 10, 26, 31, 33, 34, 36, 39, 49, 63, 91, 95, 102, 103, 112, 114]. Advances in micro and miniature molding have enabled new ways of creating small plastic parts [25, 30, 32, 43, 55, 56, 81, 80, 100, 105, 113]. In-mold assembly has also been successfully demonstrated at the macro-scale [11, 42, 44, 48, 50, 60, 89], with some specific extensions to the meso-scale [6, 7, 105]. This was shown to be an effective manufacturing process to develop multi-material, multi-functional parts with reduced production times and lead times. Considering the success of functionally-enhanced polymer composites, multi-material molding and the in-mold assembly at the macro-scale, it is envisaged that in-mold assembly and polymer composites can be potentially combined to develop a manufacturing process for realizing truly multi-functional structures for miniaturization of devices.

1.2 Motivation and Challenges

In-mold assembly methods for realizing multi-material structures have been developed and successfully demonstrated in the past [6, 11, 21, 42, 48, 60, 89]; however, these methods do not fully address the issues specific to the size scale imposed by miniaturization. Interest in miniaturization has increased for many emerging and novel applications where size and weight play an important constraint. Some of these applications include hard disks, cameras, cell phones, micro air vehicles, medical robots, and drug delivery systems. Miniature robotic applications require structures to be multi-functional, which offers structural strength as well as other functions, such as heat dissipation, selective compliance and/or energy storage. In-mold assembly eliminates manual assembly operation and reduces the part count in final assembly by utilizing function-specific materials. Development of a

comprehensive approach to realize truly multi-functional miniature structures via in-mold assembly requires addressing several challenges.

Embedding actuators using in-mold assembly methods is expected to eliminate the manual assembly and overall part count in the assembly, both highly desirable in miniature scale. However, most of the actuators on the market generate heat while operating. If the heat dissipation is insufficient, the heat generated by actuators will increase the temperature of the interface between the embedded actuator and anchoring polymer structure, causing either the polymer at the interface to soften, resulting in failure of the anchoring point for the actuator, or the overheating of the actuator, both of which leading to a subsequent failure of the device. Therefore a multi-functional structure is required to serve both as the structural housing and also as the heat sink for the embedded actuator. Small scale restricts the utilization of heat sinks commonly used at the macro-scale, which are not a viable option due to reduced weight and size budget. Using an active cooling method may also not be an acceptable option due to the additional power consumption, weight and complexity it introduces. Thermally conductive filled polymers are promising for the heat dissipation function. Many injection-moldable filled polymers currently available on the market have thermal conductivities which are an order of magnitude higher than bulk unfilled polymers (see Table 3.1). Using these materials allows for the creation of polymer heat sinks. However, evaluation of the heat dissipation capabilities of the structure to match the functional requirements on the design stage is not a trivial task, as the thermal properties depend on many factors, including the structure geometry, the material filler volumetric content and its orientation in the solidified part. The

fiber orientation is moreover a function of the flow pattern during the mold filling, which is a function of the gate size, shape and processing conditions. Modeling such complex thermal properties is a tedious process, requiring detailed analysis of the fiber orientations and the assignment to the resulting orthotropic thermal conductivities to the design regions.

Next important challenge is the ability for the actuators to survive the in-mold assembly process. Injection of a polymer melt into a mold cavity under high pressure has the potential to destroy delicate features of the actuators before they are fully embedded, which may prevent proper functioning. An example of a DC motor housing being plastically deformed during the in-mold assembly process is shown in Figure 1.5.

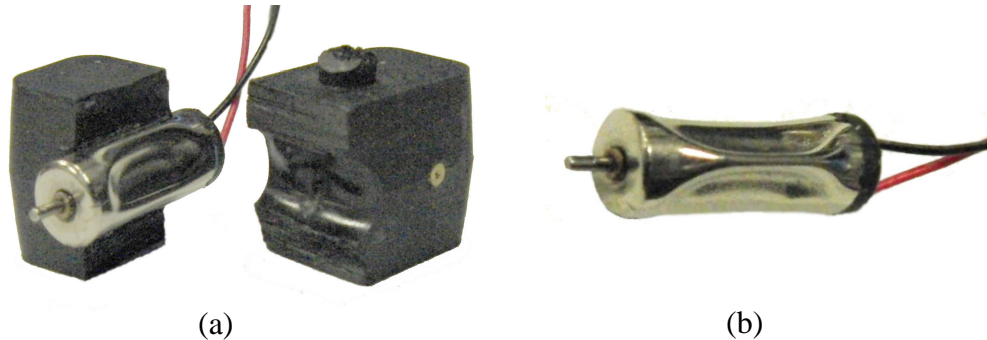


Figure 1.5 DC motor disabled during in-mold assembly due to excessive deformation: (a) assembly and (b) deformed motor housing

One of the main challenges in multi-material molded objects is the connectivity between the materials. Realizing different functions across the same structure may require the choice of materials which are not chemically compatible and will not bond

during the in-mold assembly process. Compliant mechanisms are a good example of a multi-functional structure that faces this issue, where the compliant and rigid materials are usually chemically incompatible. Several researchers have studied the bonding problem based on compliant mechanisms [21, 28, 37, 42]. Bruck et al. [21] presented a method to manufacture multi-material compliant mechanisms using multi-shot molding. However, these macro-scale assembly-based approaches impose restrictions on the size and geometric complexity of the multi-material interfaces, which leads to highly suboptimal solutions.

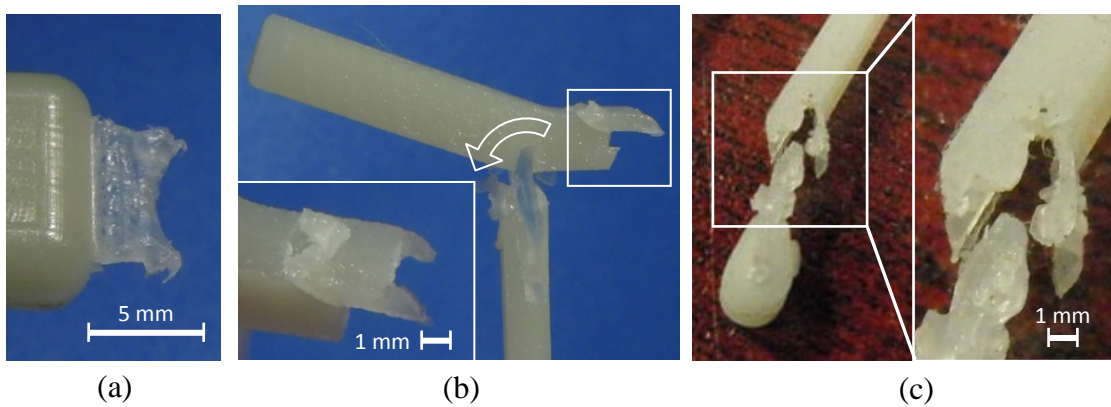


Figure 1.6 Failure modes of multi-material interface due to excessive stress concentration: (a) compliant hinge interlocking feature, and (b), (c) link encapsulation

One of the reasons, why these strategies cannot be scaled to the miniature scale is due to the stress concentration on the interlocking features. This problem arises due to the fact that the miniature-scale features have significantly less structural rigidity and durability than the macro-scale equivalents. Under a load, which is transferred by the compliant joint, the stress levels on the weakest point of the interface may

exceed the material limits, resulting in a feature fracture and the hinge fail. This failure mode is shown in Figure 1.6(a). Additionally, the loads transferred can cause overloading of the encapsulating link structure and its subsequent failure. This is shown in Figure 1.6(b).

Another important issue arises with the development of the multi-material assembly design optimization for miniaturization of devices. The possible choice of geometries and their orientations to realize the material interface is virtually endless; however the selected entities have to satisfy the ejection criteria. An improper selection of design features' shapes and their relative orientations may result in mold configurations which require sub-optimal number of mold pieces, resulting in increased lead costs and molding equipment requirements. Additionally, parametric models of all the interface design features necessary to allow for both motion and load transfer do not exist, which along with numerous injection molding constraints, restricts from obtaining optimal solutions for the miniaturization of devices.

The final challenge is connected with the design optimization of runner systems used for in-mold assembly of complex structures using multi-cavity molds. Multi-cavity molds require a complex, multi-branch runner system to supply all the cavities with the molten polymer in order to fill the mold. Again, compliant mechanisms are a good example of a multi-functional structure that faces this issue, where the molding cavity layout is fixed by the mechanism kinematic design, and the cavities are separated by the first stage components. This configuration requires each of the cavities to have a supplying runner segment. Additionally, the existence of the pre-molded parts poses a significant challenge itself. Due to the miniature scale of these

components, they are sensitive to the dynamic force fields imposed by the molten polymer during the second stage mold filling. If the flow fronts arrive at the first stage part from adjacent cavities in an unsynchronized manner, the differential pressure exerted on the insert results in its displacement, and hence, failed assembly. This failure mode observed on two exploratory designs is shown in Figure 1.7.

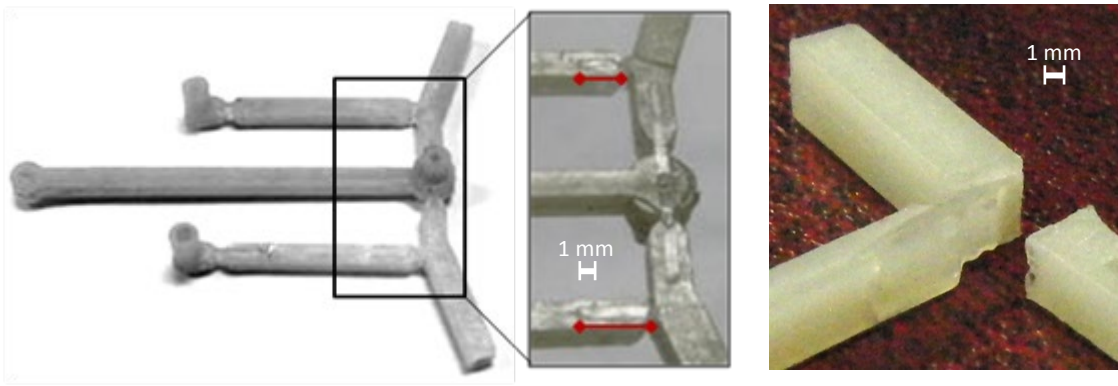


Figure 1.7 Failure modes of multi-material interface due to hinge displacement caused by unbalanced flow fields

Therefore, it is desired to minimize the time difference in flow arrivals to the pre-molded components. This objective is however dependent on the already complex runner layout, sizing, processing parameters and material properties; therefore it requires a mold filling simulation to calculate the time difference between the flows arriving at the pre-molded components. The need of mold filling simulation being involved in the runner optimization routine poses additional challenges concerning the software integration.

Because of the issues outlined above, the in-mold assembly of miniaturized multi-functional structures is still a challenging problem, which cannot be solved in a comprehensive manner. This dissertation is therefore seen as a step to overcome the main challenges in in-mold assembly of multi-functional structures used towards the miniaturization of devices.

1.3 Dissertation Goals and Scope

The challenges outlined in the previous section demonstrate that in-mold assembly of multi-material multi-functional structures with miniature components is a non trivial problem. Presence of the pre-molded component inside the second stage mold, and the utilization of functionality enhancement coming from the novel polymer composites, both make the resulting molding process significantly different from the conventional injection molding. The goals of this dissertation are to (1) develop in-mold assembly process to allow embedding of actuators in thermally-conductive polymer structures , (2) develop models for optimization of multi-material compliant mechanisms realized using in-mold assembly process, and (3) develop methods to optimize runner systems unique to multi-cavity molds used for in-mold assembly process. This dissertation identifies some of the imminent challenges in the in-mold assembly of multi-functional structures with miniature embedded components. Several part and process design strategies have been developed to address some of these challenges. Computational models have been developed to understand the in-mold assembly process involving miniature components.

Because the concepts of “multi-functionality” and “compliance” are used in many research fields, it is important clarify the use of these terms across this dissertation.

The “multi-functional structure” is used in this work to describe a structure, which in addition to its structural integrity function, serves as an anchoring point for an embedded actuator and additionally dissipates the heat generated by the actuator in operation. The “compliant mechanism” refers to elastic continua utilizing local compliance and stiffness variation to realize the motion and load transfer functions in a mechanism. Finally, the “miniature” and “small” scale when referred to a design feature is understood as a size scale in which minimization of the assembly weight is desired.

To develop a deep understanding of the issues specific to this dissertation and explore the state-of-art modeling and manufacturing methods, Chapter 2 presents the review of the relevant literature. First, the in-mold assembly process is described in terms of multi-material molding technology and the insert molding technology. Next, a review of literature concerning manufacturing multi-functional structures is presented. This includes the research related to embedding actuators, the characterization of filled polymers, and the manufacturing of the mechanisms utilizing a local compliance. Finally, the literature dealing with issues related to the design of the injection molding process is reviewed. This concerns molding system design optimization, including gate positioning and runner sizing to achieve desired part properties and process conditions through balanced flows.

One of the challenges in embedding small scale actuators in multi-functional structures is due to the heat generated by the actuator in operation. To prevent the actuator from overheating, thermally conductive filled polymers were introduced to allow for additional heat dissipation through the anchoring structure. However,

evaluation of the heat dissipation capabilities of the structure to match the functional requirements on the design stage is a challenging problem, as the thermal properties depend on various factors, including the structure geometry, material properties, gate design and processing parameters. Chapter 3 presents a simplified thermal modeling approach which allows for fast and accurate evaluation of the heat dissipation performance of structures with embedded miniature actuators. The models are used to determine the required effective thermal properties of the material. The influence of the fiber orientation on the functionality of filled polymer structures for embedding actuators is characterized using the developed models.

Another challenge is the ability for the small scale actuators to survive the in-mold assembly process. Injection of a polymer melt into a mold cavity under high pressure has the potential to destroy delicate features of the actuators before they are fully embedded, which may prevent proper functioning. Therefore Chapter 3 describes an integrated part and process design optimization approach to ensure the survivability of the actuator embedded in a thermally conductive structure.

One of the main challenges in creating multi-material molded objects is the connectivity between the materials used to realize the different functions across the in-mold assembled structure. In particular, multi-material compliant mechanisms with miniature hinges require the material interface to be able to transfer the loads between the adjacent components. Macro-scale assembly-based approaches impose restrictions on the size and geometric complexity of the multi-material interfaces, which leads to highly suboptimal solutions. Chapter 4 describes in detail the

necessary design features to facilitate the physical interlocking strategy between the incompatible materials in multi-material compliant mechanisms.

Another important issue arises with the development of the multi-material assembly design optimization for miniaturization of devices. An improper selection of the required design features' shapes and their relative orientations may result in highly sub-optimal mold configurations. Chapter 4 presents the development of parametric model of the general multi-material interface design, which includes both functional and manufacturing constrains. The model allows for the design optimization to concurrently minimize the part weight and the process cost. The developed methodology is applied to a case study of a multi-material compliant mechanism used as the drive mechanism in a miniature bird-inspired robot.

The final challenge is related with the design optimization of runner systems used for in-mold assembly of complex structures using multi-cavity molds. Multi-cavity molds require a complex, multi-branch runner system to supply all the cavities with the molten polymer in order to fill the mold. Additionally, the miniature pre-molded components are sensitive to the dynamic force fields imposed by the molten polymer during the second stage mold filling. Chapter 5 characterizes the runner design considerations unique to in-mold assembly of complex multi-material structures with miniature components. These considerations are then incorporated into a complete runner system optimization problem through a detailed mathematical formulation of the problem. The developed optimization model is implemented on a case study of a runner system used for the in-mold assembly of a multi-material drive mechanism of a miniature bird-inspired robot. The case study is used to investigate the possible

solution methods. The performance of several optimization methods is analyzed, followed by the identification of the most suitable method to obtain optimal solutions.

Finally, Chapter 6 presents the intellectual contributions of this dissertation. It also suggests the possible future directions that can be initiated as a continuation of this research work.

2 Literature Review

In-mold assembly process combined with wide functionality of polymer materials is expected to result in creation of novel multi-functional structures, which can be utilized towards miniaturization of robotic devices. The current state of the art however lacks comprehensive solutions to the challenges emerging from this combination. This chapter presents the review of literature in the individual fields of research considered in, and relevant to this dissertation. First, in-mold assembly process is described in terms of multi-material molding technology and the insert molding technology. Next, a review of literature concerning manufacturing multi-functional structures is presented. This includes the field of embedded actuators, characterization of filled polymers and manufacturing of the mechanism utilizing lumped (local) compliance. Finally, literature dealing with the issues connected to the design of the injection molding process is reviewed. This concerns the molding system design optimization, including gate positioning and runner sizing to achieve desired part properties and process conditions (balanced flows).

2.1 In-mold Assembly

In-mold assembly process is a molding process in which the assembly operation takes place inside the mold. This can include a subsequent injection of two (or more) polymers into a cavity, forming a multi-material structure, or injecting a polymer into a mold pre-loaded with elements (such as actuators, electronic components or other functional parts), as a result of which the part with embedded components gets assembled inside the mold. In-mold assembly eliminates post-molding assembly

operations, which reduces the time and cost of the product. In addition, at miniature scale, in-mold assembly not only eliminates a tedious and time-consuming precision manual assembly, but can also enable manufacturing assemblies otherwise impossible to achieve. For successful realization of multi-material, multi-functional in-mold assembled structures, the understanding of the multi-material molding technology and the insert molding technology had to be developed. The following sub-sections review the necessary literature published in these fields.

2.1.1 Multi-Material Molding

Multi-Material Molding (MMM) is generally understood as a molding process involving subsequent or instantaneous injection of more than one material into the mold cavity. The MMM definition, classification, evaluation and tooling overview was described in detail by Fowler in [37].

Multi-functionality of devices can be addressed by combining materials carefully selected to perform a specific function (compliance, heat dissipation, structural strength). One of the technologies where this is utilized is Molded Interconnect Device (MID). A MID is an “injection-molded thermoplastic substrate that has incorporated onto one or more of its surfaces a conductive circuit pattern, which effectively integrates mechanical functions with basic electrical functions” [35]. The electric circuit is obtained by coating one of the materials on the part with a conductor (copper, tin, nickel, gold) [50]. Since adhesion of subsequent shots is a considerable parameter in MIDs, researchers have studied interconnection strength for various materials. Figure 2.1 presents example interface strength results obtained by Islam

et al. [54]. Islam [55] also conducted a detailed study of two-material molding for MIDs .

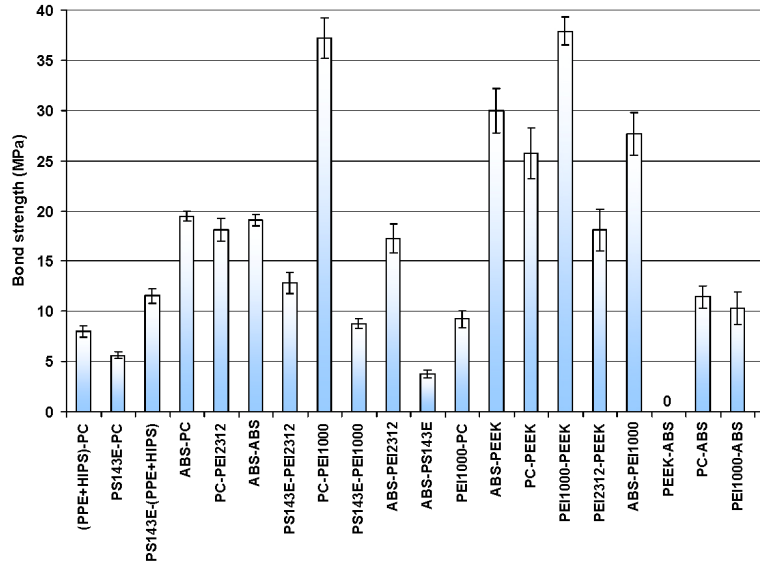


Figure 2.1 Bond strength of two component test specimens [55]

Raw Material	ABS	ASA	CA	EVA	PA 6	PA 6.6	PC	PE-HD	PE-LD	PMMA	POM	PP	PPO	PS-GP	PS-HI
ABS	■	■	■	■	■	■	■	■	■	■	■	■	■	■	■
ASA	■	■	■	■	■	■	■	■	■	■	■	■	■	■	■
CA	■	■	■	■	■	■	■	■	■	■	■	■	■	■	■
EVA	■	■	■	■	■	■	■	■	■	■	■	■	■	■	■
PA 6	■	■	■	■	■	■	■	■	■	■	■	■	■	■	■
PA 6.6	■	■	■	■	■	■	■	■	■	■	■	■	■	■	■
PC	■	■	■	■	■	■	■	■	■	■	■	■	■	■	■
PE-HD	■	■	■	■	■	■	■	■	■	■	■	■	■	■	■
PE-LD	■	■	■	■	■	■	■	■	■	■	■	■	■	■	■
PMMA	■	■	■	■	■	■	■	■	■	■	■	■	■	■	■
POM	■	■	■	■	■	■	■	■	■	■	■	■	■	■	■
PP	■	■	■	■	■	■	■	■	■	■	■	■	■	■	■
PPO	■	■	■	■	■	■	■	■	■	■	■	■	■	■	■
PS-GP	■	■	■	■	■	■	■	■	■	■	■	■	■	■	■
PS-HI	■	■	■	■	■	■	■	■	■	■	■	■	■	■	■

Figure 2.2 A compatibility matrix for various polymers [37]

Figure 2.2 presents another compatibility test results [37]. However, the chemical bonding between subsequent shots may not be strong or possible at all when specific

materials are chosen to obtain required functionality of the final multi-material assembly.

Bruck et al. [21] studied the effects of geometric complexity on interfacial strength of heterogeneous structures created using multi-stage, multi-piece molding. They compared the planar interface with two geometrically complex interfaces, with rectangular and circular interlocking features, shown in Figure 2.3. They have included both bonded and debonded geometrically complex interfaces. Their results show that geometric complexity at the interface can increase the interface strength by 20-25% or create a bond along the interface of heterogeneous materials that are not chemically compatible.

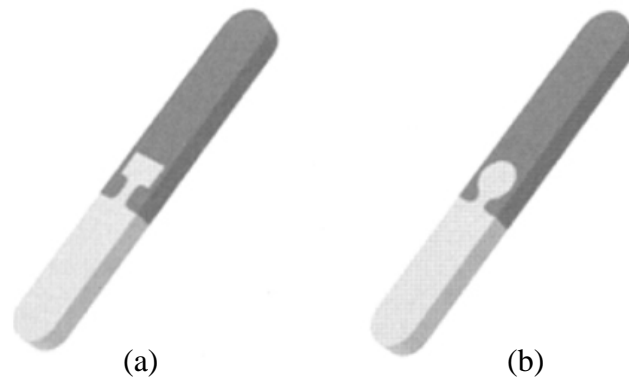


Figure 2.3 Interlocking features for macro-scale heterogeneous structures:

(a) rectangular and (b) circular [21]

Kumar and Gupta [66] described a geometric algorithm for automated design of multi-stage molds for manufacturing multi-material objects. The algorithm performs object and mold decomposition needed to ensure the assembly and disassembly of

mold-pieces during mold-stage assembly and generates the complete molding sequence of the multi-stage molds.

Li and Gupta [73] then developed geometric algorithms for generating mold stages for rotary-platen type multi-shot process. They have shown improvement over the algorithm described in [66] to be able to handle the constraints of the rotary platen process, more complex curved interfaces and to guarantee disassemblability of the generated mold pieces.

Gouker et al. [42] presented a method to manufacture multi-material compliant mechanisms using multi-shot molding. They have shown the necessity to achieve high levels of bonding between the compliant and rigid material which may or may not be chemically compatible. They described several different types of interfaces used to design compliant joints providing 1–3 DOF with an application to compliant mechanisms. For each joint design a feasible mold design was presented to realize that joint. An example of a 3 DOF joint using geometrical complexity of the interface is shown in Figure 2.4.

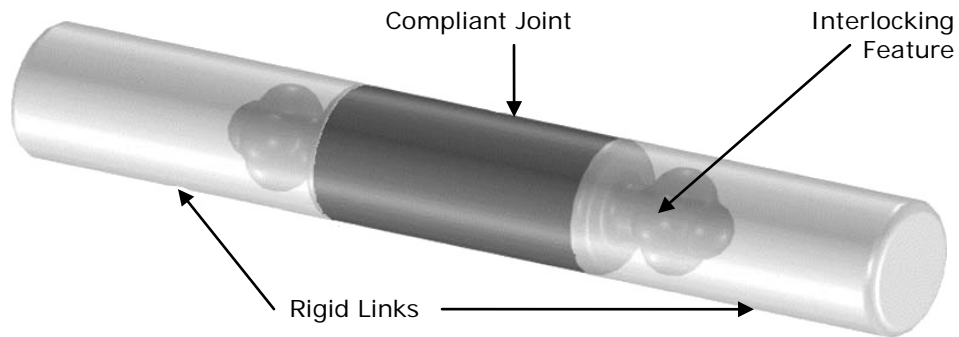


Figure 2.4 3-DOF compliant joint with complex interlocking features [42]

Banerjee et al. [11] developed a systematic methodology for performing manufacturability analysis during design of molded multi-material objects and suggested design changes required for fabricating the part using in-mold assembly methods.

Priyadarshi et al. [89] made a step towards creating a systematic methodology for creating articulated joints using in-mold assembly. They presented a first order approximation guideline for designing assemblies and molding process to achieve desired joint clearances by shrinkage prediction. They have also presented mold design templates for realizing revolute, prismatic, and spherical joints using in-mold assembly. An example case study of a 2 DOF gimbal model with four pin connections is shown in Figure 2.5.



Figure 2.5 2-DOF movement of in-mold assembled gimbal [89]

Ananthanarayanan et al. [7] focused on the in-mold assembly process applied to meso-scale rigid body revolute joints. They presented a mold design strategy and a detailed mechanics-based modeling approach to characterize and control the plastic deformation of pre-molded components. Their approach elucidates the interaction physics between the melt flow and pre-molded parts at the meso-scale in multi-shot

injection molding processes. Their work was the first demonstration of in-mold assembly process using a varying cavity shape mold to successfully manufacture an articulating meso-scale revolute joint. A practical guideline resulting from this study, allowing for the pre-molded pin deformation control by radial support, is shown in Figure 2.6.

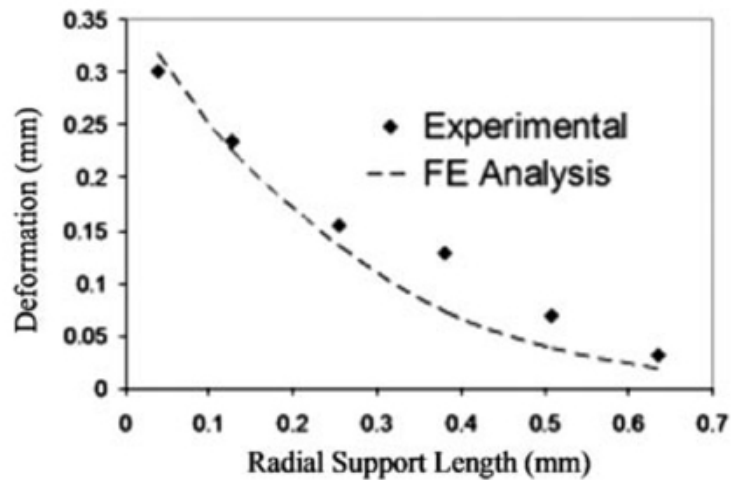


Figure 2.6 Deformation of the mesoscale core versus radial support length for in-mold assembled revolute joints [7]

In the field of micro assembly using injection molding, Michaeli et al. [80] developed a process to manufacture hybrid micro systems by sequential molding of polymer combinations. Different processing aspects of micro assembly injection molding are shown in Figure 2.7. As part of their recent work [81], they have applied the process of micro assembly injection molding to achieve miniaturization of medical instruments.

Steward [105] recently published a review of industry applications of in-mold assembly, overmolding, and other multi-component injection molding techniques.

New opportunities are presented for processors to take advantage of advances in tooling and machinery for multi-component molding technology. These opportunities include cost cuts by eliminating downstream cleaning and assembly operations, reducing scrap, and conserving floor space. Parts produced in a single cycle from multiple materials can also significantly improve quality and add value to finished products.

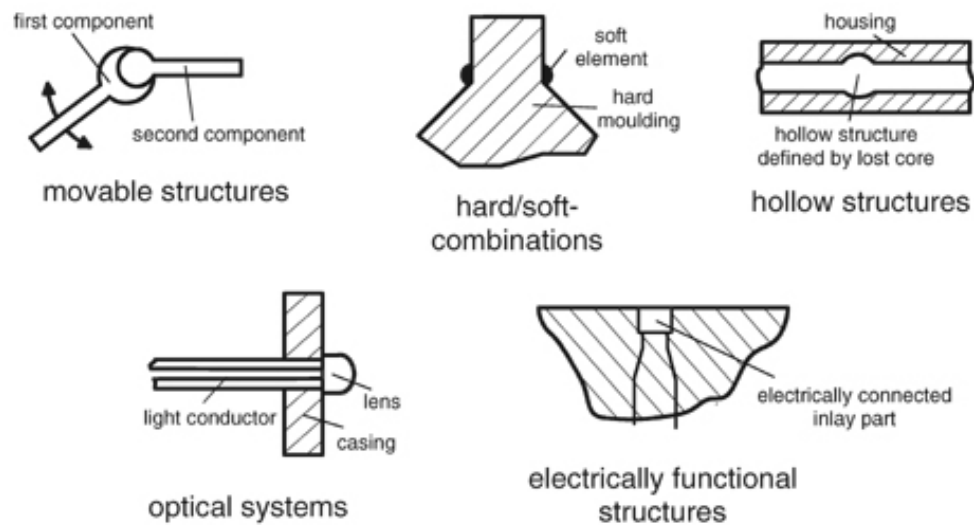


Figure 2.7 Various processing aspects of micro assembly injection molding [80]

Dimov et al. [30] reported findings from a road-mapping study conducted by the FP6 Network of Excellence in Multi-Material Micro Manufacture (4M), concerning current trends and application requirements in the development of Micro- and Nano-manufacturing Technologies (MNT) for the batch-manufacture of micro- components and devices. According to this study, injection molding was the sixth perceived important technology for the future, for both research and industry.

2.1.2 Insert Molding and Over Molding

Insert molding is an in-mold assembly process. It is characterized by having a pre-loaded component inside the mold cavity before the final polymer injection. Since it involves a single material injection to form a part around the pre-loaded component, it can be implemented with standard injection machines and molds. There also exists a process distinction to account for the insert type: insert molding for metal inserts and overmolding for plastic inserts. However, in this work Insert Molding is used to describe both, since this distinction is not important from multi-functionality point of view. Insert molding has become a popular manufacturing process for several applications, which include composite fabrication [82], packaging [108], microfluidics [113] and polymer-metal-hybrid (PMH) structures in automotive industry [46, 44, 45]. The main idea behind these structures is to employ materials complementing each other to create parts with structural performance not achievable by these constituent materials independently.

Chang et al. [23] developed a numerical approach to simulate insert molding for a complex geometry part. The proposed analysis framework contains several stages. First input data (including mesh data, material data, and process conditions) has to be read. Next, a 3D filling simulation is performed. Finally, 3D cooling simulation is conducted to obtain part temperature distribution. The cycle-average temperature served as input boundary condition for warpage analysis. Presented integrated analysis ensured coupling between filling and cooling simulation results. Studied insert-moldings are shown in Figure 2.8.

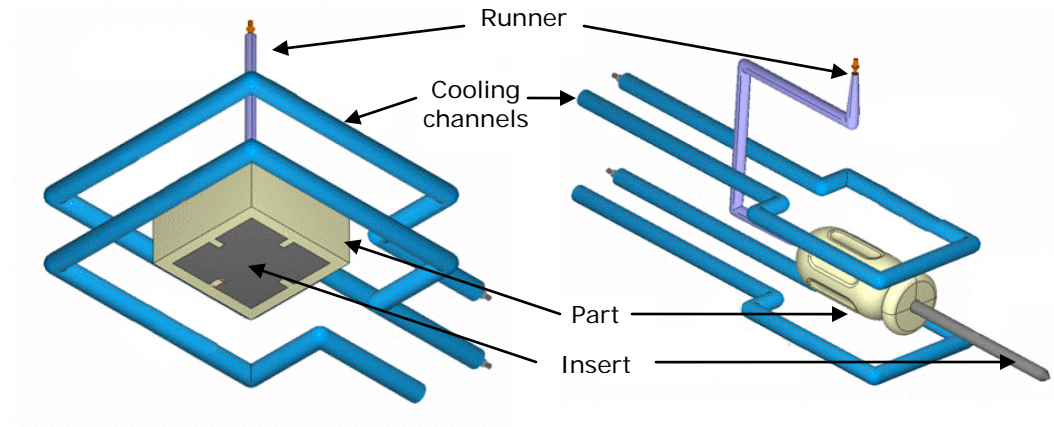


Figure 2.8 Insert-molded parts molding simulation [23]

Huang et al. [53] investigated the warpage behavior in sequential overmolding. Finite Volume Method was employed to solve the transient flow field using Moldex3D software. The influence of product geometry and material choice on the warpage of final products was analyzed. Their results aid understanding of warpage and provide design guidelines for fabricating multi-component molding products.

Grujicic et al. [44] reviewed direct-adhesion methods for manufacturing polymer-metal-hybrids (PMH). PMH technology is currently replacing all-steel structures in load-bearing car body components. Direct-adhesion between the subcomponents is obtained by direct adhesion of the injection-molded polymer to the metal insert, without the use of adhesives or interlocking rivets or over-molded edge. They categorized the reviewed work into four distinct approaches: a) micro-scale mechanical interlocking at the interface surface; (b) pre-coating for enhanced adhesion; (c) chemical modification of the polymer and (d) other strategies to improve polymer-to-metal direct-adhesion. As a result, the micro-scale mechanical

interlocking strategy was identified as the most promising for load bearing PMHs. Example PMH technologies are presented in Figure 2.9 and Figure 2.10.

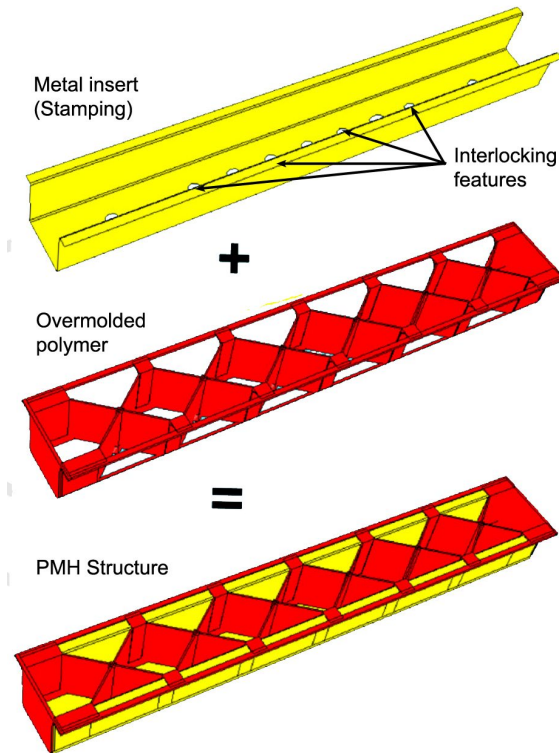


Figure 2.9 Simplified load-bearing component manufactured using metal overmolding PMH technology with interlocking holes ensuring adhesion [44]

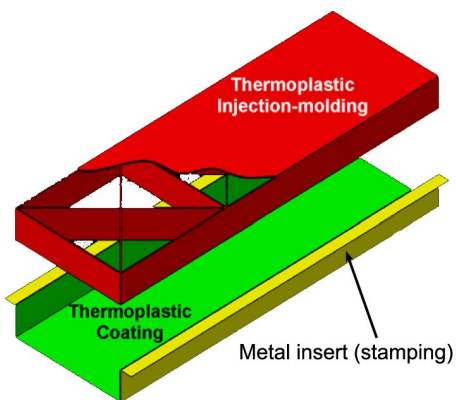


Figure 2.10 Simplified load-bearing component manufactured using metal overmolding PMH technology with a thermoplastic coating promoting the adhesion [44]

Grujicic et al. [45] also performed the analysis to assess the extent of residual stresses and warping in direct-adhesion PMH components. The magnitude and distribution of residual stresses and distortions are critical for the component assembly, performance and durability. For that purpose they combined injection-molding filling and packing stage simulations with a structural analysis involving polymer/metal adhesion analysis. They report that the adhesion at the metal/polymer-subcomponent interfaces has a profound effect on the distribution and magnitude of residual stresses/distortions in the PMH component due to interconnection (and constrained displacement) of the polymer during the cooling stage. The interface adhesion was modeled using a cohesive-zone formulation. A special set of interfacial elements was used where constitutive mechanical response was defined using appropriate normal and shear traction vs. interfacial-displacement discontinuity laws. Figure 2.11 shows the model of each four-node iso-parametric interface element in deformed state, where nodes 1 and 4 and nodes 2 and 3 coincide in the un-deformed (reference) configuration.

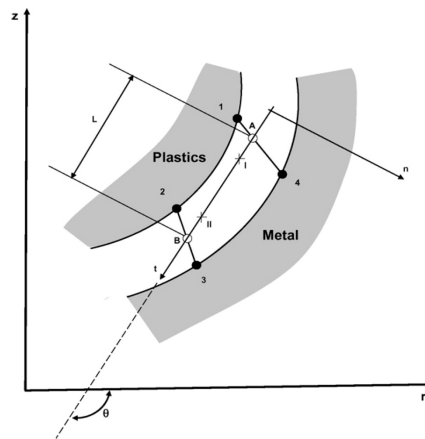


Figure 2.11 Definition of the linear four-node axi-symmetric interface element [45]

Recently, Grujicic et al. [46] also investigated a new concept for mechanical interlocking between the metal and polymer in PMH. The proposed approach utilized the ideas from spot-clinching joining process. First shallow indentations within the metallic insert (stamping) were produced using a common stamping process. These dove-tail shape indentations were then used to anchor the injection-molded polymer ribs to the metal insert. The authors performed a set of finite-element based sheet-metal forming, injection molding and structural mechanics computational analyses. They reported that stiffness and buckling resistance levels are maintained when compared to other PMH processes, however the weight of the polymer subcomponent was reduced and the need for holes and overmolding the metal free edges was eliminated. The two types of clinch-lock concepts analyzed are shown in Figure 2.12.

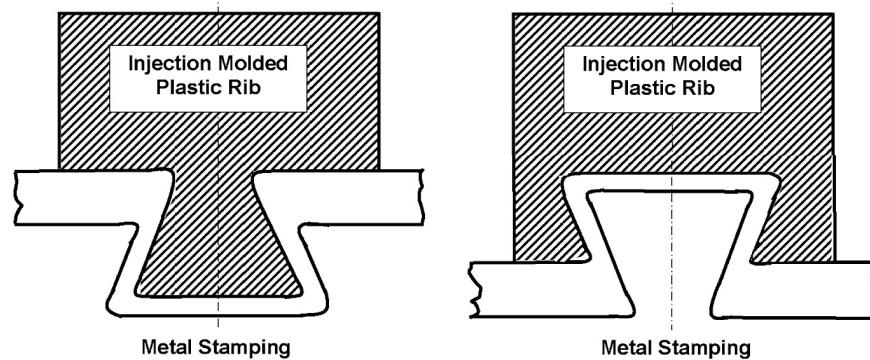


Figure 2.12 Schematics of two types of clinch-lock concepts [46]

2.2 Manufacturing of Multi-Functional Structures

The scope of this work, as defined in Section 1.3, involves two distinct types of structure functionality: (1) embodiment of external actuators and the heat dissipation by the structure, and (2) motion and load transfer by utilizing specific local

compliance and stiffness. Actuators embedded directly in the mechanism structure generate heat during operation. The structure should therefore provide the heat dissipation function along with providing for structural integrity and an anchoring point for the actuator. Such structures are classified as multi-functional structures in this work. Thermally conductive polymers are promising for the heat dissipation function, offering thermal conductivities an order of magnitude higher than bulk unfilled polymers. The thermal conductivity of injection-moldable polymers is achieved by adding conductive fillers (usually carbon) to the polymer. The selection of market available filler materials and forms allows also for an increase in rigidity by using short and long glass or carbon fibers as polymer fillers. The existence of the filler however poses certain challenges in part and process design. The properties of a fiber-reinforced composite are highly dependent on the orientation of the fibers, and the orientation is generally a function of the flow pattern with respect to time during the mold filling. Accurate modeling of the fiber orientation and the properties resulting from it is a very complicated task and has been approached by many researches [1, 9, 10, 26, 33, 34, 36, 39, 49, 63, 91, 95, 102, 103, 112, 114]. Representative literature related to the scope of this dissertation is reviewed in the following sub-sections.

Another interpretation of multi-functionality of the structure is the motion and load transfer by utilizing local compliance and stiffness to realize kinematic mechanisms. This can be realized by using function-specific materials. Fiber-filled polymers are capable of increasing the rigidity of mechanism links. Highly flexible polymer compounds on the other hand can provide the necessary degrees of freedom, often

allowing for elimination of revolute joints and resulting in a lower part count of the assembly. Therefore the term “compliant mechanisms” is used in this work to describe elastic continua that utilize local compliance and stiffness variation to realize the motion and load transfer functions in a mechanism. Compliant mechanisms can also utilize elasticity distributed over the whole mechanism to store energy, which can be returned to the system in the aid of mechanism efficiency. This can reduce the number of actuators and simplify the controls. However, this function of compliant mechanisms lies outside the scope of this dissertation.

This section presents a review of literature concerning manufacturing multifunctional structures. At first, the field of embedded actuators is reviewed. Next, the literature reporting characterization of filled polymers is presented. Finally, manufacturing of the mechanism utilizing a lumped (local) compliance is investigated in the published literature.

2.2.1 Embedded Actuators

This section presents the review of literature dealing with embedding actuators. In many small scale applications, size and accessibility limitations often exclude classic motor-based actuation strategies, both direct and remote. Several types of actuators are currently being embedded in micro-electro-mechanical structures (MEMS). These actuator types include piezoelectric, thermal (SMA), electrostatic and electromagnetic materials and components. Manufacturing of micro-actuators integrated within MEMS is usually realized by multi-material prototyping methods such as layered deposition or micro-surface machining [25, 32, 56, 64].

Chien and Yu [25] presented a technology to fabricate actuators on polymer material. This technique utilized conventional photolithography technology, electroplating and hot embossing. The metal layer was first deposited on the silicon wafer and then it was transferred into the polymer substrate by hot embossing technology. Since the adhesion between the metal and polymer was greater than with silicon wafer, the wafer was easily debonded, resulting in the metal layer being embedded in the polymer substrate. They have also fabricated and tested a PMMA cantilever beam actuator driven by electrostatic force using this technology.

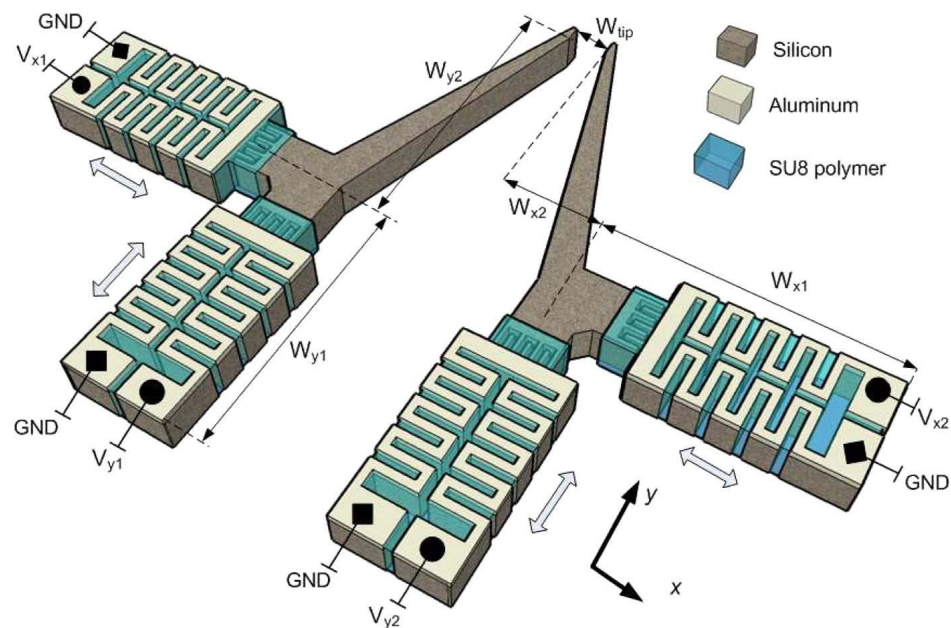


Figure 2.13 2D micro-gripper with four silicon-polymer forward actuators [32]

Duc et al. [32] described in detail the fabrication process of a novel electro-thermal micro-actuator and showed its applicability in a 2-DOF micro-gripper. The schematic micro-gripper assembly is shown in Figure 2.13. The actuator realizing in-plane

forward motion consists of a deep silicon skeleton structure with a thin-film aluminum heater on top and filled polymer in the trenches among the vertical silicon parts. The fabrication was based on deep reactive ion etching, aluminum sputtering, SU8 filling, and KOH etching.

Iverson and Garimella [56] reviewed MEMS micro-pumping techniques that have been reported in the literature in the recent years. The range of applications was presented along with limitations of various micro-pumping technologies. However manufacturing technologies of micro-pumps were not discussed in detail, with exception of screen-printing and thin-film deposition technologies being used for attachment of PZT materials in piezoelectric actuators.

Rosmarin and Asada [92] developed a humanoid hand with hybrid DC motor–SMA actuator arrays embedded in the palm. ABS fingers are actuated by a series of pulleys driven from the palm, which is composed of steel plates. The authors mention using cooling fans, which suggests that even though the SMA wires are not directly embedded in the polymer structure, there is a need for active cooling. The robot was created using manual assembly operations.

Kim and Tadokoro [64] published a review of electroactive polymers (EAP) actuators and sensors for robotic applications. They have introduced a novel antagonistically driven linear actuator (ANTLA) and presented its possible implementation in realizing different types of motion. The actuator was produced by layered deposition rapid prototyping. One of the applications included three ANTLAs embedded in a polymeric annelid structure to form a segment of an inchworm micro-robot. The actuators not only provide actuation by reproducing muscle combination,

but also serve as a frame, making it a multi-functional structure. The prototype was capable of translational motion. It was manufactured using layered deposition technology, however authors point to possibility of extension to injection molding as well. Actuation sequences of the robot segment are illustrated in Figure 2.14.

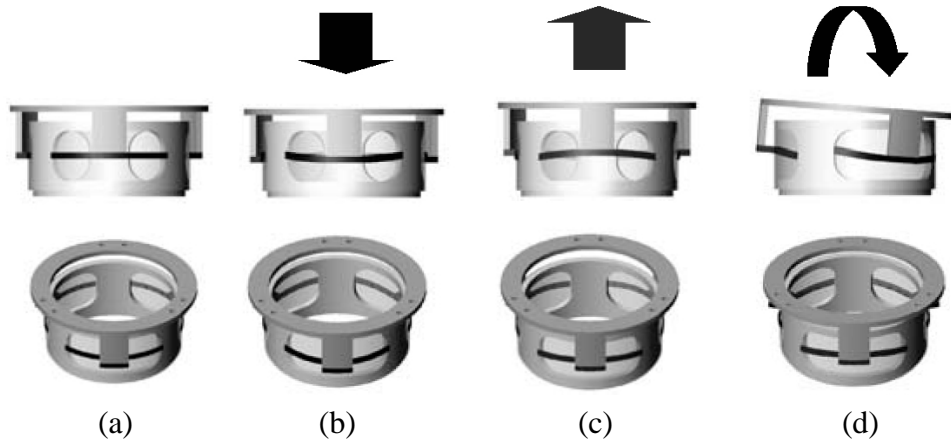


Figure 2.14 Actuation sequences of ANTLA robot segment: (a) neutral state (b) upward actuation (c) downward actuation (d) asymmetrical actuation (turning) [64]

Gyger et al. [48] developed an approach for creating multi-functional bio-inspired structures with controllers, actuators, and sensors integrated into a modular segment of a robot. They successfully embedded electronic systems in a polymer structure using multi-stage molding process to form an integrated module of a snake-type robot. The second stage of the two-stage transfer molding process was used to make a universal joint allowing for 2-DOF. The model of in-mold assembled robot modules is shown in Figure 2.15. The presented approach resulted in Thermal and Impact Protected (TIPed) Embedded Sensing Controls Actuation Power Element (ESCAPE) Structures for compact and rugged robotic applications. However, their

work did not include issues connected with embedding actuators like heat dissipation and survivability of the embedded components during molding process.

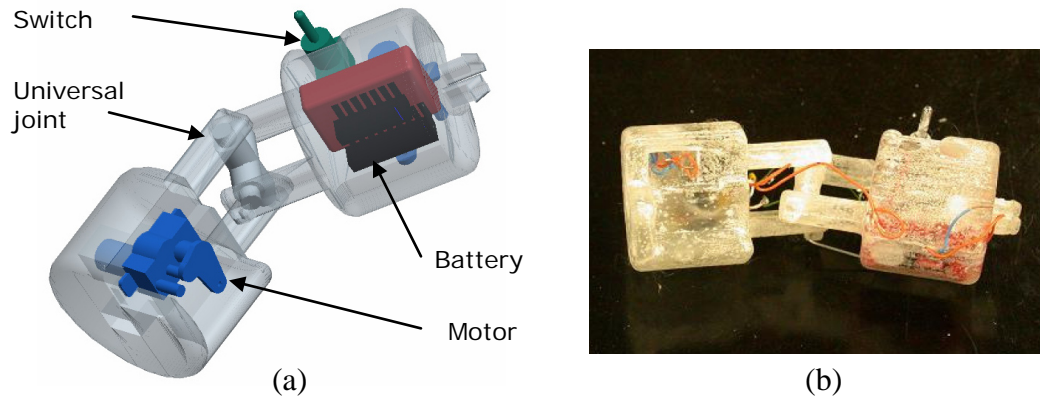


Figure 2.15 Multifunctional Structural Module with embedded electronic components: (a) solid model, (b) molded prototype [48]

2.2.2 Filled Polymers

This section presents the review of literature dealing with characterization of filled polymers relevant to the scope of this dissertation. It is worth mentioning here that the reviewed work did not consider manufacturability aspects related to thermally conducting filled polymers. Properties of the thermoplastic compounds can be enhanced by adding filler to the polymer matrix, resulting in a composite material. The selection of market available filler materials and forms allows for production of engineering materials with properties serving particular functions of the molded product. Using short and long fibers increases the stiffness of the composite, however the strength and brittleness depend on the volume fraction and orientation of the filler. Addition of metallic or carbon fillers to the polymer results in polymer

composites capable of conducting heat and electricity. The conductivity results from the physical connection of the filler particles inside the polymer matrix and is directly proportional to the volume fraction of the filler. Carbon-filled polymers offer thermal conductivities an order of magnitude higher than bulk unfilled polymers. Finally, filled polymer composites can reduce the mass of the final product by replacing metallic counterparts and thereby offering improved stiffness-to-mass ratio.

The existence of the filler however poses certain challenges in part and process design. When the filled polymer is injected into the mold, the fibers tend to get aligned with the flow [58], resulting in non-isotropic thermal and mechanical properties. The properties of a fiber-reinforced composite are highly dependent on the orientation of the fibers. The orientation of fibers affects the strength, thermal expansion and elastic modulus when the composite is solid; viscosity when liquid; and thermal conductivity for both solid and liquid forms [26]. The degree of fiber orientation across the molded part is described by a 3D fiber orientation tensor described by a probability density function. It is defined as the probability of a fiber being oriented within an angular range to a pre-defined direction [1]. The orientation tensor is generally a function of the position, and for filling simulations, time. Numerical prediction of the 3D fiber orientation during mold filling is usually based on an equation of motion for rigid particles in a fluid suspension. The analysis consists of two identifiable terms: (1) the hydrodynamic term [58], and (2) the interaction term [36]. Accurate modeling of the fiber orientation itself and the properties resulting from it is a very complicated task and has been approached by

many researches [1, 9, 10, 15-17, 26, 31, 33, 34, 36, 39, 49, 63, 91, 95, 102, 103, 112, 114].

Weber et al. [114] observed synergistic effect of combining different carbon fillers on thermal conductivity of carbon filled nylon 6,6 and polycarbonate based resins. The three carbon fillers investigated included an electrically conductive carbon black, synthetic graphite particles, and a milled pitch-based carbon fiber. They determined the effects and interactions of each filler on the thermal conductivity properties of the conductive resins.

Bahadur and Bar-Cohen [10] investigated the thermal performance limits of a polyphenylene sulphide polymer composite pin fin heat sinks cooled with air. They analytically predicted the thermal performance across an extensive parametric space in terms of the primary thermal metrics and identified the thermal performance limits. They showed that PPS heat sinks are a viable alternative material for energy efficient heat sink design with thermal performance comparable to aluminum and copper heat sinks at low fin densities and pumping power.

Bahadur [9] also presented thermal simulations and measurements with application to heat sink design fabricated out of thermally conductive polymer composites. He presented theoretical models and validation techniques to predict and optimize the filler orientation for the heat dissipation function, however this work addressed only fin pins heat sink designs.

Dogruoz et al [31] studied thermal performances of advanced heat sink materials via computational models, and compared them with Aluminum heat sinks. They

presented transfer functions based on the heat sink geometry, material properties (thermal conductivity) and the base temperature.

Egelkraut et al. [34] demonstrated the potential of highly filled polymers for packaging solutions in power electronics and present a packaging technology for passive devices. They used a choke for a high power multiphase DC/DC converter packaged in a highly filled thermal conductive thermo-plastic polymer using an injection molding process. Based on thermal simulations, polymers with different Al_2O_3 filler volume fractions were produced and used as housing. The high filler volume fraction and the thermal conductivity led to changes in process conditions, especially with respect to temperature and pressure during the molding process.

2.2.3 Compliant Mechanisms

This section presents the review the published literature dealing with the design and fabrication of compliant mechanisms and their novel applications. Conventional mechanism consists of rigid links connected with joints, forming a dynamic system realizing desired transduction function (force, motion or energy transfer). In these mechanisms, elasticity can be incorporated as a discrete component such as a spring. Compliant mechanisms are designed elastic continua. They utilize elasticity distributed over the parts or the whole mechanism [96, 106]. The main advantages over conventional mechanisms are:

1. Friction and backlash losses reduction
2. Noise and vibration reduction
3. Light weight
4. Cost reduction:

- a. Manufacturing
- b. Maintenance

Additionally, a local (lumped) compliance in the mechanism can be used to eliminate revolute joints from the assembly, resulting in reduced part count and improved system precision. Finally compliant mechanisms allow for reduction of the degrees of freedom when combined with reciprocating actuators by storing energy and restore it during the return cycle. All these advantages make compliant mechanisms promising towards miniaturization of devices. The main fabrication methods of compliant mechanisms include precision milling, laser cutting, lithography-based technologies and molding techniques. Some of the main application areas of compliant mechanisms include precision instrumentation, micro-electro-mechanical systems (MEMS) and special-purpose designs like centrifugal clutches [27] or MAV drive mechanisms [5, 14, 18, 40, 83, 107].

On the other hand, metal compliant mechanisms eliminate creep and stress relaxation and are suitable for high-temperature applications. Also, material properties of metals are more reliable and easily modeled. Manufacturing processes include bending of sheets, laser cutting, stamping, wire electrical discharge machining (EDM) and CNC machining [87]. This section presents the work most relevant to the scope of this dissertation that was published in the field of compliant mechanisms.

Tantanawat [106] investigated modeling and optimization of compliant systems for dynamic applications. The main goal of his research was to use distributed compliance to reduce peak input power and average input power of a mechanism and

its entire system. He explored different modes of optimal designs and developed a framework for dimensional synthesis of compliant systems. The explored applications included a power converter, input actuator and a compliant mechanism of a small MAV, schematically shown in Figure 2.16.

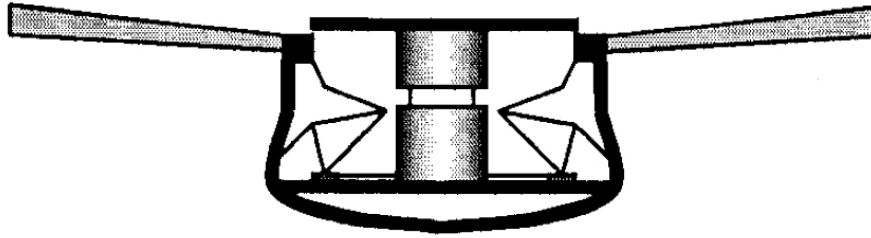


Figure 2.16 Flapping wing air vehicle compliant mechanism concept [106]

Tantanawat and Kota [107] also reported that power input needed to drive the proposed compliant flapping mechanism was 15% less than a rigid-link four-bar flapping mechanism with a spring. The reduction of peak input power was accredited to the exploitation of elasticity in compliant members.

Tian et al. [109] explored the influence of the geometric parameters on the characteristics of the filleted V-shaped and cycloidal flexure hinges. They have developed empirical equations and dimensionless graphical expressions for designing hinges in compliant mechanisms. However, they considered the hinges to be manufactured monolithically with other components of the entire mechanism by numerically-controlled WEDM (wire electrical discharge machining) technology. Nevertheless, the main results from this work are valuable for the current study in scope of the hinge geometry design, therefore they are cited in detail with relation to Figure 2.17.

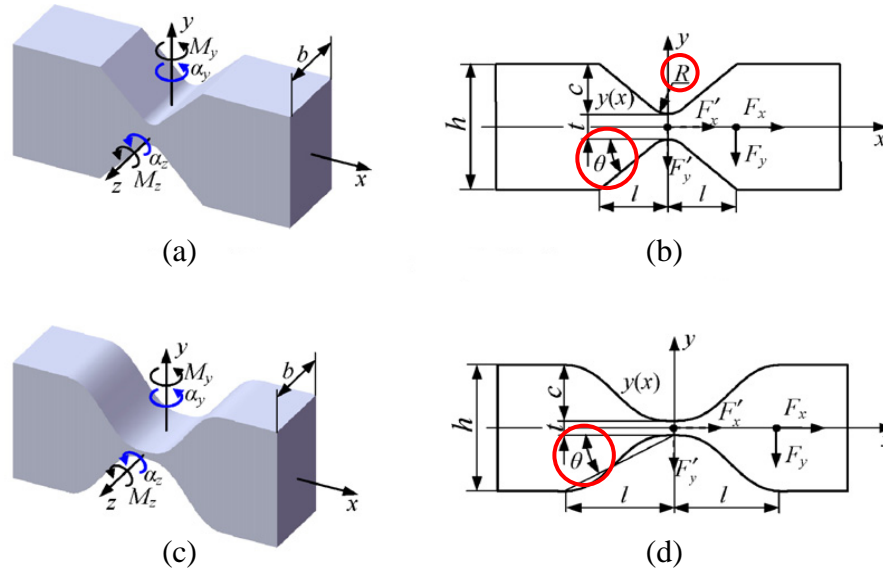


Figure 2.17 Diagram of filleted V-shape hinge: 3D (a), 2D (b);
and cycloidal hinge: 3D (c), 2D (d) [106]

The stiffness and rotational precision of the filleted V-shaped flexure hinges increase with the increasing angle Θ and decreasing radius R , respectively. For small ranges of Θ the cycloidal flexure hinges are more compliant than the filleted V-shaped flexure hinges, and for large values of Θ this relation is opposite. When the filleted radius R approaches to the half length of the flexure hinge, the filleted V-shaped flexure hinges have larger compliance than the circular flexure hinges and the stiffness reduces with decreasing angle Θ .

Gouker et al. [42] proposed utilizing the multi-material molding process for creating compliant mechanisms and described feasible mold designs for creating different types of compliant joints. They have presented practical applications for the use of multi-material molding to create compliant mechanisms: a compliant clip and a rotor system, shown in Figure 2.18. For joints with a flat interface a sliding core

molding method can be used. For more complex joint interfaces as well as more complex mechanism assemblies cavity transfer method has to be used.

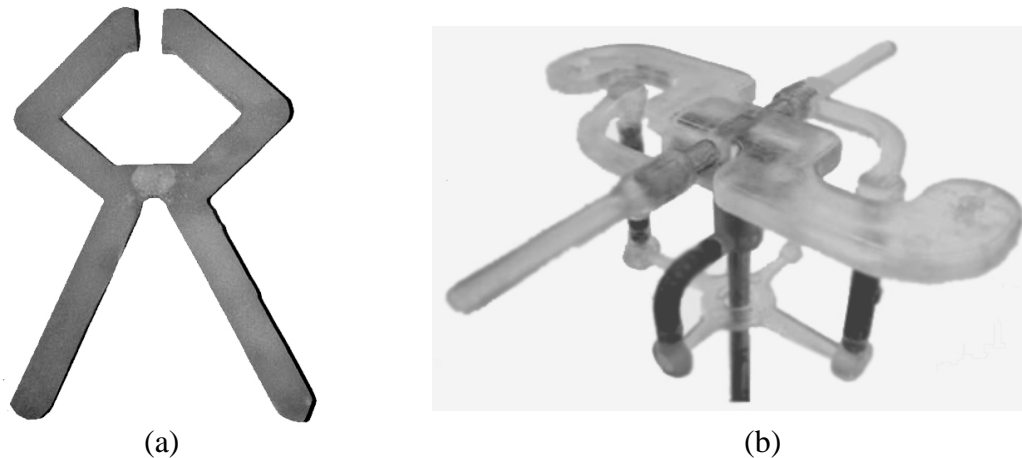


Figure 2.18 Compliant structures manufactured using multi-material molding: (a) compliant clip, (b) rotor system [42]

Bejgerowski et al. [14] performed parametric optimization of injection-molded compliant drive mechanism and demonstrated its application in a successfully flown MAV. This novel mechanism design used distributed compliance to allow for small displacements of anchoring points for the flapping-motion. This work included mold manufacturability considerations, as well as minimization of mold pieces.

Cutkosky and Kim [28] recently published methods for design and fabrication of multi-material structures for fabrication of bio-inspired robots. They used shape deposition manufacturing (SDM) with polymers and fabric or fiber reinforcement. They explored the design of a leg of hexapedal running robot, which was actuated by a push-pull cable system, driven by a motor through a slider-crank mechanism. The compliant polymer was used to create elastic flexures and friction dampers, as shown

in Figure 2.19. They have also presented a hierarchically compliant structure of a gecko-inspired robot climbing vertical surfaces. Hierarchical compliance included (a) flexible body articulation, (b) serial compliances with force sensor at the limbs and differential cable system, (c) under-actuated cable-driven toes and (d) segmented toe structure with directional polymeric stalks. Each compliant element was composed of soft and hard polymers. The compliance hierarchy is shown in Figure 2.20. They also presented a way of manufacturing flexural components containing elements like fibers, wires or fabrics that traverse the boundary between two different part materials. This is schematically shown in Figure 2.21.

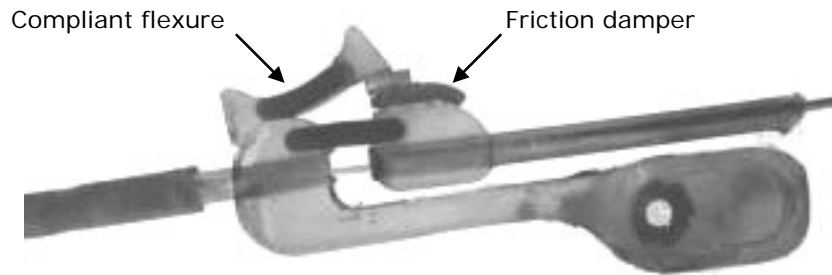


Figure 2.19 Running robot leg design made using hard and soft viscoelastic materials for compliance and damping [28]

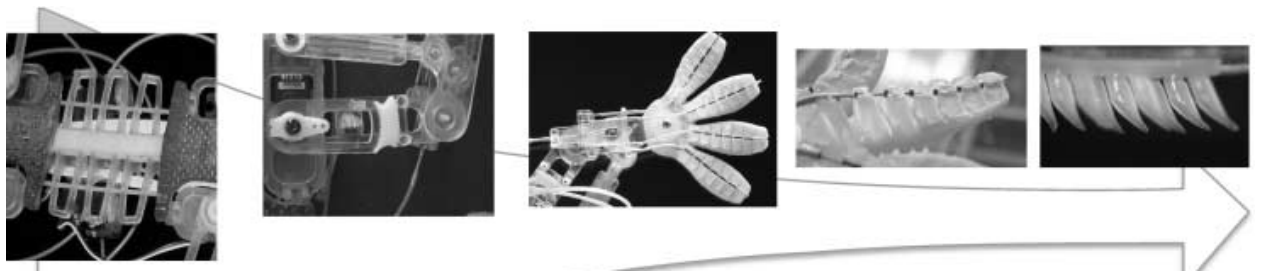


Figure 2.20 Hierarchical compliance structure of a gecko-inspired robot [28]

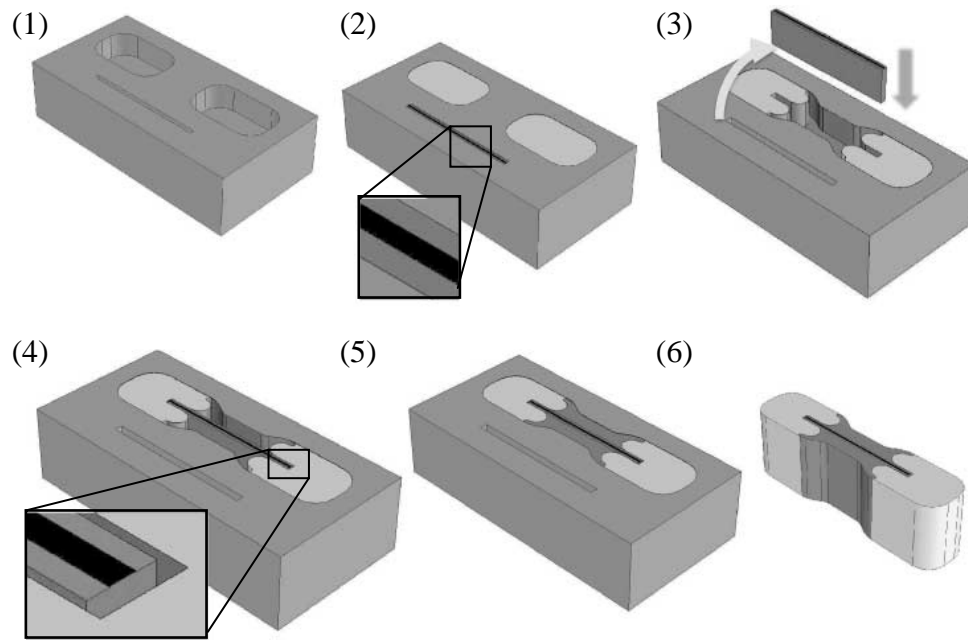


Figure 2.21 SDM process plan for creating multi-material parts with fibers traversing material boundaries [28]

Zelenika et al. [116] presented flexural hinge shape optimization for monolithic micro-devices. They considered high-precision milling, electro-discharge-machining (EDM) and lithography-based technologies as manufacturing techniques. They compared several predefined and freeform parametric shapes in terms of compliance, strength, stress concentration factors and parasitic shifts. They report that the optimized hinge shapes result in improved performance compared to conventional circular notches.

Cannon and Howell [22] presented a compliant contact-aided revolute (CCAR) joint, a scalable planar mechanism realizing torque transfer and partial rotation. The CCAR joint consists of multiple flexures fixed at one end and free at the other. The free ends of the flexures are constrained by the cam surface of the gauge pin. Pseudo-

rigid-body model was used for modeling the CCAR joint behavior, which was validated by finite element analysis and prototype testing. General design guidelines for CCAR joints were given: more flexures for designs requiring high torque and small rotation and fewer flexures for designs requiring low torque and large rotation. The manufacturing considerations are discussed for the macro, meso, and micro scales, involving prototypes manufactured using CNC-milling, micro wire electrical discharge machining (EDM) and Sandia Ultra-planar, Multi-level MEMS Technology 5 (SUMMiT V) respectively. Two prototypes of CCAR are shown in Figure 2.22.

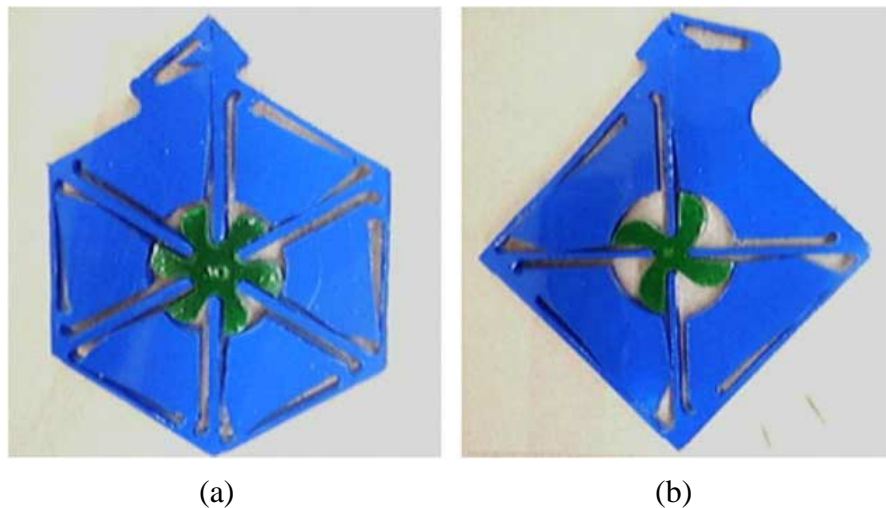


Figure 2.22 Prototypes of contact-aided revolute joints: (a) drive rotor and (b) gate rotor [22]

Pendleton and Jensen [87] demonstrated compliant mechanisms formed from a single pre-shaped wire, called wireform mechanisms. They presented a simplified pseudo-rigid-body model of the mechanically tri-stable mechanism and validated it by FEA and experimental measurements. Two types of wireform mechanisms were

studied: (1) wire coils as torsional springs to approximate joints and (2) sections of a wire placed in torsion. The later is shown in Figure 2.23. This work created an alternative fabrication method of metal compliant mechanisms.

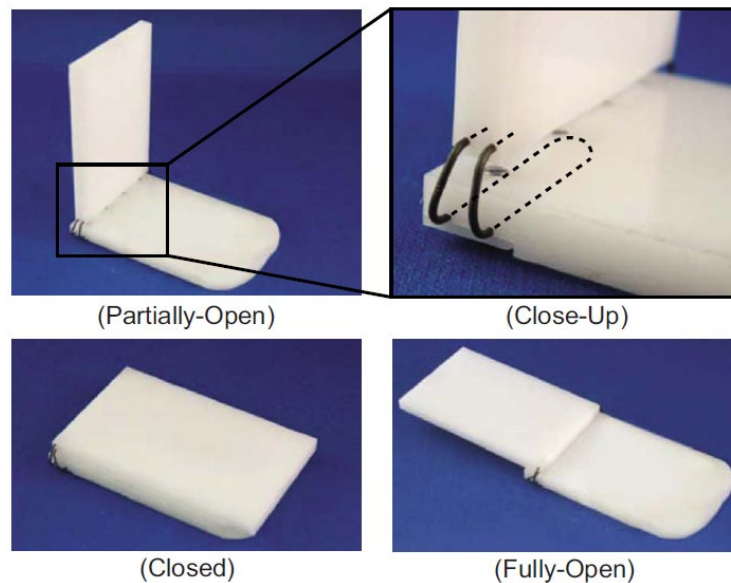


Figure 2.23 Wire-form torsion-bar mechanism prototype hinge [87]

2.3 Molding Process Design

This section reviews the literature which deals with the issues connected to the design of the injection molding process. Injection molding process consists of the following stages:

1. Mold closing
2. Mold cavity filling – polymer melt is being injected at injection temperature
3. Packing stage, during which the cavity is additionally filled under high pressure to compensate for material shrinkage

4. Cooling stage – time required for the part to solidify
5. Mold opening
6. Part ejection

The quality of injection molded parts is generally described by its dimensional tolerance, visual defects and strength. The dimensional tolerance defines the allowable warpage and shrinkage. Warpage occurs when different regions of the part cool (and shrink) over different periods of time. To minimize this effect injection pressure and temperature within the cavity need to be evenly distributed, resulting in balanced filling process. Visual defects are caused mainly due to flash, improper gate size or formation of the weld-lines. Strength of the part can also be significantly reduced by the presence of weld-lines. However, in some cases weld-lines are unavoidable, for instance whenever the polymer melt flows around a core or mold insert. In these cases, the weld-line region should be designed to be sufficiently strong, or in multi-gate cavities, weld-lines should be moved to structurally (or aesthetically) non-critical regions by relative positioning of the gates.

To ensure the quality of products, design optimization theory is being widely applied to injection molding design. Usually, the molded part has its functional requirements and its dimensions may not be changed. The gate dimensions are directly related to the pressure and temperature distribution of the molding while runner layout is determined by the part geometry and cavity layout. Therefore gate location and runner size are the most common design parameters for optimization of injection molds [2, 3, 29, 43, 57, 59, 62, 67, 69, 68, 70-72, 84, 94, 98-100, 104, 115, 117, 120, 121, 118, 119].

2.3.1 Gate Placement Optimization

Gate location is an important design variable in injection mold design. It largely affects the fill pattern in the cavity. An improper choice of gate location induces an unbalanced flow, which causes overpacking, high shear stress, and excessive warpage. The gate position also influences the fiber orientation for the filled polymers, affecting the properties of the molded part. Therefore gate placement is of a great importance to achieve high quality products with required properties. The state-of-the-art in gate placement optimization in injection molding is reviewed in this section.

Pandelidis and Zou [84] used the combined scheme of a simulated annealing and a hill-climbing optimization method for the gate location. The quality of a gate design was represented as an additive function of a temperature differential term, an overpack term, and the frictional overheating term, with appropriate weighting factors. Even though the methodology is applicable to any complex mold geometry, it is not computationally efficient.

Lee and Kim [68] developed a methodology to predict the optimal gate location based on user-defined design evaluating criteria for warpage, weld/meld lines, and Izod impact. The methodology determines the initial design based on the human designer's intuition, and then locates the optimal gate by the adjacent node evaluation method. The scheme can be used for complicated parts, but it requires an extensive number of design evaluations to obtain the optimal gate location.

Smith et al [104] optimized gate location and injection pressure profile through minimization of fill time, while satisfying constraints on injection pressure, injection

flow rate, and mold clamp force. They used the Newton-Raphson iteration to solve the nonlinear equations for the polymer melt pressure field which are formed via the isothermal Hele-Shaw flow analysis and Galerkin finite element method. To compute the fill time and filling pattern, a moving boundary analysis was developed based on the volume-of-fluid (VOF) technique. They applied the Design Sensitivity Analysis (DSA) to optimize gate locations in planar mold cavities, addressing only isothermal problems.

Kabanemi et al. [59] extended the DSA-based numerical simulation method to non-planar geometries and non-isothermal filling problems. Their optimization problem formulation follows [104]. Their algorithm uses direct differentiation method to evaluate the sensitivities of Hele-Shaw equations, filling fractions and energy equations. The finite element evaluated objective and constraint functions are passed to Design Optimization Tools (DOT). The numerical optimizer systematically modifies the design variables to minimize the fill time. Both linear and quadratic sequential programming algorithms were used.

Kim et al. [62] presented a single gate placement design guideline for parts with hinges. They investigated resin flow patterns obtained by numerical analyses for several different gate positions of a simple strip with a hinge. The analyses showed that the resin at the hinge did not flow until the other side of the part was filled. Once the resin at the hinge did not flow for a long enough time to be solidified, short shots or hesitation marks formed due to the secondary resin flow over the partly solidified flow front occurred. Therefore, they presented a design guideline to properly locate gate positions to minimize flow hesitation at hinge areas and hence to avoid

formation of defects. They present a practical application of the guidelines on a design of automobile junction box cover.

Shen et al. [98] proposed a gate location optimization by using modified hill-climbing algorithm. Their method predicts the optimal gate location based on simulation. The cost function contains filling pressure, filling time difference between different flow paths, temperature difference and overpacking percentage, which are the functions of gate location. A modified hill-climbing algorithm that combines the designer's intuition with a deterministic hill-climbing search is used to search the optimal gate location. They quantitatively relate the properties that the gate location has a large effect on, such as inlet pressure, filling pattern, and shrinkage, to the flow simulation results. However, they discuss only the single-gate location problem.

Lam and Jin [67] developed a gate location optimization method based on the minimization of the Standard Deviation of Flow Path Length (SDL) or Standard Deviation of Filling Time (SDT) during the mold filling process. They implemented hill-climbing algorithm for flow path determination, subsequently utilized for gate location optimization. SDT was claimed superior to SDL for parts with non-uniform thickness in locating optimal gate positions.

Zhai et al. [119] proposed a general methodology called Flow Resistance Search Scheme (FRSS) (Figure 2.24) to find the optimal gate location. They used the minimum mold fill time as a proxy to balanced flow. The mold fill time was related to the flow resistance: higher the flow resistance - longer mold fill time. The flow resistance was reflected by the pressure gradient; the largest pressure gradient

represented the highest flow resistance. By moving the gate along the direction with maximum flow resistance, the mold fill time was reduced to achieve a balanced flow pattern. They have concluded that the FRSS method is as efficient as the BFGS gradient-based method, however based on an example study of a telephone cover mold the FRSS method was claimed to be superior when applied to complex parts.

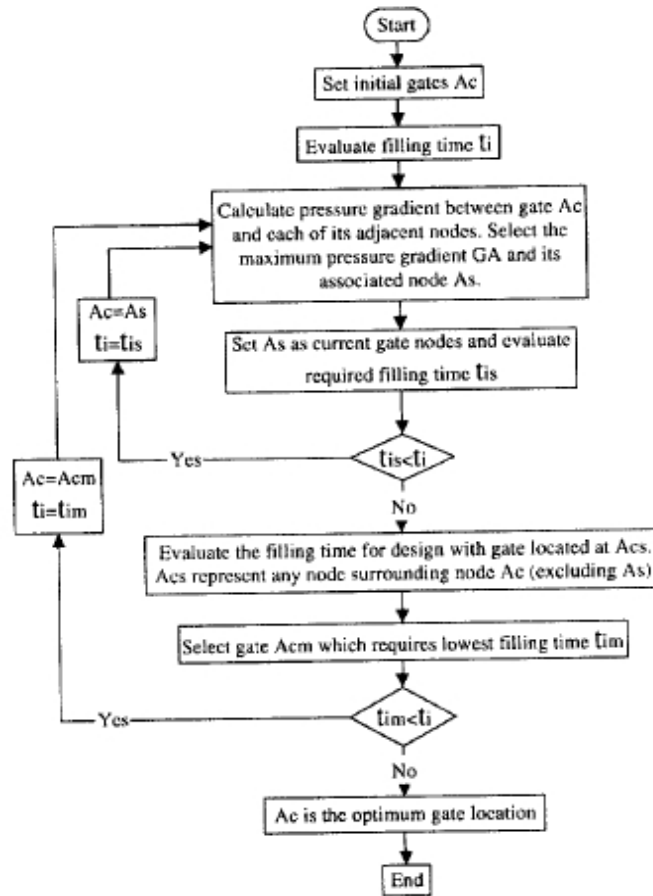


Figure 2.24 Flow Resistance Search Scheme flowchart [119]

Zhai et al. [118] also proposed a gate placement optimization approach to achieve balanced polymer flow and reduce the warpage of the part. The proposed objective function was based on minimizing injection pressure at the end of fill time and

compared it with objective function in [67]. They used the concept of flow paths (standard deviation of flow path length or fill time, or range of fill time) as a measure of balanced flow. They showed that the proposed optimization algorithm (Figure 2.25) based on pressure gradient method is more efficient compared with the algorithm based on the flow path and avoids the necessity of identifying a set of boundary nodes when compared with the objective function of range of fill time. The performance of the gate location optimization method is demonstrated by two single-gate design examples.

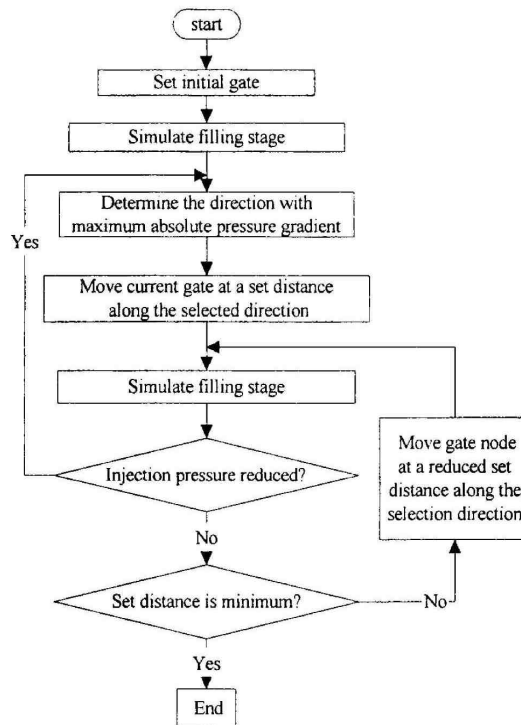


Figure 2.25 Gate placement optimization approach to achieve balanced flows [118]

Zhai et al. [117] also presented an efficient search method for the two-gate location optimization problems in injection molding. They increased the efficiency of optimization process based on the Pressure Gradient Search Scheme (PGSS) by

employing a heuristic strategy to select the candidate. This method was found to be computationally efficient as it required over 90% less number of numerical simulations compared to genetic algorithm (GA).

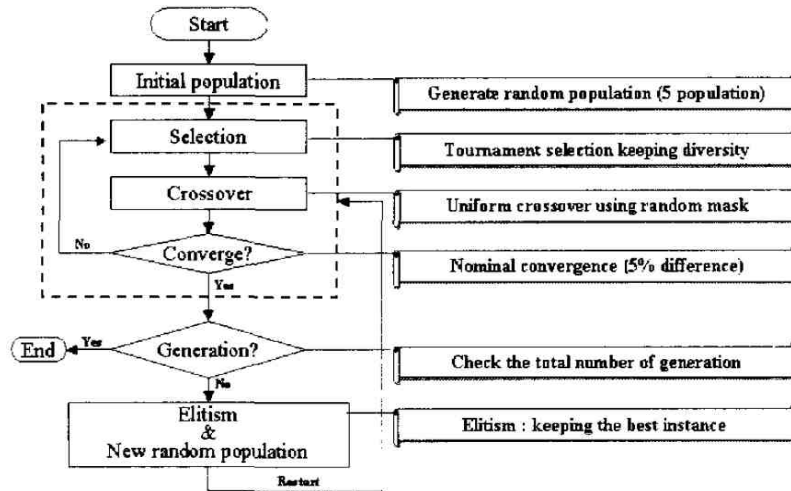


Figure 2.26 Gate placement optimization mGA algorithm [70]

Lee and Kim [70] explored the design of injection mold system using micro genetic algorithm (mGA). They proposed two design objectives to locate gate positions: (1) by minimizing maximum injection pressure at the injection port and (2) minimize maximum pressure difference among all the gates on a product, with constraints on shear stress and/or weld-line. The analysis of filling process was conducted by the finite element based software for polymer flow – Computer Aided Plastics Application (CAPA). Due to the nature of inherent nonlinearity in flow analysis, mGA process shown in Figure 2.26 was used as a global optimization tool. Proposed design strategies were evaluated on different design applications, showing effectiveness of mGA in the context of optimization of molding system.

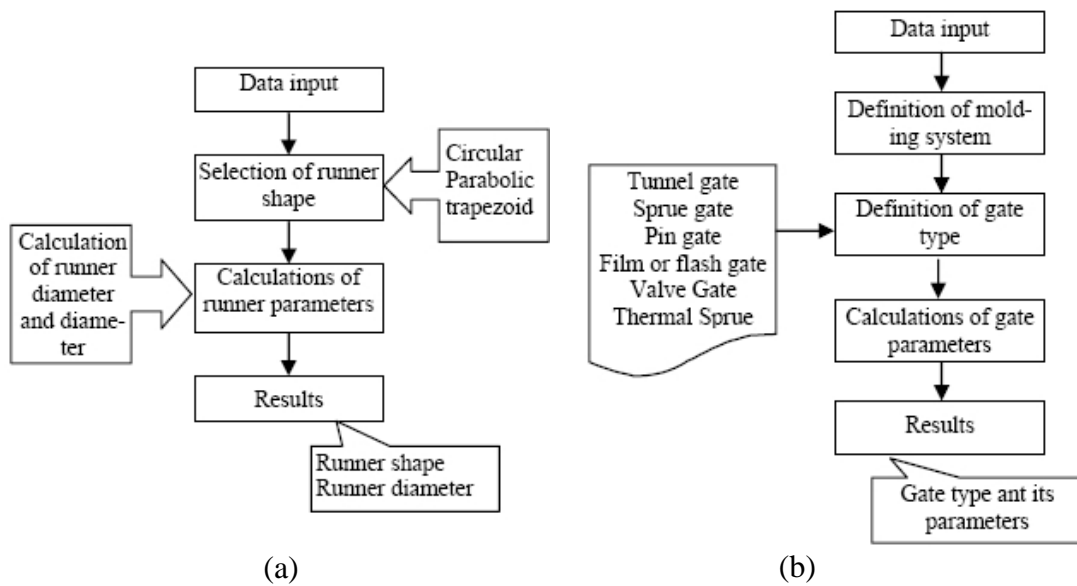


Figure 2.27 Algorithms for designing injection molding system: (a) automated gate type definition and (b) runner type selection and parameter calculation [94]

Rutkauskas and Bargelis [94] developed a method to replace routine work of human experts by artificial intelligence knowledge-based method in gate and cold runner's design for injection molding. They systemized the engineering data and facts available in various references and companies for the molding system of injection mold. They developed the algorithms for the definition of gates and runners and calculation of their parameters based on production volume and delivery time of the part, its geometrical form, dimensions, mass and quantitative-qualitative parameters and molding machine characteristics. These algorithms are shown in Figure 2.27. The developed method was tested by comparison to experimental data of seven molded plastic parts with acceptable error.

Deng et al. [29] proposed strategies and methods for the optimization of multi-class design variables in injection molding using particle swarm optimization (PSO). They combined variables from different classes: part thickness from part geometry class, melt temperature, mold temperature, injection time belonging to processing parameters class and gate location for the mold design class and optimized them to maximize the quality of the part by minimizing the warpage, length of weld-lines and size of air traps. They presented a mathematical model, subsequently reformulated for a PSO algorithm and the procedure of the optimization process. Based on a case study, authors show that the PSO algorithm can handle multiple objectives and multiple classes of design variables with ease. The main limitation of this method is that a single best or optimal solution from a PSO algorithm cannot be obtained. Hence the designer has to choose the final solution from a set of reported elites.

Shen et al. [99, 100] presented a mathematical model for thin-walled injection molded parts, defined by thickness smaller than 1 mm, or the ratio of flow length to thickness larger than 100. They present the mathematical model for the non-isothermal, generalized Newtonian fluid and use the control volume finite element method to solve the mass, momentum and energy conservation governing equations. The authors analyze different gate positioning strategies for a thin-walled battery cover and choose single point on two sides, double gate placement as the optimal result by numerical simulation.

2.3.2 Runner Optimization

The runner system is one of the most important basic elements of thermoplastic injection molds [57] [69]. The main function of the runner system is to supply mold

cavities with a molten polymer from the injection nozzle. Multiple cavity molds are used for injection molding of (1) many parts from a single shot to increase productivity and/or (2) parts with cavities separated by pre-loaded inserts for in-mold assembly applications. The main design consideration for the runner system is to achieve balanced flow. A balanced flow results in minimum variations in pressure and temperature in all cavities at the end of filling phase [72]. An unbalanced flow leads to overpacking, high shear stress, and excessive warpage, resulting in inconsistent and/or low quality products. Therefore the literature dealing with runner system optimization had to be reviewed to understand the flow balancing problem, which is presented below.

Li and Shen [72] combined optimization theory with flow simulation to automatically balance flows in a multi-cavity molds. They assumed the flow balanced if all cavities fill at the same time and under the same conditions. For that purpose the variation of pressure and temperature between the gates was minimized. Galerkin FEM was used to simulate the flow in a one-dimensional channel.

Lee and Kim [69] incorporated the compressibility of the polymers in the runner optimization problem. The effects of packing phase were accounted for by minimizing the differences in pressure between cavities over the entire molding cycle. Each runner system design was evaluated by the packing simulation software C-PACK[®], developed by AC Technology. This software models the injection-molding process based on the generalized Hele-Shaw flow model of a compressible and non-Newtonian viscous polymer melt. The proposed methodology was tested on two

multi-cavity molding systems, one with four identical cavities, and the other being a family mold with different cavity volumes and geometries.

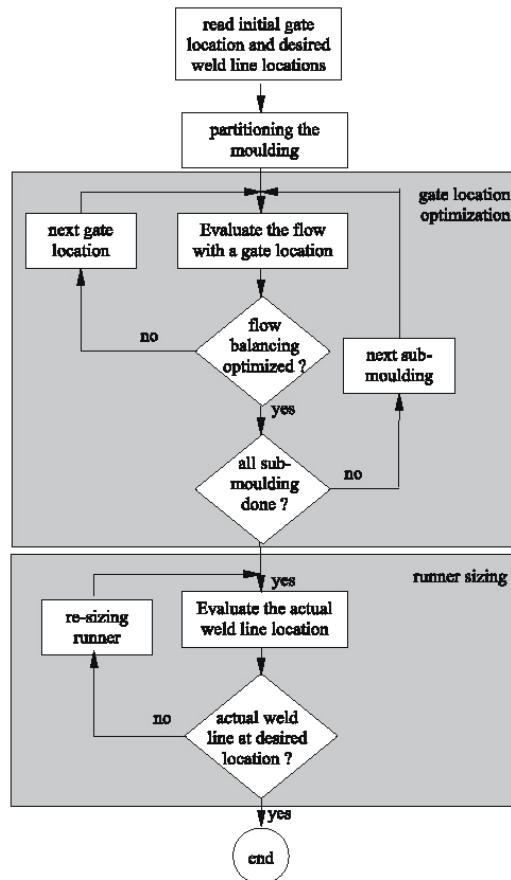


Figure 2.28 Two-stage flow balancing optimization methodology for a multi-gated cavity [120]

Zhai et al. [120] proposed two-stage flow balancing optimization methodology for a multi-gated cavity. The optimization stages consisted of (1) gate location determination and (2) runner sizing. This allowed for addressing the issue of different nature in the design parameters. The flowchart of the proposed optimization scheme is shown in Figure 2.28. The objective was to achieve balanced mold filling

pattern, represented by minimum injection pressure, with constraints set on specified weld-line locations. Initially the weld-line locations were estimated by the principles of Voronoi diagram. Next, gate locations resulting in minimum injection pressure within a sub-molding cavity were identified using a pressure-gradient search scheme [117]. Finally, runners were sized to compensate for differences in filling times of sub-cavities and consequently, keep the weld-lines at the desired or specified region of the part. The optimization was reported to be performed automatically, with solutions evaluated by MoldFlow[®] simulation. This research was sponsored by Moldflow Pty Ltd.

Yen et al. [115] proposed abductive neural network approach to optimize the runner system for minimum warpage of injection molded parts with free-form geometry. The design methodology integrated MoldFlow[®] simulations, Taguchi method, neural network approach and simulated annealing method. The diameter and length of the runner and gate were used as design variables. The abductive network model for predicting warpage was trained using MoldFlow[®] simulation results. During optimization, the FEM simulation model was replaced by abductive network model. The relationship between runner parameters and warpage was obtained based on the best model of abductive networks. This study was performed only on a single runner molding system. Lee et al. [71] extended this approach to multi-cavity molds.

Alam and Kamal [2] noted that using indirect quality measures during flow balancing in multi-cavity molds can penalize runner systems with inconsistent temperature and pressure among the cavities. To overcome this issue, they suggested maximum difference in shrinkage between the cavities as the quality-related

objective. The cost-related objectives included runner volume and cycle time. The balanced runner system consisted of four identical cavities and primary and secondary runners with diameters and lengths and design variables. Additionally, the influence of processing conditions was also included. The optimization was conducted using multi-objective genetic algorithm combined with MoldFlow[®] simulations. Authors reported that a balanced runner system characterized by minimum difference in shrinkage between the mold cavities can have lower product costs than systems characterized by similar fill times and cavity pressure profiles. The optimization of the secondary runners and processing conditions allowed for further cost reduction.

Alam and Kamal [3] later extended the above methodology to perform a robust optimization. This included an additional objective – the extent of the dimensional tolerance violation. A two-factor sensitivity matrix was used to simulate process variation. The robust balanced runner systems were found less sensitive to the effects of process variation.

Griffiths et al. [43] performed an experimental study to investigate the polymer melt flow behavior in the filling stage of micro cavities. They focused on the relationship between the filling of micro parts and the size of the runner system. Based on the flow length study results, they reported runner sizes with optimal surface-to-volume ratio and shear heating balance with regard to the filling performance for PP and ABS. They also noted that increasing runner dimensions had a negative effect and both materials failed to fill the micro cavities with the larger runner. Test part

geometry used, containing multiple spiral-like micro cavities and the supplying runner system, is presented in Figure 2.29.

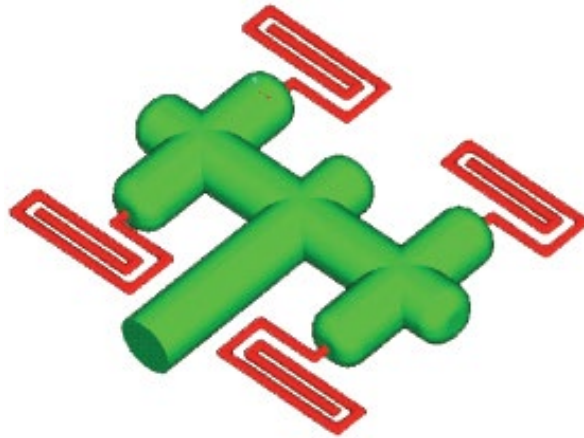


Figure 2.29 Experimental investigation of filling stage in micro-molding [43]

Recently, Zhai et al. [121] presented a non-dominated sorting genetic algorithm to perform the multi-objective optimization of a runner system in multi-cavity molds. Runner size and processing conditions were used as design variables. The proposed objectives were: (1) minimize the difference in end of fill time between the cavities; (2) minimize the average pressure difference between the cavities; (3) minimize the average temperature difference between the cavities; (4) minimize the volume of the runners and; (5) minimize the injection pressure. Objectives (1) and (2) were used to balance the flow between cavities. Objective (3) was utilized to achieve uniform cooling rate. Objective (4) aimed at minimization of material wastage. Objective (5) was used to minimize part warpage. The optimization algorithm evaluates a population of solutions using MoldFlow[®] simulation and promotes individuals within

the population according to Pareto-optimal criteria. Finally, weighted sum method is used to select appropriate designs from the Pareto set.

2.4 Summary

This chapter summarizes the body of work conducted in the following fields:

- 1) Multi-material molding
- 2) Embedding actuators
- 3) Characterization of filled polymers
- 4) Manufacturing of novel compliant mechanisms
- 5) Gate design optimization
- 6) Runner system design optimization.

Several new functional design possibilities have been enabled by the advances in in-mold assembly of multi-material structures. The reported investigations show the importance of incorporating special geometrical features at the material interface, as most of the already characterized polymer grades are not chemically compatible and do not bond to each other. However, the developed multi-material manufacturing methods allow only for (a) high-throughput production at the macro-scale, or (b) prototyping techniques at the micro-scale. Methods allowing for scaling the existing in-mold assembly methods to miniature multi-material interfaces capable of transferring loads do not exist.

Multiple prototyping methods for embedding various actuators in the structural elements have been developed for micro-electro-mechanical structures (MEMS). There are also few studies reporting embedding macroscale actuators inside polymer

structures. However, methods ensuring the survivability of miniature actuators during the automated embedding process do not exist.

Thermally conductive polymer composites have been studied by researchers for several years now. The focus of the research in this area had been on modeling and characterization of the fiber orientation and the resulting properties of the part. However, there is no published work which allows for the part and process optimization of thermally conductive structures with embedded miniature actuators with respect to the heat dissipation task and manufacturability constraints.

Several multi-material compliant mechanisms and their manufacturing methods have been developed. Available literature is oriented towards enhancement of mechanism efficiency and functionality. Some novel applications are also reported. However, the majority of published work utilizes prototyping manufacturing methods to achieve the miniature multi-material interfaces in compliant mechanisms. On the other hand, the existing mass production techniques consider only macro-scale assemblies. There are no published models allowing for high-throughput manufacturing of multi-material compliant mechanisms with miniature hinges.

To ensure the quality of polymer products, design optimization theory is being widely applied to injection molding design, with the gate location and runner size as the most common design parameters. The gate type, position, and size influence the properties of the molded part and the occurrence of molding defects. Therefore, the available gate design optimization approaches needed to be fully understood to utilize the functionality enhancement of the filled polymers and prevent from known defect modes.

Complex runner systems are prominent in multi-cavity injection molds. Many researchers have developed runner optimization approaches to balance the flows during the mold filling. However, none of the current methods consider the existence of miniature pre-molded components and their sensitivity to the melt fronts as the flow balancing criteria.

3 Embedding Actuators in Multi - Functional Structures

This chapter introduces design methodology for filled polymer structures with embedded heat-generating actuators using an in-mold assembly process, taking into account the processing conditions¹. The thermal behavior of thermally conductive filled polymers was characterized and modeled for the in-mold assembly process. Both thermal and processing models were developed for predicting thermal management and survivability of the embedded actuator respectively using commonly available software packages. Experiments were designed and performed using resistors as surrogate heat generating elements to calibrate the models. Both unfilled Polyamide 12 and a PA 12-based thermally conductive filled polymer were used in order to determine the difference in operating temperature for unfilled and filled structures. The thermal models were then used to investigate the sensitivity of the filler orientation resulting from the in-mold assembly process to the heat dissipation function. Experiments were then conducted to determine if the thermal properties of the thermally conductive filled polymers are sufficient to run embedded actuators at an acceptable temperature that ensures both structural and thermal functionality. Finally, the processing model was used to determine processing conditions ensuring motor survivability during in-mold assembly, and then experiments were conducted to demonstrate feasibility of creating multi-functional

¹ The material presented in Chapter 3 is based on publications [15-17]

structures from thermally conductive polymers by embedding actuators through an in-mold assembly process.

3.1 Motivation and Challenges

In-mold assembly can improve the miniaturization process by overcoming manufacturing limitations related to the challenges of integrating small functional components, such as actuators, into miniaturized polymeric structures by eliminating the manual assembly operation [7]. This however poses two important challenges. The first is thermal management, since embedded actuators generate heat during operation that must be dissipated. If the heat dissipation is not sufficient, the heat generated by actuators will increase the temperature of the interface between the embedded actuator and anchoring polymer structure causing either (a) the polymer at the interface to melt resulting in failure of the anchoring point for the actuator or (b) overheating of the actuator, both of which lead to subsequent dysfunction of the actuator. Therefore a “multi-functional” structure is required, which serves as a structural housing and also as the heat sink for the embedded actuator. The second important challenge is the ability for the actuators to survive the in-mold assembly process. Injection of a polymer melt into a mold cavity under high pressure has the potential for destroying delicate features of the actuators before they are fully embedded, which may prevent proper functioning of the actuator.

Miniature robots illustrate the problems associated with thermal management of heat generated by embedded actuators. For example, insufficient dissipation of heat generated by embedded actuators has been observed in miniature robotic devices, such as the Minimally Invasive Neurosurgical Intracranial Robot (MINIR) [85] or

flapping wing micro-air vehicle (MAV) [14]. The MINIR, developed in the RAMS Lab, was assembled from Delrin™ machined parts and SMA wires threaded through them. The assembly is shown in Figure 3.1. Due to the absence of active cooling or adequate passive heat dissipation, the embedded SMA wire actuators heated up the anchoring polymer structure during operation, causing the anchoring polymer structure to reach its softening temperature which resulted in loss of load transfer to the structure.

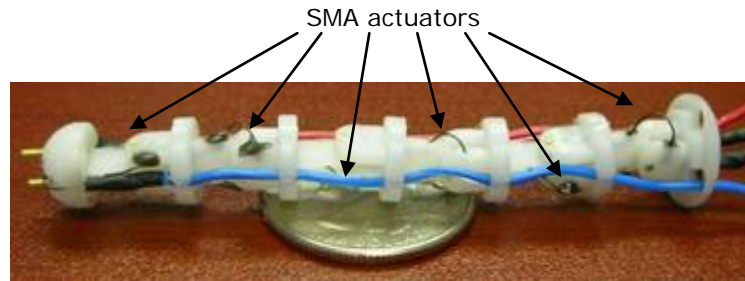


Figure 3.1 Minimally Invasive Neurosurgical Intracranial Robot (MINIR) [85]

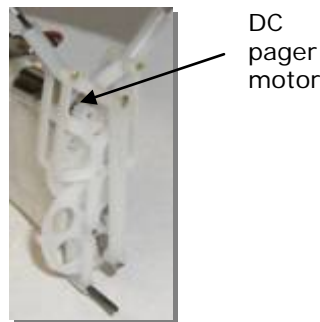


Figure 3.2 Flapping wing MAV mechanism [14]

In the MAV application, a DC motor used as an actuator was placed in an ABS mechanism frame, as shown in Figure 3.2. This actuator was cooled in-flight by the

air flowing over it, and hence functionality was maintained. However, overheating was observed while testing the MAV in a fixed stand over the long periods of time due to reduced air flow.

In many small scale applications the utilization of heat sinks commonly used at the macro-scale is not a viable option due to reduced weight and size budget. Using an active cooling method may also not be an acceptable option due to the additional power consumption, weight and complexity it introduces. Since thermally conductive filled polymers are promising for the heat dissipation function, their thermal behavior needs to be characterized when using them for the embedding of actuators. Many injection-moldable filled polymers currently available on the market have thermal conductivities which are an order of magnitude higher than bulk unfilled polymers (see Table 3.1). Using these materials allows for creating multi-functional structures that offer both anchoring points for actuators, as well as heat dissipation function.

3.2 Overview of the Design Process

This section describes the overall approach for designing structures with embedded actuators to be manufactured using in-mold assembly process. The goal of the approach is to concurrently optimize the choice of material, size of the structure and processing conditions. The objective function of this optimization is to minimize the weight for miniaturization of robotic devices, but it can be also chosen to be compatible with any other design requirements. In order to perform this optimization process, first a selection of moldable material needs to be made for ensuring the thermal performance. Next, the appropriate thermal model of the structure needs to be developed to assess if the heat from the actuator is dissipated sufficiently through

the filled polymer structure. The actuator to be embedded imposes certain constraints due to its strength to eliminate the possibility of damaging the actuator due to forces exerted by the manufacturing process. Finally, the geometry of the structure and in-mold assembly processing conditions needs to be parameterized. The overall general approach is outlined in Figure 3.3.

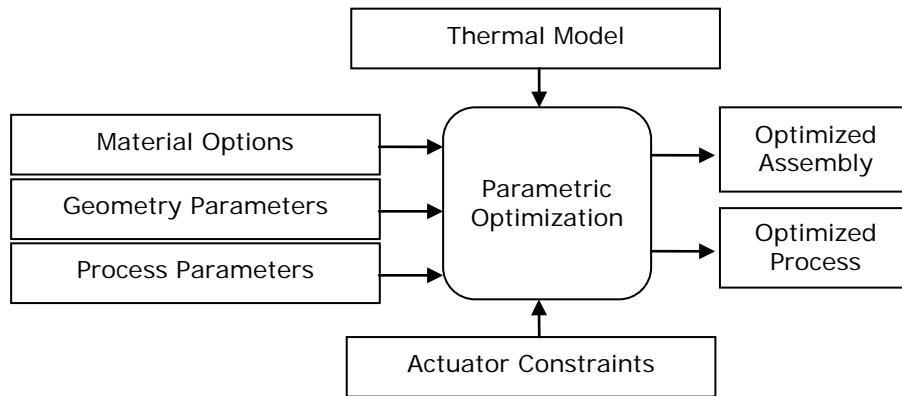


Figure 3.3 Parametric optimization of in-mold assembly using thermally conductive polymers

The development of thermal model of the structure with embedded actuator is usually not straight forward due to various parameters that need to be considered. Thermal conductivity of injection-moldable polymers is enhanced by adding conductive fillers (usually carbon microfibers) to the polymer. These fillers tend to get aligned with the polymer flow during injection into the mold, resulting in non-isotropic thermal and mechanical properties. These properties can be controlled through careful gate positioning in the mold to control fiber orientation during flow of the polymer melt. Accurate modeling of thermal properties resulting from the fiber

orientation is a very complicated task. However, for the heat dissipation capability assessment, the tedious orthotropic modeling may not be required once a material with sufficient thermal conductivity is chosen, since only sufficient heat transfer path is required from the design point of view. Nevertheless, the actual value of thermal conductivity has to be chosen with care. Also, establishing the natural free convection coefficient for the thermal model is not obvious, as it depends on both material characteristics and the geometry. Section 3.3 presents a systematic approach of determining these thermal modeling variables with sufficient accuracy for the heat dissipation task.

After developing the appropriate thermal model, the structure geometry and process parameters need to be parameterized for the optimization procedure. Depending on the functional requirements of the designed part the design variables and parameters have to be chosen appropriately. These include the parameterized geometry of the structure as well as the processing conditions. The mold used for in-mold assembly, in addition to all regular mold designing rules, needs to be designed in a way to allow for fixating actuators in order for them to be embedded correctly. This also requires securing heat sensitive features of the actuators from the hot polymer melt. The actuator to be embedded also poses certain constraints on the process parameters. The injection temperature and pressure are the most important parameters to be controlled, ensuring both proper filling of the mold and survivability of the embedded actuator. The temperature of the polymer melt has to be chosen correctly, so that the viscosity of the melt is sufficient to fill the mold cavity. At the same time, it cannot thermally shock the embedded component. The injection pressure has to be also

chosen correctly to allow for filling of the entire mold cavity and ensure that the embedded component will not experience plastic deformation over the acceptable limit. Therefore the actuator constraints on the process parameters need to be incorporated to the parametric optimization to ensure functionality of the final product, which is discussed in Section 3.4.

3.3 *Development of Thermal Model*

Since thermal modeling of embedded electronic components is a research area on its own [4, 9, 10, 31, 33, 34, 41], a modeling approach based on FEA was developed on an experimental foundation for verification and calibration. Also, because of the complexity of modeling a real actuator, the experimental foundation consisted of using a resistor as a surrogate with similar heat generation and geometric characteristics. After establishing the modeling approach, it was possible to study the sensitivity of the analysis with respect to different characteristics of the thermal conductivity for the filled polymer. Finally, the modeling approach was applied to a more complex motor assembly model and experimentally verified, which is discussed in detail in Section 3.4, to test the versatility of the modeling approach.

3.3.1 Acquiring Experimental Data for Model Calibration

A heat dissipation experiment was designed and performed to verify and calibrate the thermal FEA modeling approach for a structure with an embedded electronic element as a heat source. For sample preparation, Grilamid L16 Natural from EMS-Chemie was used as the bulk polyamide material and thermally conductive NJ-6000 TC polyamide compound from PolyOne as the filled polymer. Hence, it was possible

to quantify and justify the difference made by using thermally conductive polymers to dissipate heat from embedded actuators. The main physical properties of the materials are listed in Table 3.1.

Table 3.1 Properties of materials used in the experiment

Measure	Units	Grilamid L16	NJ-6000 TC	Test Method
Density	$kg.m^{-1}$	1010	1610	<i>ASTM D792</i>
Thermal Conductivity	$W.m^{-1}K^{-1}$	0.22	11	<i>ASTM C177</i>
Tensile Strength	<i>MPa</i>	42	110	<i>ASTM D638</i>
Elongation at Break	%	275	1.9	<i>ASTM D638</i>
Flexural Modulus	<i>GPa</i>	1.3	22.2	<i>ASTM D790</i>
Flexural Strength	<i>MPa</i>	59	109	<i>ASTM D790</i>
Volume Resistivity	<i>Ohm cm</i>	10^{14}	10^2 to 10^3	<i>ASTM D257</i>
Melt Temperature Range	$^{\circ}C$	190 to 270	260 to 277	

A 1 Watt, 1 k-Ohm metal-oxide resistor from Radio Shack was used as the electronic component producing heat during operation. The resistor was placed in the center of the cylindrical cavity of the mold. Precision-milled cavities on the parting surface of both mold halves ensured adequate clamping, and hence accurate positioning of the resistor. A thermocouple was also placed in the mold cavity to allow for experimental verification of the modeling approach by direct temperature measurement of the embedded resistor. The thermocouple was supplied through a hole in the back of the mold, opposite to the sprue/gate. The mold assembly is shown in Figure 3.4. Distance disks were used to overcome mold filling difficulties. Babyplast[®] injection molding machine was used to assemble the samples in-mold

during injection. The resistivity of the resistor was measured before and after embedding with a Fluke 87 True RMS Multimeter and determined to be within 8% from the nominal value, thereby verifying that no damage occurred during the in-mold assembly process. The specimens after demolding are shown in Figure 3.5 and Figure 3.6.

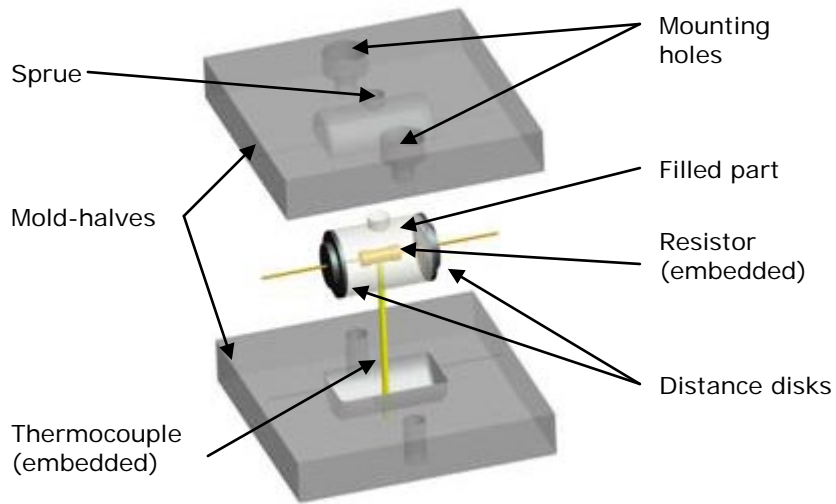


Figure 3.4 Embedded resistor: in-mold assembly

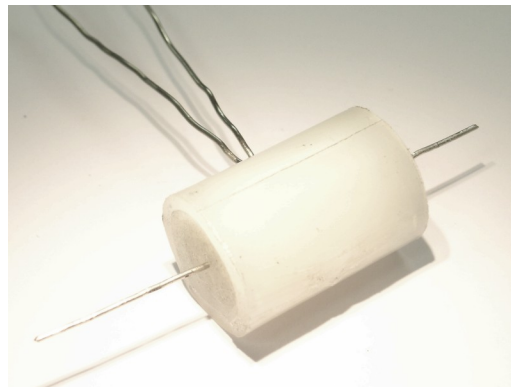


Figure 3.5 Resistor embedded in Grilamid L16 (PA 12)

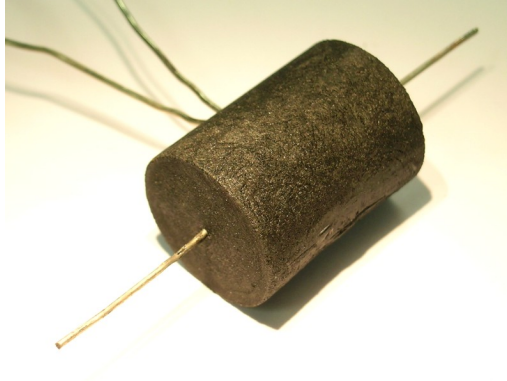


Figure 3.6 Resistor embedded in NJ-6000 TC (PA 12-F)

In order to control the amount of heat generated, the embedded resistors were connected to a HP Harrison 6205B Power Supply at 31.62 V. The amount of heat generation was verified by direct measurement of the current in the resistor circuit. The temperatures were recorded by Omega® HH506R Thermometer, which transferred the data to a PC through a RS-232 port. Using Omega® IV Recording Software, it was possible to automatically measure two temperatures for extended periods of time. This, along with shielding of the experimental setup, ensured the steady-state natural convection conditions. First, the ambient temperature was recorded along with temperatures in different points on the surface of the cylinder. In the second setup, the ambient temperature was measured along with the embedded thermocouple reading. All thermocouples used in the experiment were Omega® 5TC-GG-K-20-36. Table 3.2 contains the dimensions of prepared samples. A schematic of sampling points is shown in Figure 3.7. However, sectioning of in-mold assembled samples showed that the embedded thermocouple may not necessarily be in contact with the resistor, which is further discussed in Section 3.3.3.

Table 3.2 Embedded resistor sample dimensions

Parameter	Symbol	Unit	Grilamid L16	NJ-6000 TC
Resistor radius	r_1	m	1.91E-03	1.91E-03
Cylinder radius	r_2	m	9.27E-03	9.27E-03
Cylinder length	L	m	3.18E-02	2.54E-02

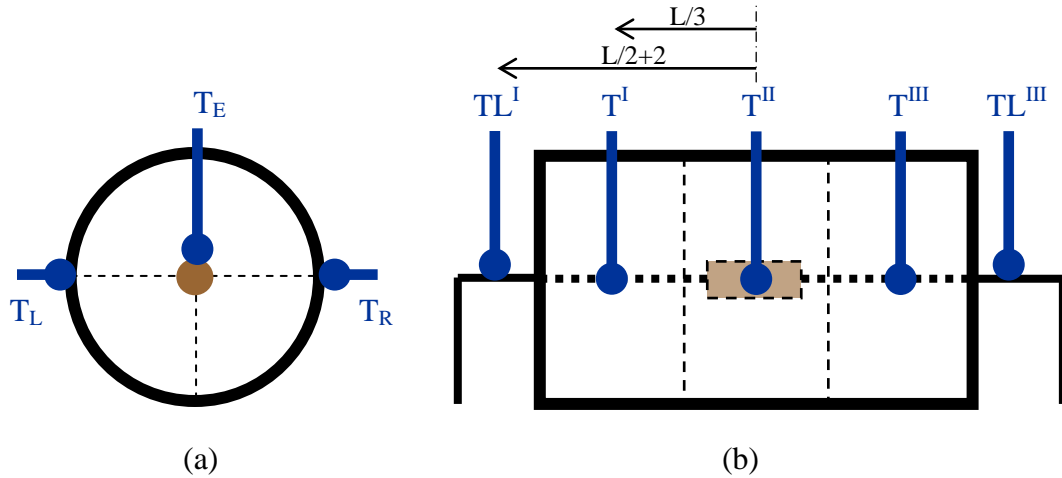


Figure 3.7 Schematic of temperature sampling points: (a) cross-section (b) side view

3.3.2 Thermal Model Description

The thermal FEA model of the samples described in Section 3.3.1 was developed using SolidWorks™ 2007 software. The model consists of an assembly of resistor and polymer casing with heat power and convection boundary conditions applied. The resistor is an assembly of two leads and a ceramic casing, with the 1W heat power applied to the inside cavity surfaces in a ratio corresponding to surface area. The free convection is applied to all outside surfaces of the sample assembly. The FEA model is shown in Figure 3.8, and the applied boundary conditions are

illustrated in Figure 3.9. The assembly was meshed with an element size of 1.046 mm and a tolerance 0.052 mm, which resulted in 83,823 total nodes and 59,002 tetrahedral elements. The mesh generated is shown in Figure 3.10.

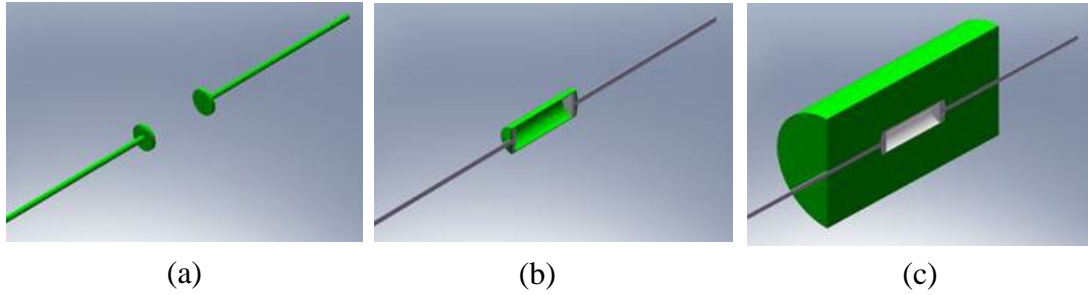


Figure 3.8 FEA model assembly: (a) leads (b) ceramic casing (c) polymer casing

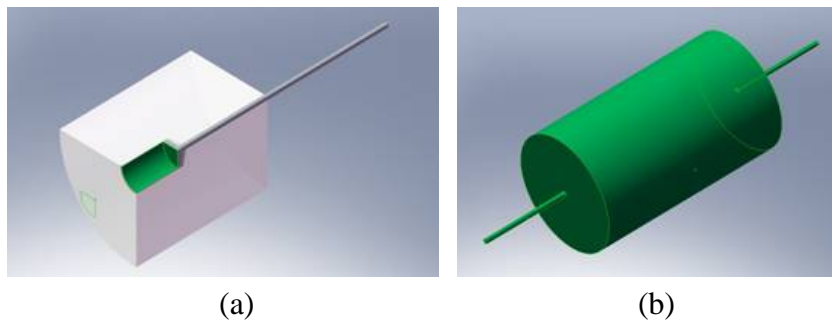


Figure 3.9 Surfaces for applying FEA boundary conditions (highlighted): (a) heat power, (b) convection to air

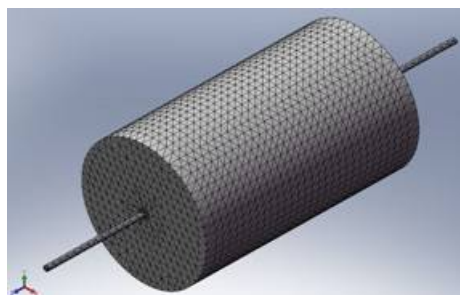


Figure 3.10 FEA model mesh

3.3.3 Model Calibration

The thermal conductivity of the filled polymer depends on fiber orientation of the filler, which is not necessarily uniform across the sample. Therefore, experimental results from a bulk Polyamide sample without filler were first used to validate and calibrate the model. Since the thermal conductivity of the unfilled polymer is isotropic and does not change substantially after injection molding, it ensures uniform heat dissipation and accurate material properties for input into the simulation.

In order to assign adequate material properties to model the embedded surrogate, the resistor was disassembled to determine the materials that were used in its fabrication, as well as their geometries. The casing material was a carbon ceramic measured to be 0.15 mm, while the electrical leads were determined to be copper.

Free convection was applied to all outside surfaces of the sample assembly. However, the resistor leads have two orders of magnitude higher thermal conductivity compared to the other components, and the heat from the embedded resistor dissipates through them more quickly than through the polymer casing. Due to the much smaller area of the leads and their higher temperature, natural convection conditions with different coefficients were applied to the leads and the casing. The values of h were calibrated with experimental data to be 60 and 30 W/m²-K respectively. The thermal properties of the materials used in the FEA model are listed in Table 3.3.

Table 3.3 Thermal properties used in FEA

Material	Thermal conductivity	Mass density
	[W/m-K]	[kg/m ³]
Resistor copper leads	230	8400
Resistor carbon ceramic casing	15	2300
Grilamid L16	0.22	1010
NJ-6000TC	11	1610

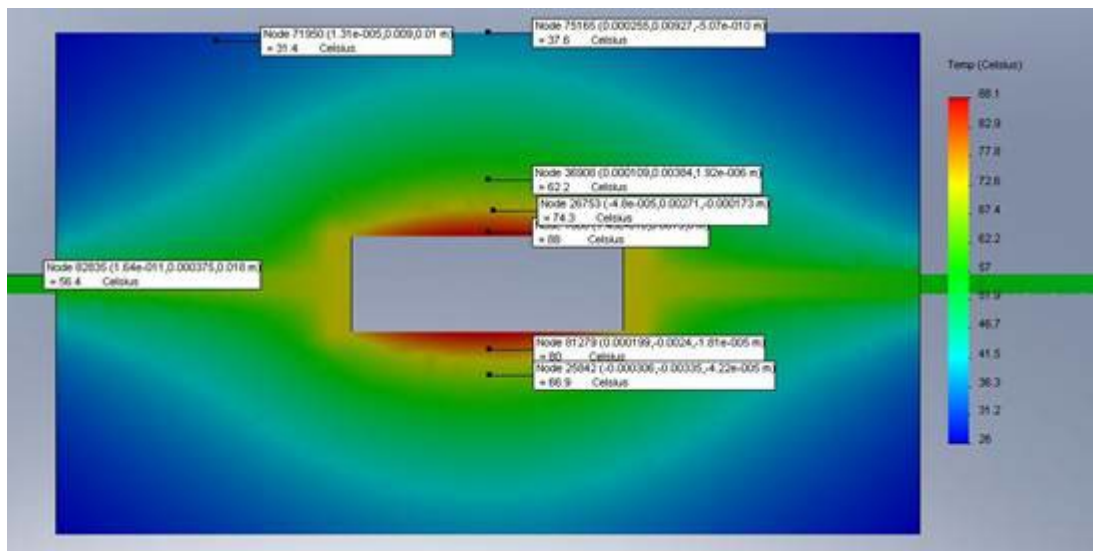


Figure 3.11 Temperature field FEA result for unfilled Nylon 12 sample

Sectioning of the bulk polymer sample showed that the thermocouple was 1.5 mm away from the resistor, due to forces imposed on it while melt injection to the mold. Therefore, the temperature field resulting from the FEA simulation was compared with corresponding experimental data at the thermocouple location. The thermocouple reading was 63.3°C, the corresponding FEA result was 66.9°C and the embedded resistor surface temperature resulting from FEA was 88°C. The cross

section temperature field FEA result is shown in Figure 3.11. Since the maximum error in the FEA prediction was less than 10%, it was determined that the modeling approach was capturing the physics of the thermal conduction process with sufficient accuracy to warrant proceeding to modeling and experimental validation of the thermally conductive filled polymer specimen.

3.3.4 Modeling of Thermally Conductive Polymer Structures

Since thermal conductivity of the filled polymer depends on fiber orientation of the filler and will not necessarily be uniform across the sample, the modeling approach had to be modified to account for the directionality of the heat conduction that would result from the fiber orientations obtained after the in-mold assembly process. In addition, due to more demanding processing conditions for the filled polymer, voids can potentially develop inside the specimen that must be accounted for in the modeling. Voids (or air traps) are formed when converging flow fronts surround and trap a bubble of air. This is usually caused by racetrack effect, hesitation, unbalanced flow paths or improper venting [101]. Since this work so far was focused more on the practical application of the filled polymers for their improved thermal conductivity, rather than optimizing the runner system to achieve balanced flow, we tried to model the actual sample as realistically as possible. Therefore, sectioning of the experimental sample was performed by placing it in a milling machine and removing 1 mm thick layer of the material at a time, followed by photographic examination of the cross-section. The photographs revealed the actual void distribution inside the sample, as seen in Figure 3.12. This data was then used to introduce simplified voids in the model of the polymer in which the electronic

component is embedded. The resulting model with voids is shown on Figure 3.13 and substituted for the previous model to perform the thermal analysis.

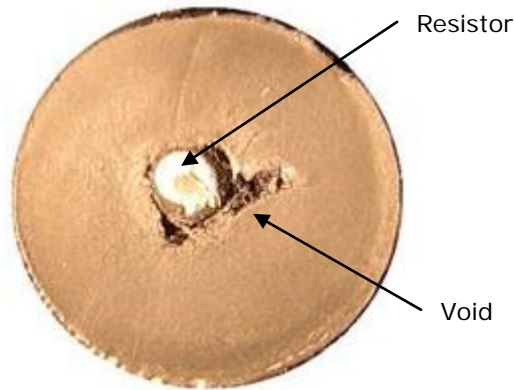


Figure 3.12 Cross-sectioning of the embedded resistor specimen

After modeling the voids, the fiber orientation had to be accounted for inside the filled polymer specimen. For this purpose, a CFD flow simulation was performed inside the mold using MoldFlow[®] Plastics Insight 6.1 to obtain the 3D fiber orientation tensor (degree of orientation). Numerical prediction of the 3D fiber orientation during mold filling in MoldFlow[®] is based on an equation of motion for rigid particles in a fluid suspension. The analysis consists of two identifiable terms: (1) the hydrodynamic term [58] and (2) the interaction term [36]. The process simulation settings used are listed in Table 3.4. The resulting “tensor principal vector as segments” was plotted and scaled to display only the vectors which were aligned more than 75%. These plots were obtained for 5 mm long portions of the cylinder to clarify variation of the results across the axis of the specimen. Sample plots are shown in Figure 3.14.

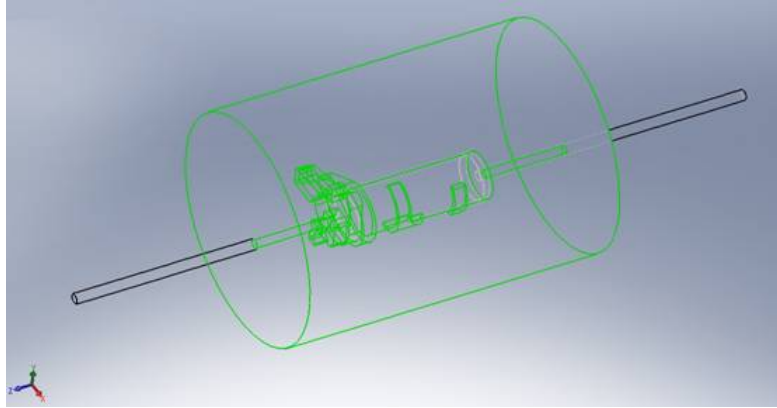


Figure 3.13 FEM model with voids

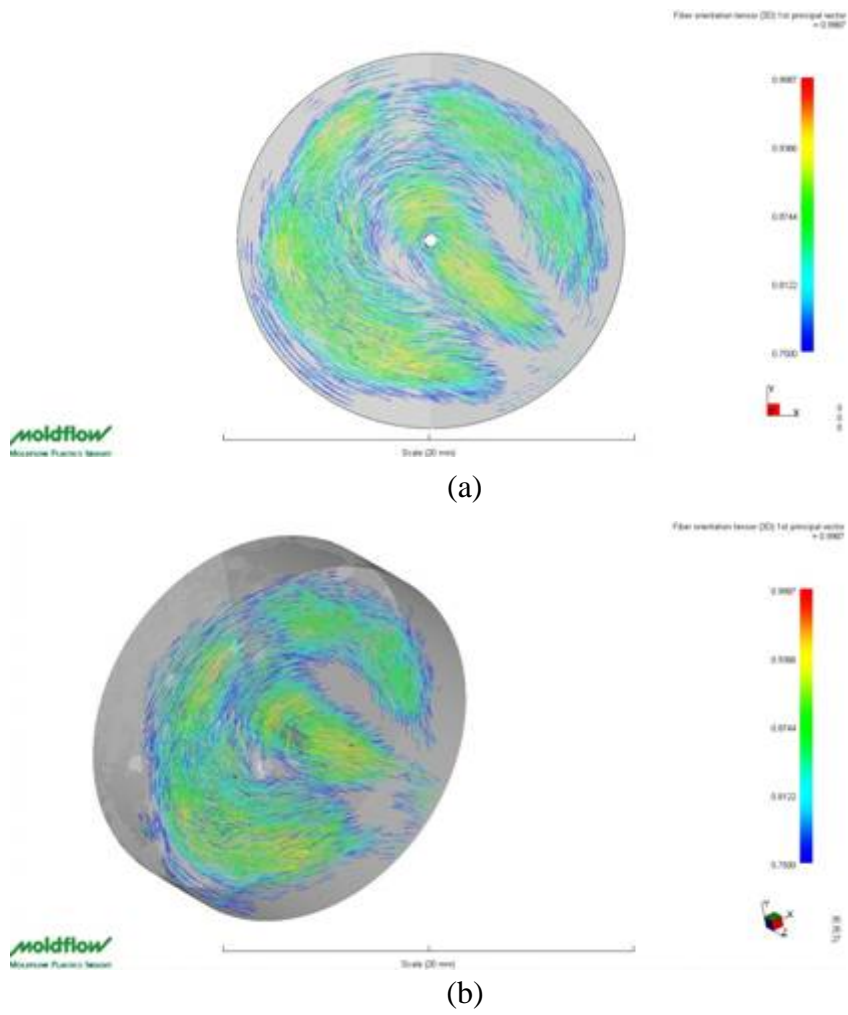


Figure 3.14 Mold flow simulation sample result: (a) side view and (b) isometric view of a segment

After careful analysis of the above results, it was determined that the cylinder model for the polymer composite could be partitioned into two sub-parts along the length to reflect the directional thermal conductivities based on fiber orientation. These “discretization” approaches have been previously used in modeling processing and performance effects on complex material distributions in composite materials such as Functionally Graded Materials, where the compositions can be continuously varying [20, 90, 97].

Table 3.4 Process settings used in flow simulation

Parameter	Value
Injection material	POLYONE NJ-6000 TC Black
Fibers/fillers	51.8% Cytec DKD Filled
Injection temperature	270 C
Mold temperature	35 C
Injection velocity	6.2 cc/s
Mold-open time	5 s

Due to the directionality of the fibers, the “high” value of k is used along the hoop direction in the bigger partition and along the radial direction in the smaller partition. According to the manufacturer, the thermal conductivity along the perfectly aligned fibers is 11 W/m-K. Given the level of misalignment that was permitted in defining the partitions, the “high” value of k was taken to be 10 W/m-K along the fiber orientation direction. Using a standard rule-of-mixtures formula for transverse and longitudinal conduction relative to the direction of fiber reinforcement for a

transverse isotropic material, a value of 1 W/m-K was used in the two other principal directions [86]. The final simplified model is shown in Figure 3.15.

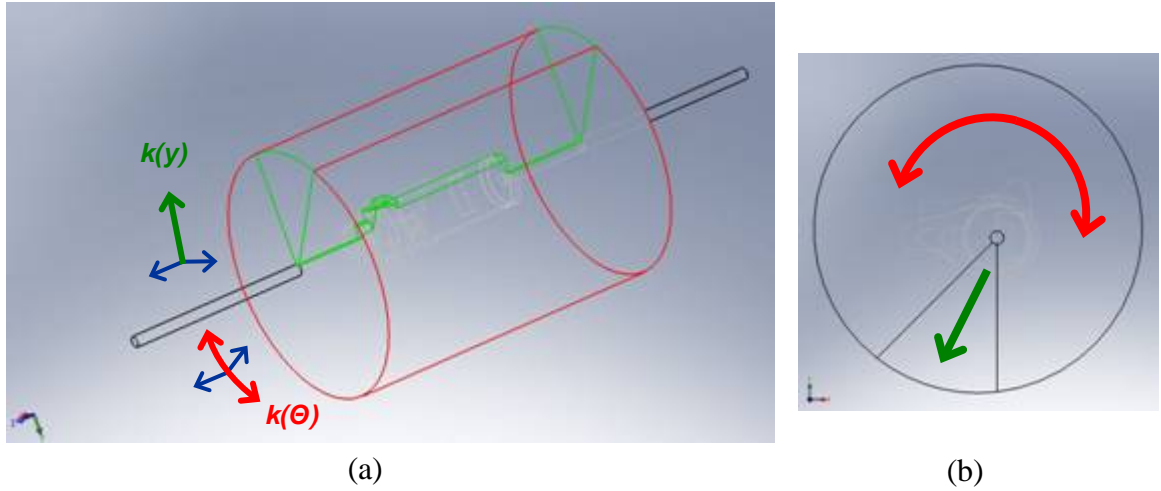


Figure 3.15 FEM model with orthotropic thermal conductivities assigned:

(a) isometric view and (b) side view

Using this model and the same boundary conditions as in the bulk polymer sample, the thermal FEA simulation was performed, and the resulting thermal plot shown in Figure 3.16 was compared with experimental data for the filled polymer sample shown in Figure 3.6. The maximum predicted temperature error was found to be less than 11%, therefore verifying that the model approach was sufficiently accurate for thermally conductive filled polymers. The thermocouple reading was 50.5°C, the corresponding FEA result was 45.3°C and the embedded resistor surface temperature resulting from FEA was 51.1°C. These values when compared with the results from the bulk polymer case indicate a significant 40% reduction in the operating temperature of the embedded resistor. Therefore, these results justify the use of

thermally conductive filled polymers as the material of choice for embedding actuators. However, one has to keep in mind that a high filler volume fraction responsible for the increased thermal conductivity of the polymer also affects the composite mechanical properties, making the material more brittle. Therefore additional analysis may be needed for structurally critical designs.

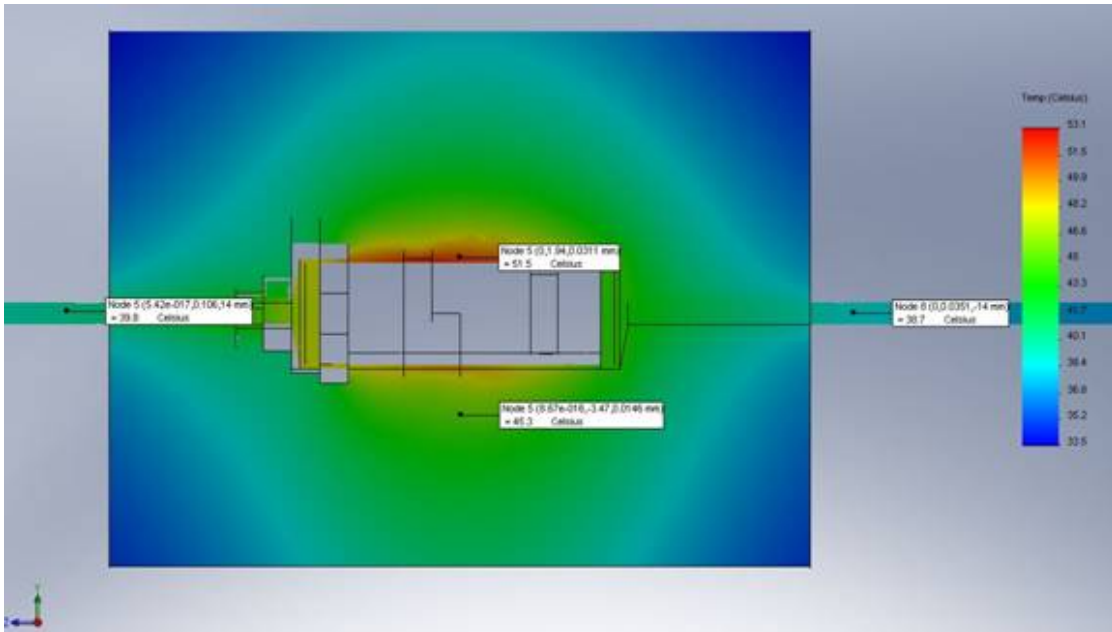


Figure 3.16 Temperature field FEA result for NJ-6000 TC filled polymer composite

3.3.5 Analysis of Thermal Conductivity for Filled Polymers

After developing a suitably accurate thermal FEA model accounting for the effects of fiber orientation in the filled polymers resulting from the in-mold assembly process, it was possible to predict trends for the thermally conductive, filled polymers. First, the sensitivity of the actual operational temperature and heat dissipation of the embedded component was assessed relative to the directional

thermal conductivity resulting from the in-mold assembly process. The model described in Section 3.3.2 was used with some modifications to the polymer cylindrical casing. Instead of a single part with uniform isotropic properties, it was modeled as an assembly of three cylinders, which combined together to form the original part. Then, different directional values of thermal conductivities were assigned to each of the three cylinders. The modified FEA model is shown in Figure 3.17. To address the processing conditions, the “high” thermal conductivity direction of the middle part was modeled to be aligned with the injection direction, marked on Figure 3.17 with a dotted arrow. For the outer cylinders, the directional thermal conductivity was aligned with the axis of the leads. Then, the values of these thermal conductivities were varied to assess their influence on actual heat dissipation.

Table 3.5 Embedded resistor temperature [C] as a function of directional thermal conductivity

$k^I \backslash k^{II}$	<i>1-10-1</i>	<i>2-8-2</i>	<i>3-6-3</i>	<i>4-4-4</i>
<i>1-1-10</i>	43.5	41.5	40.9	40.9
<i>2-2-8</i>	43.1	41.2	40.6	40.7
<i>3-3-6</i>	43.0	41.2	40.6	40.7
<i>4-4-4</i>	43.2	41.4	40.8	40.8

The variation of the values was done in the following manner: using integer increments, the “high” k (i.e., along the orientation of the fibers) was varied from 4 to 10 W/m-K, while keeping the sum of thermal conductivities in all three principal directions at a constant value of 12. Note, that in the case of $k=4$, the model had a uniform distribution of k in all directions and represented an isotropic case. With this

model, it was possible to predict the maximum surface temperature of the embedded resistor with respect to the fiber orientation. The results of this study are presented in Table 3.5. The temperature field for the most anisotropic case (principal values 1-1-10/1-10-1) is shown in Figure 3.18.

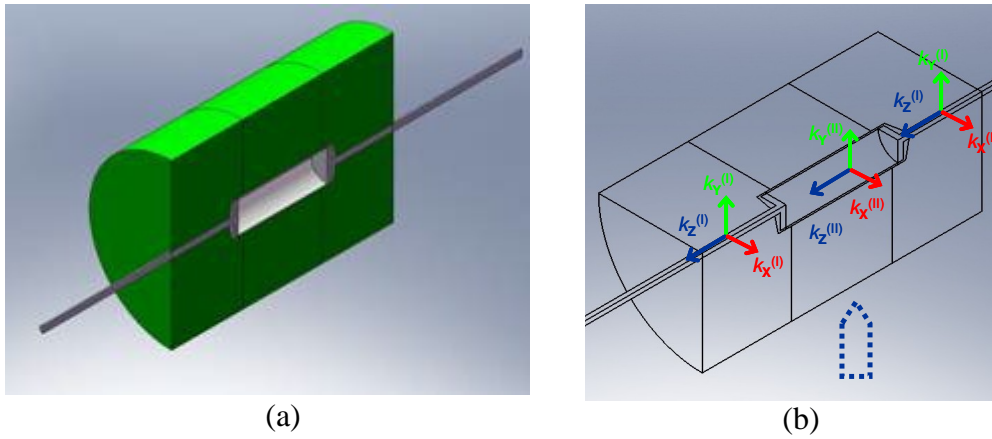


Figure 3.17 Modified FEA model: (a) assembly, (b) directional thermal conductivities

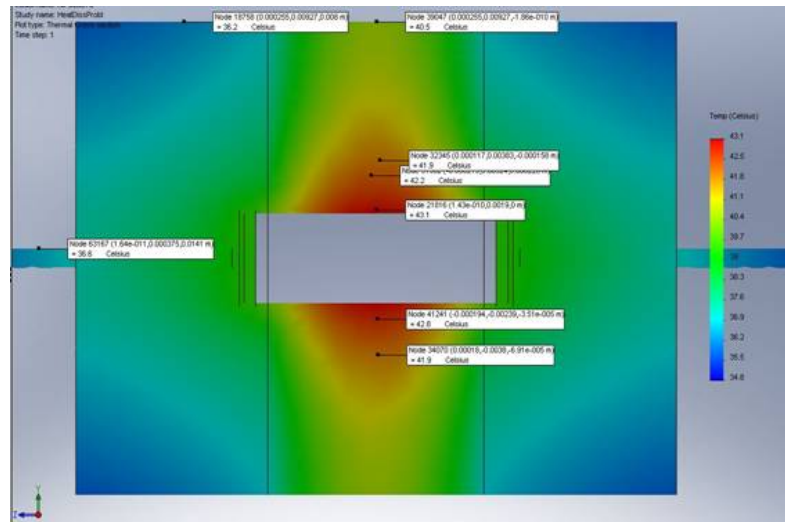


Figure 3.18 Temperature field FEA result for the most anisotropic case (1-1-10/1-10-1)

It can easily be concluded from Table 3.5 that the variation of the directional thermal conductivities across the sample does not influence the operating temperature of the embedded heat-generating electronic component in a significant manner, as long as the value of k is high enough. Therefore it was concluded that for this structure with an embedded electronic component, tedious and sophisticated modeling of directional thermal conductivities resulting from manufacturing process can be significantly simplified and reduced, or even omitted.

Next, it was desirable to understand how much can be gained by using polymers with increased thermal conductivity. Therefore based on the previous results, the value of k was varied isotropically and plotted against the predicted surface temperature of the embedded resistor. The resulting plot is shown in Figure 3.19. From this numerical study, it was concluded that increasing the value of thermal conductivity of the polymer from 0.22 to 2 W/m-K results in a 50% temperature drop of the embedded resistor in operation. However, further increase of k does not substantially decrease the surface temperature of the resistor therefore this value represents an effective “cut-off” for the change in the surface temperature of the resistor with thermal conductivity. This cut-off point can be attributed to free convection in air being the “bottleneck” for heat dissipation. Nevertheless, using thermally conductive polymers shows significantly improved heat dissipation and promising use of these materials as multi-functional anchoring structures to facilitate miniaturization of devices.

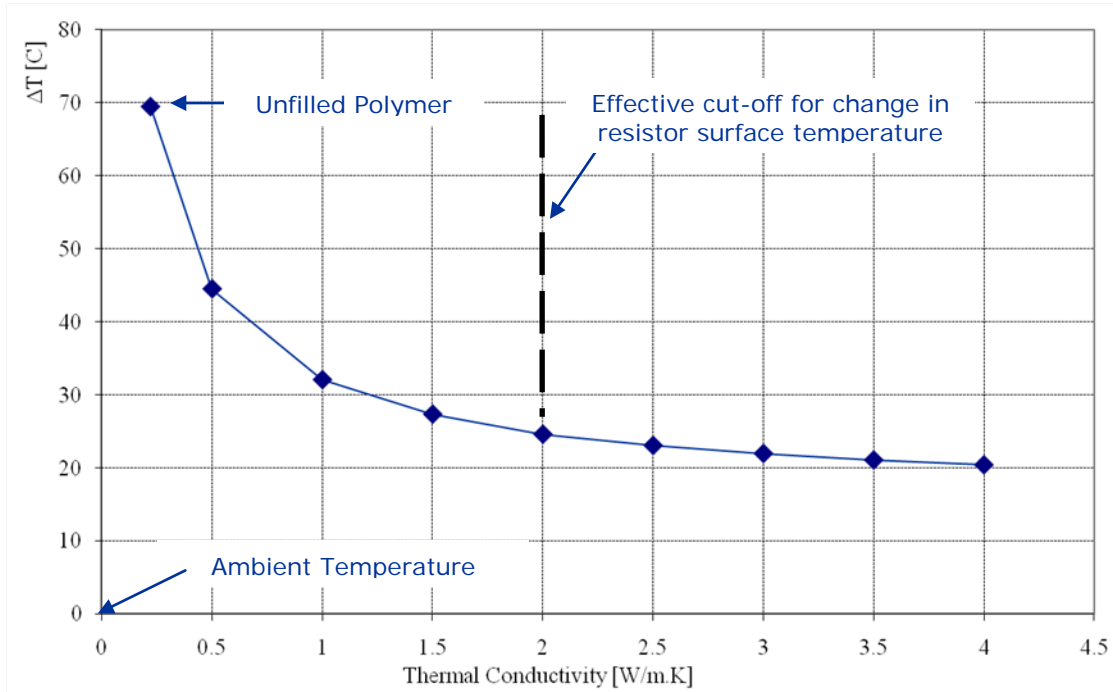


Figure 3.19 Isotropic thermal conductivity influence on the temperature of embedded component

3.4 Incorporating In-mold Assembly Process Constraints during Optimization

The mold used for in-mold assembly, in addition to all regular mold designing rules, needs to be designed in a way to allow for fixating actuators in order for them to be embedded correctly. This also requires securing heat sensitive features of the actuators from the hot polymer melt. During injection molding, the high-pressure polymer melt being injected into the mold cavity has the potential to destroy delicate features of the actuator before it is fully embedded, which may prevent the actuator from functioning properly. The injection temperature and pressure are the most

important parameters to be controlled, ensuring both proper filling of the mold and survivability of the embedded actuator.

To demonstrate the feasibility of embedding actuators using the in-mold assembly process, a case of an actuator anchored in a polymer structure was studied. A simple motor holder was designed to reveal the difference in heat dissipation when the actuator is placed in a thermally conductive polymer versus a bulk polymer structure. The same polymers were used as in the experiment described in Section 3.3.1, while a Didel SS 7 mm blue pager motor producing a maximum of 1.5 W was used as the power input. The structure was designed for a 12-teeth pinion on the motor shaft to be engaged with a 60-teeth spur gear on the output shaft. The output shaft was placed in an in-mold assembled brass sleeve to minimize friction.

Initial experiments indicated that the steel motor housing was being permanently deformed while injecting the polymer into the mold cavity. This survivability issue had to be addressed by determination of correct size of the embedding structure and the packing pressure during injection. Reduction of the part thickness reduces the area of the compressive pressure being exerted on the actuator, however it was constrained in this case by the tooling available for manufacturing the molds. On the other hand, reduction of packing pressure may lead to incorrect filling of the mold. Therefore a numerical model of the motor casing and the pressure applied during polymer melt was developed using ANSYS 11.0 FEA software to quantify this interaction and determine the injection pressure needed for successful in-mold assembly of the actuator without preventing proper functioning of the actuator. The motor housing was modeled as a series of cylinders to reflect the actual part and

applied boundary conditions. The housing thickness was measured to be 0.4 mm and modeled accordingly. Measurements of the motor coil inside the housing determined the clearance between these elements to be 0.25 mm in the radial direction. The physical motor assembly examined and corresponding dimensions are shown in Figure 3.20. It was assumed that the actual deformation should not exceed 1/3rd of the clearance value to practically ensure the functionality of in-mold assembled actuator.

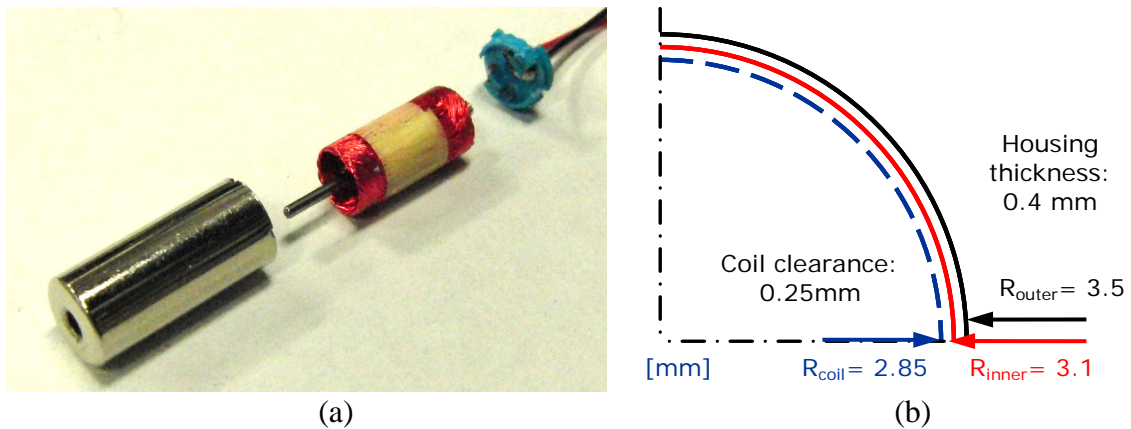


Figure 3.20 Embedded motor: (a) physical assembly exploded and (b) cross-section dimensions

The ANSYS model was meshed with SOLID92 elements, and material properties for steel were used for the metal housing (Young's Modulus of 200 MPa and Poisson's ratio of 0.27). The boundary conditions applied were zero-displacement of the cylindrical part of the housing tightly constrained by the mold cavity and a pressure applied to the neighboring cylindrical segment, which was exposed to the

injection pressure during the in-mold assembly process. Figure 3.21 shows the part dimensions, a schematic of the applied boundary conditions, and a mesh of the model.

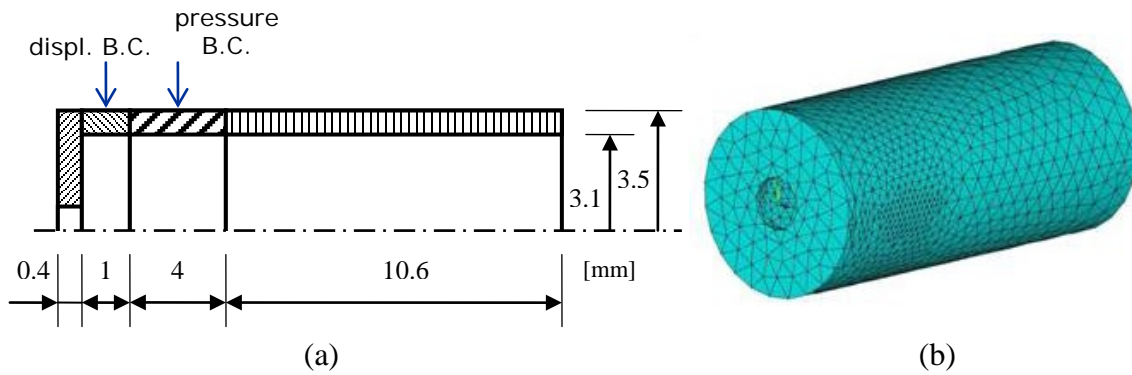


Figure 3.21 ANSYS model: (a) key dimensions and boundary conditions, (b) mesh

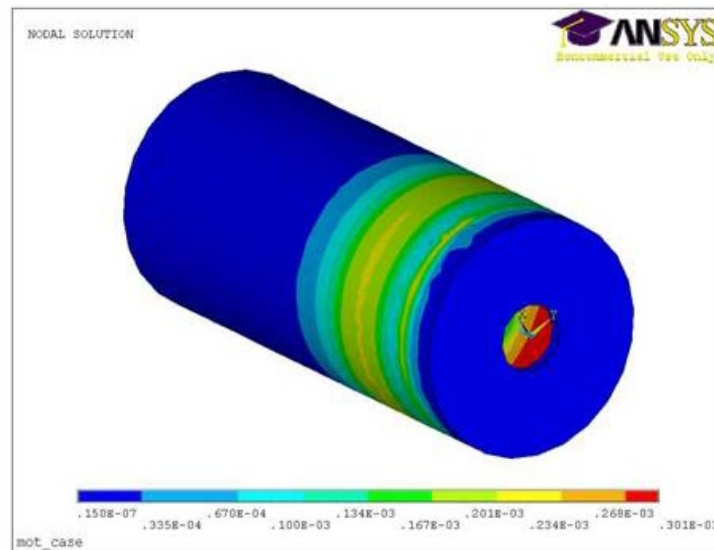


Figure 3.22 ANSYS results for the total von Mises strain plot on motor housing

As a result of the ANSYS FEA, the acceptable pressure applied to the motor housing during the in-mold assembly process was determined to be 5.59 MPa, which resulted in a permanent deformation of 0.087 mm that was within the acceptable

range. The von Mises total strain plot is shown in Figure 3.22. MoldFlow® simulations were performed to ensure this value results in correct mold filling.

After determining the appropriate injection pressure to maintain actuator functionality, motor holders were manufactured using the in-mold assembly process. The in-mold assembly mold setup is shown in Figure 3.23 and the successfully in-mold assembled parts are shown in Figure 3.24. The injection parameters used for the in-mold assembly process are listed in Table 3.6.

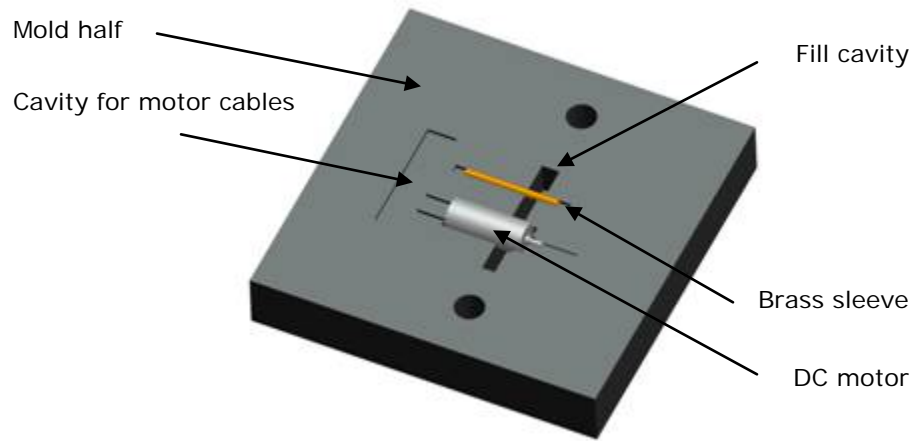


Figure 3.23 In-mold assembly setup for manufacturing the motor holder

Table 3.6 In-mold assembly process parameters

Parameter	Value
Packing pressure	5.59 MPa
Cycle time	2.7 s
Injection time	0.4 s
Injection temperature	195 C (Grilamid L16) 270 C (NJ-6000TC)
Mold temperature	35 C

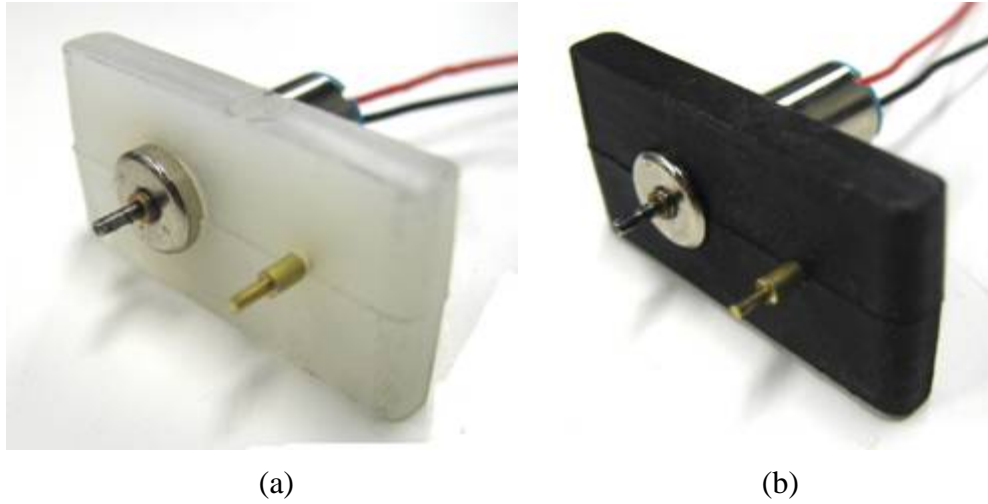


Figure 3.24 In-mold assembled motor holders: (a) PA 12, (b) PA 12-F

For the heat dissipation experiment, a load was applied to the motor shaft to generate maximum power. With careful control of the voltage supplied to the motor and the current drawn, it was possible to maintain a constant power of 1.5 W. An Omega® 5TC-GG-K-20-36 thermocouple was used to measure the surface temperature of the embedded DC motors. The results of the experiment are listed in Table 3.7. The thermal studies were modeled using the approach described in Section 3.3 except for the following:

1. a different geometry was used for the encasing polymer
2. the resistor was replaced with the pager motor assembly
3. there was no void structure around the motor assembly.

The resulting temperature distribution plots are shown in Figure 3.25.

Table 3.7 Results of the embedded motor experiment

Parameter	Unit	Unembedded	PA12	PA12-F
Voltage	V	3.00	3.00	3.00
Current	A	0.5	0.5	0.5
Temperature	C	120.2	96.0	65.5

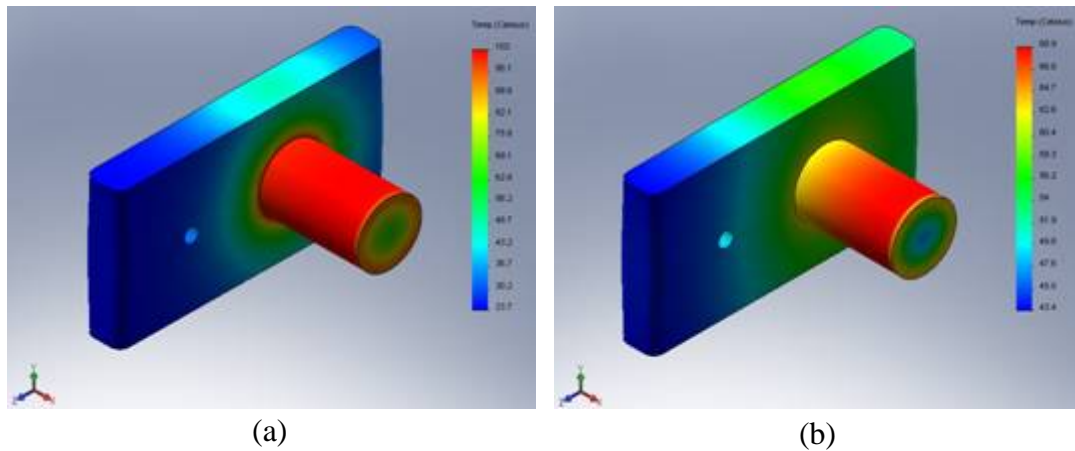


Figure 3.25 FEA thermal analysis results: (a) PA 12, (b) PA 12-F

For the unfilled polymer sample, the FEA prediction of the embedded motor temperature was 102°C, which was 6% more than the measured value. For the filled Nylon 12 sample, where thermal conductivity was modeled to be 4 W/m-K in all principal directions, the FEA result was 68.9°C, which was 5% more than the measured value. The accuracy of these results were consistent with the previous experimental and numerical comparisons. Thus, this case study clearly shows that embedding the DC pager motor in a thermally conductive filled polymer results in reduction of its working temperature by 46% when compared to the bulk polymer casing. This further proves the concept that thermally conductive polymers are more

effective in terms of heat dissipation, and hence are the material of choice for building multi-functional structures with embedded actuators. The modeling approach was also established for enabling feasible design of embedded actuators using the in-mold assembly process.

3.5 Summary

This chapter described a systematic approach for designing multi-functional, filled polymer structures with embedded actuators using in-mold assembly process to facilitate the miniaturization of devices. The novel aspects of this work include: (1) determination of effective thermal conductivity of filled polymer composites for heat dissipation task and (2) determination of design and processing conditions to ensure survivability of the embedded actuator using in-mold assembly process through concurrent optimization of choice of material, size of the structure and processing conditions.

The method described in this chapter is applicable to any multi-functional structure with embedded actuators that can be manufactured using filled polymers and in-mold assembly process. An integrated design methodology for these structures have been described, taking into account: (1) selection of a moldable material for ensuring thermal performance, (2) a mold design for successfully realizing in-mold assembly, (3) influence of gate placement on thermal performance, and (4) influence of processing conditions on survivability of the embedded actuator. The following new results were reported in this chapter. First, an integrated thermal modeling methodology for designing multi-functional structures using filled polymers under functionality and moldability constraints was presented. Second, this methodology

was used to assess effective thermal conductivity of filled polymers for the heat dissipation task. Next, the influence of the fiber orientation on the functionality of filled polymer structures for embedding actuators was determined. Finally, an approach for determining processing conditions resulting in successful in-mold assembly of embedded actuators was described.

The design framework was experimentally verified to be sufficiently accurate for predicting thermal behavior of filled polymer multi-functional structures. The use of these thermally conductive polymers resulted in significant improvement in dissipation of heat from actuators embedded in the structure when compared to unfilled polymers. The influence of gate placement was determined to be of minor significance on the heat-dissipation task. Once a critical level of thermal conductivity of the polymer is reached, there exist a heat-transfer path and natural free convection becomes the bottleneck for the dissipation of heat from embedded actuator. Therefore it was shown that tedious and computationally-expensive modeling of fiber orientation resulting from process design is not necessary from the thermal management point of view, as long as thermal conductivity of the polymer exceeds 2 W/m-K. Successful in-mold assembly of an example multi-functional structure consisting of an actuator embedded in a motor holder assembly was obtained through optimal design of the structure and processing conditions for the choice of filled polymer. Therefore, the feasibility of designing multi-functional structures from filled polymers was demonstrated for embedding actuators using in-mold assembly to facilitate the miniaturization of devices.

4 Design and Fabrication of Miniature Compliant Hinges for Multi-Material Compliant Mechanisms

In-mold assembly is a promising technology to realize the miniaturization of devices. Replacing rigid body revolute joints with compliant ones can result in reduced part count and improved performance, leading to lighter and more reliable assemblies. This investigation was performed on a platform of a MAV prototype. The main challenge in MAV applications is the vehicle weight reduction to enable realization of various missions by allowing for more payload capacity. Hence the experimental MAV platform is considered as a representative example to miniaturization of devices. The prototype MAV utilizes a drive frame converting rotary motion of the motor to the flapping motion of the wings. This drive frame utilized incompatible materials and the idea of local compliance to replace revolute joints. The MAV drive frame serving as the experimental platform was manufactured using in-mold assembly.

This chapter further advances the in-mold assembly process by describing the design and fabrication methods of miniature compliant hinges for multi-material compliant mechanisms¹. First, a design methodology for the miniature compliant joints is described. To allow for a robust interconnection between the incompatible materials used to perform different functions in the compliant mechanism, several interlocking strategies are presented and characterized according to the joint requirements. Next, a modeling approach is developed to evaluate the interlocking of

¹ The material presented in Chapter 4 is based on publications [14, 18]

compliant hinges. Towards this end, an experimental method is presented to validate the analysis results. Next, an in-mold assembly process to create compliant mechanisms with miniature hinges is presented. This includes the process overview and specific mold design considerations. Finally, a case study of a multi-material compliant micro air vehicle (MAV) drive mechanism is presented. This case study shows the great potential of the in-mold assembly process developed in this chapter towards miniaturization of devices being manufactured on a large scale. Methods described in this chapter are applicable to any lightweight, load-bearing compliant mechanism manufactured using multi-material injection molding.

4.1 Motivation and Challenges

Compliant mechanisms, defined as flexible structures that elastically deform to produce a desired force or displacement, have recently been integrated into many mechanical systems to provide improved functionality, simpler manufacturing, and greater reliability. Some of the main application areas of compliant mechanisms include bi-stable mechanisms, orthoplanar springs, centrifugal clutches, overrunning pawl clutches, near-constant-force compression mechanisms, near-constant-force electrical connectors, bicycle brakes, bicycle derailleur, compliant grippers, and micro-electro-mechanical systems (MEMS) [18, 21, 22, 27, 28, 42, 51, 76, 87, 107, 122]. Compliant mechanisms generally consist of rigid sections (links) with compliant sections (joints) added in strategic locations in order to control the force or displacement. Compliant mechanisms possess several advantages over traditional designs with rigid-body articulated joints. These include: (a) the reduction of wear between joint members, (b) the reduction in backlash, and (c) potential energy storage

in deflected members [51]. Using compliant mechanisms also reduces the noise levels generated by mating components in operation. Additionally, localized (lumped) compliance in the mechanism can be used to eliminate joints from the assembly, resulting in reduced part count and improved system precision. Part reduction results in reduced assembly labor, purchasing, inspecting, and warehousing costs [93]. Furthermore, when polymer materials are used to create a compliant mechanism, there is a significant weight reduction of the mechanism. Finally, using polymers makes the component more amenable to high-throughput polymer processing techniques, such as injection molding, to provide additional cost savings. All of these advantages have made compliant mechanisms a promising replacement of the conventional mechanisms with rigid articulated joints, and have also enabled the potential towards miniaturization of common devices.

Utilization of different polymer grades to create compliant mechanisms using selective (lumped) compliance to realize miniature joints by in-mold assembly method is not however a trivial task. Polymer grades designed to realize compliant joints in a rigid structure may require a choice of materials that are not chemically compatible and do not bond during the in-mold assembly process. Feasible mold designs for creating different types of compliant joints from incompatible materials at the macro-scale has been developed previously [42]. However, these interlocking strategies cannot be scaled to the miniature scale. Preliminary experiments with interlocking features developed in [42] and scaled to fit 1 mm-long compliant joints revealed excessive stress concentration on the interlocking features, which made the hinge-link assembly not capable of transferring any load useful load levels.

Therefore, new design and fabrication methods have to be developed to address issues specific to the miniaturized structures.

Several different MAV platforms were developed in Advanced Manufacturing Laboratory at the University of Maryland, College Park. Figure 4.1 shows the different size scale prototypes manufactured. Due to size and weight budget limitations a compliant mechanism was chosen for the MAV drive [51, 76, 122]. The “Small bird” was the group’s first effort in designing a fully steerable lightweight bird. The maximum wing flapping frequency was 12 Hz, the MAV net weight (without battery) was 9.7 grams and the total payload capability was 5.7 grams. Due to the light weight, however, this MAV had difficulties in flying outdoors. The development of this prototype was reported in [5, 14] with special consideration to the drive mechanism frame design and the multi-piece mold system for its manufacturing. To enable a successful outdoor flight and increase the payload to carry additional on-board sensors, the “Big bird” was developed. The increased total payload capability (19.1 g) was achieved by scaling up the wings. This resulted in increased power requirement to flap the wings, which had an effect on the design of load-transferring drive mechanism. The resulting maximum wing flapping frequency was reduced to 4.5 Hz. To further increase payload capabilities, a new “Jumbo bird” was prototyped. Utilizing machined and manually assembled drive mechanism, this MAV weighted 38 grams (excluding battery) and was proven successful in flight with 33 grams of payload. The maximum wing flapping frequency was 6.1 Hz. Videos presenting successful flights of the MAVs presented in Figure 4.1 are available on the website [47]. Preliminary experiments showed that the in-mold assembly technology

allows for creating a replacement drive mechanism with 27% less parts by utilizing compliant joints. Therefore the MAV drive mechanism was chosen as a platform representing a demanding small scale application where opposing objectives of weight reduction and functionality constraint satisfaction presents a challenging problem.

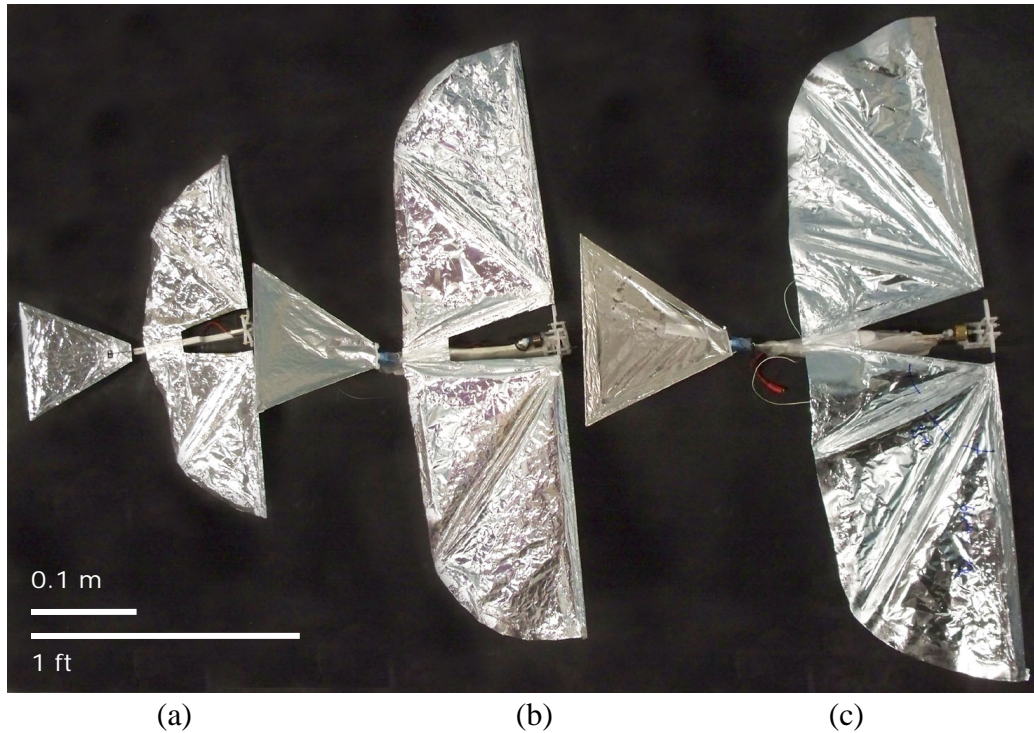


Figure 4.1 MAVs developed in AML: (a) 9.7 g “Small bird”, (b) 27.9 g “Big bird” and (c) 38 g “Jumbo bird”

4.2 Overview of the Design Process

In miniature multi-material compliant mechanisms, compliant joints, such as hinges, are required to transfer relatively large loads while allowing for the required DOF. The load transferred by the miniature compliant hinge determines not only the

sizing of the joint cross-section, but also influences the required level of bonding between the materials selected to create flexible and rigid portions of the structure. Since many heterogeneous polymers do not chemically bond during the molding stage [21, 37, 42, 50, 55, 54, 93], restricting design choices to just the material pairs that are known to bond well significantly reduces the design space. Therefore the assumption that desired materials for the compliant mechanism do not chemically bond had to be considered. To provide for physical (i.e., mechanical) bonding, interlocking features had to be incorporated into the design to ensure a robust interconnection between the materials. Therefore, to expand the design space it was necessary to consider alternative mechanisms for bonding chemically incompatible material pairs. One mechanism that has a great deal of potential is to provide for physical (i.e., mechanical) bonding through interlocking features to ensure a robust interconnection between the materials. However, if the pairs are chemically compatible, some positioning and structural considerations described in this section can still apply to the general design of the miniature hinge.

The robust interconnection strategy for incompatible materials in multi-material miniature mechanisms leads to a multi-objective optimization of the hinge design, with factors such as the part weight and the in-mold assembly process cost as the design objectives to be minimized. Whereas the part weight objective is directly proportional to the part volume and material density, the process cost is a complicated function of the manufacturing method selected, the process design, as well as the feature shapes and sizes. To allow for the optimization, the important design features have to be synthesized and parameterized with respect to all functional requirements

and manufacturing process constraints. In this chapter, the shape synthesis of a miniature hinge design in a multi-material mechanism is described, along with model parameterization and identification of the main constraints. The overall approach is shown in Figure 4.2.

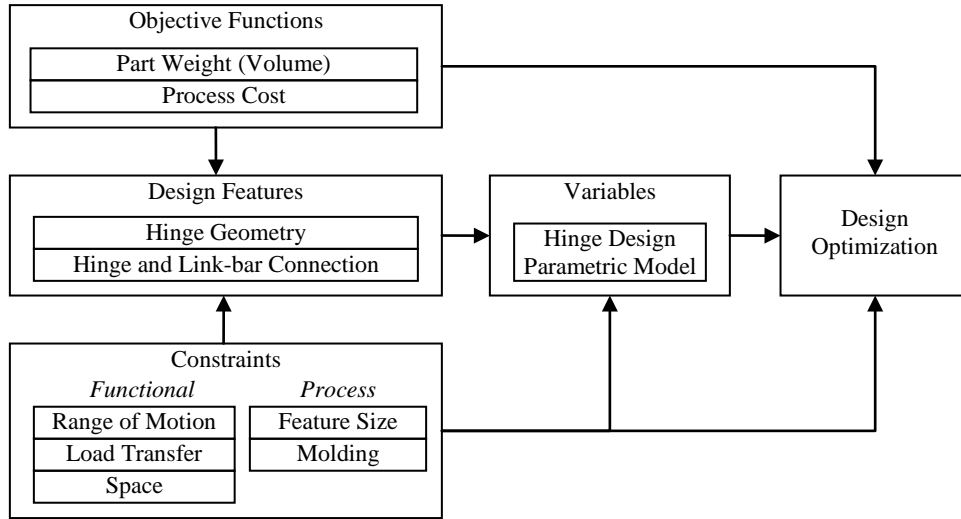


Figure 4.2 Miniature hinge design optimization approach

4.3 Shape Synthesis of Compliant Hinges

In order to select the appropriate hinge-link interface geometry, functional requirements and process constraints had to be considered, which is described in detail in the following paragraphs.

The first functional requirement for the hinge was to provide a 1 DOF angular motion with a prescribed range. To allow for rotation along the desired axis, the shape of the hinge was chosen to be a protrusion with a rectangular cross-section, varying along the hinge length. To allow for easy bending and reduce the stress

concentrations, the minimum cross-section has to be positioned in the middle of the hinge and gradually increase towards the ends of the hinge. While keeping the hinge breadth constant, the result is an arc-shaped cross-section in the plane normal to the axis rotation. A sufficient deformable length is required to provide for the prescribed angular range. To constrain the remaining DOF, the minimum hinge cross-section dimensions should have a high aspect ratio, with much greater dimension along the rotation axis and the thickness greater than a minimum value, determined from the forces acting out of the rotation plane. To further decrease any stress concentrations, all sharp edges should be rounded.

The second functional requirement was to ensure sufficient load transfer capability of the hinge. The hinge cross-sectional area has to be large enough to transfer the energy throughout the mechanism. In this approach, the minimum cross-sectional area of the hinge is determined by the tensile properties of the flexible material and the maximum loading conditions, obtained both experimentally and computationally through simulation.

Additionally, the injection molding process constrains the hinge orientation inside the mold. The orientation should result in a flow filling pattern along the hinge rotation axis [110] and allow for easy demolding. The mold parting surface design influences multiple process requirements, including number of mold pieces, number of side-action cores, and equivalent equipment; therefore, a minimum number of parting surfaces and mold pieces results in minimized process cost.

To allow for a connection interface between multiple materials, the bonding section has to be added to the design. This includes the embedded section of the hinge and

encapsulating section of the link. Due to the hinge load transfer capability requirement and the molding process considerations above, the embedded cross-sectional dimensions were set equal to those of the hinge. However, space constraints resulting from the mechanism's kinematic requirements have to be applied in the form of a constraint on maximum embedded section length. This length is utilized for the anchoring and positioning features described in the following paragraphs.

To ensure the structural integrity of the encapsulating section of the link, the embedded hinge cross-section has to be sufficient to transfer the mechanism loads. The shape of the encapsulating volume cross-section was determined based on the process cost objective. Three shapes, namely rectangular, polygonal and circular, were considered. Any sharp corners on the feature are expected to increase stress concentrations on the molded feature and turbulence the flow during mold filling. Additionally, parting surface orientations required for features with sharp corners can dramatically increase the mold complexity, and hence, process cost. Moreover, increased outside area causes more friction during demolding. Due to all of the above, an arc was determined as the optimal cross-section shape for the angular motion linkage interface. The space constraints resulting from the mechanism's functional design can again constrain the maximum section length, which has to be greater than the hinge embedded length. Such a complex geometry is expected to experience a complex stress distribution, therefore the encapsulating volume dimensions have to be assigned based on results from finite element analyses (FEA).

For the manufacturing of multi-material mechanisms, it cannot be assumed that the materials will be compatible and chemically bond during the in-mold assembly

process. Therefore the embedded section design has to incorporate anchoring features, which physically interlock the hinge with the links. Since all feasible interlocking 3D geometries cannot be possibly described, the shape synthesis of the interlocking features in this approach included single features, namely a protrusion and a void, and the combinations of both as complex interlocking strategies.

Due to the obvious fact that any voids in the hinge embedded section reduces its effective strength, and that the necessary compensation in the cross-section area around the void is followed by an increase of the links encapsulation volume, the single void interlocking feature was rejected as conflicting with the minimum part weight objective. Since the minimum cross-section area dictates the effective hinge strength, the void-protrusion feature combination was also eliminated from the possible optimal interlocking strategies as it results in redundant part mass from the load transfer capability point of view. Note, that this type of interlocking strategy, successfully applied in macro-scale multi-material compliant joints [42], is clearly conflicting with the main performance measure (weight) of a miniature mechanism design.

The choice between the remaining two options has to be made based on the physical space available, resulting from the functional mechanism design. Based on experimental investigation on sub-optimal interlocking feature designs, and FEA-based design evaluations, described in the next section, the protrusion-void interlocking feature combination was determined to be the most durable, as the void supporting the protrusion in the embedded section results in lower stress concentrations on the hinge from the load transfer capability requirement, with lower

encapsulation volume required. However, constraints set on the maximum encapsulation length may result in insufficient space to allow for this solution. In such cases, only the protrusion interlocking feature has to be used as the anchoring feature.

The protrusion interlocking feature cross-section shape selection was performed in the same manner as the encapsulating section of the link: based on the process cost objective. Rectangular, polygonal and circular geometries were considered. Sharp corners on the feature should be avoided, and the number of mold pieces should be kept to a minimum, to reduce the process cost. Therefore a rectangular cross-section with rounded edges placed symmetrically on both sides of the hinge embedded section was determined as the optimal shape, resulting in the minimum number of mold pieces. To ensure the load transfer capabilities, the total feature interlocking area had to be equal or greater than the hinge active cross-section. To prevent shearing, each feature's thickness had to be greater than its height. Finally, the minimum arc radius for the rounded edges had to be determined from the mold machining resources available and the corresponding tool sizes, with respect to the feasible domain and cost of the considered manufacturing process.

The void interlocking feature cross-section shape selection was performed in the same manner as the protrusion feature using the same performance measure guiding the selection and the same geometries considered. However, in this case the cross-section was considered in the plane of the hinge width, and not, as in previous cases, in the plane normal to the rotation. The optimal shape had to provide for the maximum interlocking area, equal to the minimum hinge cross-section reduced by the

void. Cross-section edges were rounded to avoid stress concentrations. The minimum width of the geometry surrounding the void and providing for the interlocking area had to be adjusted to available mold manufacturing resources. Note, that whenever the protrusion-void interlocking feature combination is allowed, the total interlocking area is shared between three physical anchors: two symmetrical protrusions and the void.

The final design consideration was specific to the in-mold assembly process. The second stage polymer melt can exert a relatively large force on the first stage component placed in the mold cavity. This can result in displacing the hinge and re-positioning it in the final multi-material assembly, leading to parts with reduced load transfer capabilities expected for each of the previously designed features. To fix the hinge inside the second stage mold cavity, positioning design features were added. Feature cross-section shape selection was performed similarly to the protrusion feature, with the same performance measure guiding the selection and the same geometries considered. An arc was determined as the geometry resulting in minimum stress concentrations on the hinge. The minimum radius had to be adjusted to available mold manufacturing resources. Therefore, the positioning protrusion feature length could not be greater than the hinge width. The size of this feature can be minimized using a flow balancing during the mold filling stage. The difference in times of the flow arriving at the hinge from adjacent cavities should be minimized or constrained to some small value to account for the dynamic effects. A runner optimization approach dealing with this type of problem is described in Section 5 of this dissertation.

The hinge design developed according to the approach presented in this section is shown in Figure 4.3, the corresponding connection with the link is shown in Figure 4.4, the variables of the parameterized design are listed in Table 4.1, and the constraint functions are listed in Table 4.2.

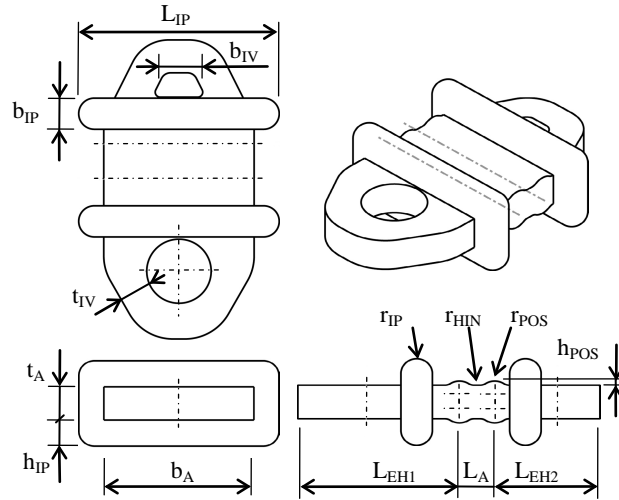


Figure 4.3 Miniature hinge design shape synthesis

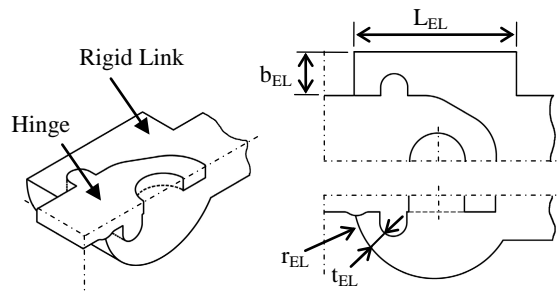


Figure 4.4 Hinge and link connection design shape synthesis (cross-section)

Table 4.1 Hinge design parameters

Feature	Symbol	Description
Hinge Active Section	t_A	Thickness (symm. wrt. rotation axis)
	b_A	Breadth (along rot. axis)
	L_A	Length (for the range of motion)
	r_{HIN}	Hinge arc radius
Hinge Embedded Section	L_{EHI}	Length (along L_A direction)
	h_{IP}	Interlocking protrusion height
	b_{IP}	Interlocking protrusion breadth
	L_{IP}	Interlocking protrusion length
	r_{IP}	Interlocking protrusion radius
	b_{IV}	Interlocking void breadth
	t_{IV}	Thickness around interlocking void
	h_{POS}	Positioning protrusion height
Link Connection	r_{POS}	Positioning protrusion radius
	L_{EL}	Hinge encapsulating length
	b_{EL}	Encapsulating breadth
	t_{EL}	Encapsulating thickness
	r_{EL}	Link ending radius

Table 4.2 Hinge design constraints

Fn#	Formula	Description
g_1	$t_A \leq k \cdot b_A$	Defines the rotation axis, where k is a coefficient dependent on the material
g_2	$t_A \geq t_{A(MIN)}$	Constrain the remaining DOF
g_3	$A_A \geq \sigma_{MAX} / \sigma_T$	Load-guided cross-section area: $A_A = t_A \cdot b_A$
g_4	$L_{EH} < L_{EL} < L_{MAX}$	Maximum embedded lengths (functional space constraint)
g_5	$A_{TOT} \geq A_A$	Minimum total interlocking area: $A_{TOT} = 2 \cdot [(L_{IP} \cdot h_{IP}) + (t_A \cdot b_{IP})] + (b_{IV} \cdot t_A)$
g_6	$b_{IP} \geq h_{IP}$	Prevent shearing of interlocking protrusion
g_7	$t_A, t_{IV}, r_{IP}, r_{POS} \geq t_{TOOL}$	Size constraints from tool size

The shape synthesis performed in this sub-section might appear similar to the topology optimization [77, 96]. However, the topology optimization approach does not consider feature interactions, and it may lead to shapes which are infeasible to manufacture.

After determining all the variables and constraints, the parameterized hinge model was used for the simulation-based design optimization, which is discussed in detail in the following section.

4.4 Modeling and Analysis of Compliant Hinges

To allow for the hinge optimization, the design has to be evaluated with respect to the posed constraints and requirements. However, due to the complexity of the shape synthesized in Section 4.3, this evaluation is not a trivial problem. A complex geometry experiences complex stress distribution fields when the hinge is loaded by the reaction forces from the links in operating multi-material mechanism. Therefore finite element analysis (FEA) has to be used to evaluate the design under maximum loading.

For FEA, the boundary conditions (BC) have to be appropriately chosen to simulate real-world loading imposed on the hinge by the rigid links of the mechanism. From the design possibilities enabled by the choice of materials that can be used in the in-mold assembly process, which is described in Section 4.5, the mechanism links can be made rigid with the actual mechanical properties of the links controlled through the composition of a glass fiber filler in a polymer. In the case study, described in Section 4.6, the composition of polyamide 6,6 (85% volume) with short glass fibers (15% volume) was used. The most intuitive way of applying the BC to the hinge

model is to constrain displacements of the model surfaces on one side of the hinge (i.e., fixed), and apply a load distribution on the opposite side of the hinge. The choice of the load type, direction, and traction surfaces should be considered carefully to correspond properly to the mechanism kinematics. Additionally, stiction forces have to be considered, as some polymer pairs may experience chemical bonding during the in-mold assembly process, which should be reflected in the modeled BC.

In some design cases, determination of load magnitudes can pose several challenges, as it can be difficult to measure the exact forces acting on the mechanism. In such case, a planar dynamics model can be used to simulate the experimentally measurable forces and their propagation onto the mechanism parts. The reaction force outputs can be then used to estimate the magnitude of the loads applied to the surfaces of the hinge model. This is presented in more detail on a case study in Section 4.6.

To evaluate the hinge design, the parameterized geometry synthesized in Section 4.3 was represented as a 3D solid model in Pro/Engineer Wildfire 4.0. The model was assigned the material properties corresponding to the polymer used to mold the hinge. Initially, Low Density Polyethylene (LDPE) from DOW Plastics, grade 722, was used for manufacturing the hinges. However, due to the insufficient fatigue resistance of this material revealed during the experimental validation, High-Impact Polypropylene (HIPP) from RTP Company, grade RTP-202, was chosen as a more fatigue-resistant replacement. The main material properties used in the FEA are listed in Table 4.3. The load BC and constraint BC are shown in Figure 4.5. The model had to be meshed separately in each design iteration.

Table 4.3 Material properties used in the FEA

Measure	Unit	LDPE	HIPP
Density	kg/m^3	918	910
Poisson's Ratio [88]	-	0.45	0.35
Young's Modulus	MPa	139	1034
Tensile Yield Stress	MPa	9	21

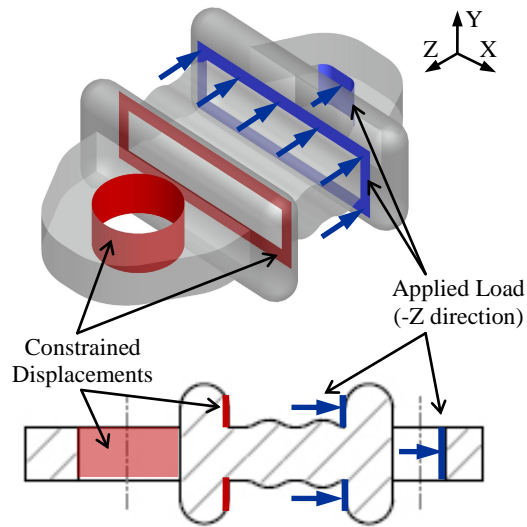


Figure 4.5 Hinge FEA boundary conditions

To characterize the level of chemical bonding between the polymers, an experimental investigation was undertaken. A dog-bone specimen, containing one of the preliminary hinge designs embedded in the gage section, was designed and injection molded using LDPE. The dog-bone specimen, shown in Figure 4.6, was designed to reflect the encapsulating geometry synthesized in Section 4.3.

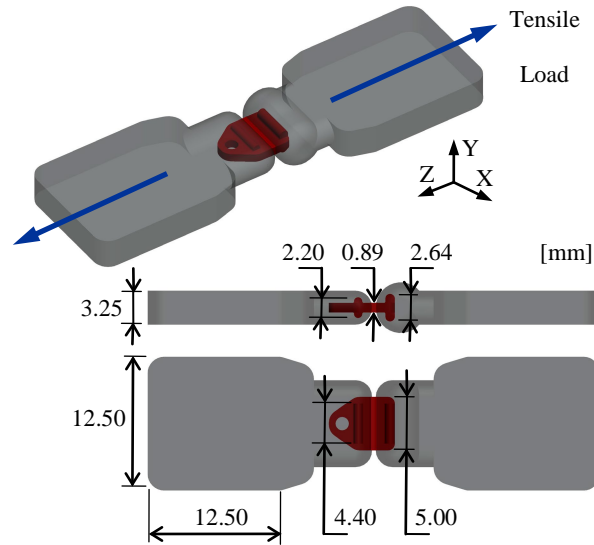


Figure 4.6 Specimen for tensile testing of the hinge

The specimens were then tested using tensile test equipment. The IMADA MX-500 Force Measurement setup with Z2H-440 Digital Force Gauge and data acquisition software were used to obtain the displacement-force plots. From these plots, the average maximum load was measured to be 34.8 N with standard deviation of 4.2 N. The spread of the results can be explained by the varying failure modes of the specimens. Half of the tested samples failed at the hinge flexible section, and half failed due to excessive deformation of the protrusion interlocking feature on the hinge itself, allowing the hinge to slip out of the encapsulating part of the specimen. Note, that the second failure mode was observed always on the side of the hinge with only the protrusion interlocking feature. This failure mode also suggested no bonding between the materials. To verify this, FEA was performed. Assuming zero bonding, the hinge design used in the experiment was loaded with the measured force at yield on one side of the hinge, and the other side was assigned the displacement constraints.

The BC are schematically shown in Figure 4.7. From the FEA, the von Mises stress distribution and displacements were plotted. The displacement result, shown in Figure 4.8, closely matched the observed failure mode. Additionally, the stress plot indicated stress levels exceeding the material tensile properties, which confirmed the dual failure mode of the tested hinge. Therefore, the assumption of the materials used in the in-mold assembly not being chemically compatible and not bonding during the process was verified.

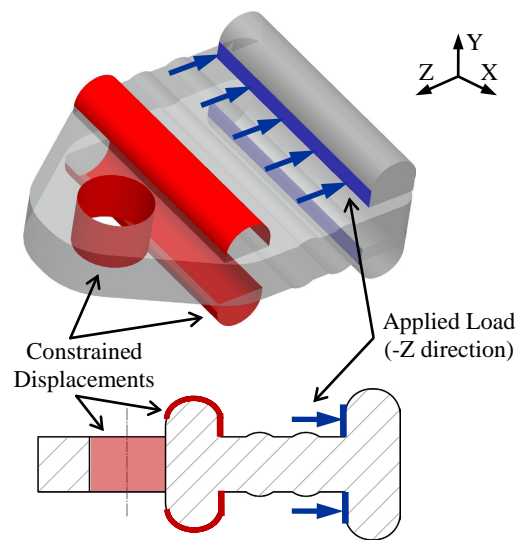


Figure 4.7 Tensile test specimen hinge FEA boundary conditions

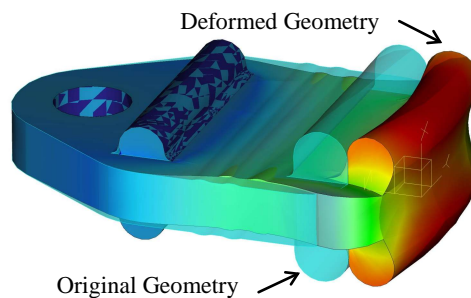


Figure 4.8 Displacement magnitude result for the tensile test specimen

After several FEA design evaluations, the main variables controlling the hinge strength were determined to be the area of the protruded interlocking feature and the cross-sectional area of the flexible portion of the hinge. Starting from the initial design, values of these variables were gradually increased, such that the resulting stress distribution would not exceed the allowable tensile strength at yield. Von Mises stresses, plotted for each design, were scaled to this value, to eliminate stress concentrations resulting from the FEA model and mesh imperfections. The mesh of the final design consisted of 11467 solid tetrahedron elements and 3723 nodes. The stress plot for this design is shown in Figure 4.9, and the key dimensions of this design are listed in Table 4.4. After determining the final hinge design, the mechanism links had to be expanded to fully encapsulate the hinge geometry.

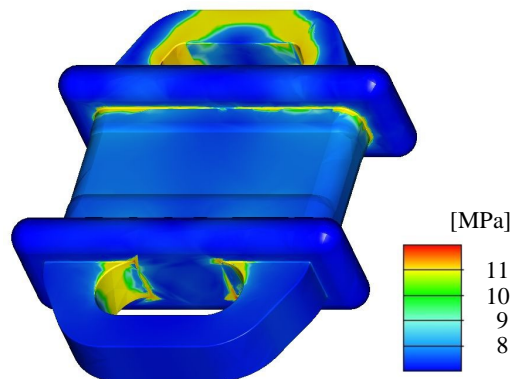


Figure 4.9 Von Mises stresses in the final LDPE hinge design

The optimized hinge was then injection molded with LDPE and in-mold assembled with the rigid links. However, endurance tests revealed a significant fatigue degradation of the LDPE hinges. Since the developed hinge was designed to be used

in a MAV drive mechanism, the fatigue life was determined to be insufficient for the desired flight duration. Additionally, the elongations of the hinges were measured optically (by a high-speed video recording analysis) to the flapping range of the wings by changing the kinematics of the drive mechanism.

Table 4.4 Key dimensions of the LDPE final hinge design

Variable	Symbol	Unit	Value
Hinge Thickness	t_A	<i>mm</i>	1.10
Hinge Breadth	b_A	<i>mm</i>	5.59
Hinge Length	L_A	<i>mm</i>	0.51
Interlocking protrusion height	h_{IP}	<i>mm</i>	0.65
Interlocking protrusion breadth	b_{IP}	<i>mm</i>	0.80
Interlocking protrusion length	L_{IP}	<i>mm</i>	6.94
Thickness around interlocking void	t_{IV}	<i>mm</i>	0.80

To overcome these issues, a high-impact polypropylene (HIPP) was used to mold the hinges. Due to differences in the properties, the hinge geometry had to be modified. Due to greater Young's Modulus of the HIPP, the hinge flexible section had to be thinned to allow for the desired bending action. This was obtained by specifying the radius of the arc boundary of the hinge cross-section. Since the overall dimensions of the mechanism assembly are fixed by the required kinematics, and the thinning had to be done on a relatively short distance to maintain the moving range, the cross-section shape radius was chosen such that the outer portions of the flexible section would remain unchanged. This allowed for a precise positioning of the hinge in the second stage mold without the risk of introducing cracks to the actual 'thinned'

flexing section. Additionally, this solution also deactivated the minimum flexing section thickness constraint, as it was imposed only by the second stage molding of a planar mechanism with multiple hinges.

Starting from the initial LDPE design, the radius of the arc thinning of the flexible section was gradually decreased, such that the resulting stress distribution would not exceed the allowable tensile strength at yield. The main material properties used in the FEA are listed in Table 4.3. Von Mises stresses, plotted for each design, were scaled to this value, to eliminate stress concentrations resulting from the FEA model and mesh imperfections. The mesh of the final model consisted of 12028 solid tetrahedron elements and 3911 nodes. The stress plot for the HIPP hinge design is shown in Figure 4.10, and the key dimensions of this design are listed in Table 4.5. After determining the final hinge design, the mechanism links had to be expanded to fully encapsulate the hinge geometry.

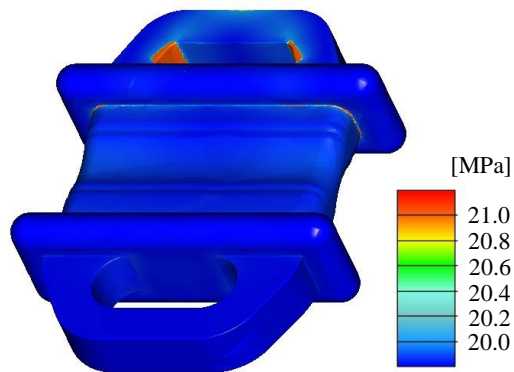


Figure 4.10 Von Mises stresses in the final HIPP hinge design

Table 4.5 Key modified dimensions of the final HIPP hinge design

Variable	Symbol	Unit	Value
Hinge thickness	t_A	<i>mm</i>	0.79
Hinge length	L_A	<i>mm</i>	1.52
Hinge radius	h_{HIN}	<i>mm</i>	1.27
Interlocking protrusion length	L_{IP}	<i>mm</i>	5.59

The HIPP hinges were observed to slightly elongate at the initial phase of operation, which could be easily accounted for and compensated by the driving elements of the mechanism.

4.5 In-mold Assembly of Compliant Hinges

In-mold assembly process is generally understood as any assembly operation that takes place inside the mold. This section describes the development of an in-mold assembly process to create multi-material compliant mechanisms with multiple miniature hinges based on the case study design of a multi-material compliant MAV drive mechanism. This process builds on the cavity transfer method, with additional considerations to the miniature scale involved and hinge processing guidelines. First, the overall process sequence is presented. This includes the first stage molding of the compliant hinges and the second stage molding of the rigid links of the mechanism. Mold designs are also described. Next, the gate design problem is solved based on the functional requirements of the mechanism. Finally, runner layout and sizing considerations are addressed in the second stage molding to account for the unique process considerations. The runner optimization approach is described in detail in Section 5 of this dissertation.

4.5.1 Process Overview and Mold Design

The choice of a specific in-mold assembly method to realize compliant structures with miniature hinges is a trade-off between the mold complexity and the cycle time. Several morphing cavity methods have been developed [89], offering a high level of automation. Due to the fact that the morphing cavity method needs to satisfy the assembly and disassembly constraints imposed on the mold pieces, the complexity of the part shape drastically affects the complexity of the molds, and hence significantly increases the tooling cost and lead times. To reduce the mold complexity, while maintaining the generality of the manufacturing approach, the cavity transfer method [42] was employed in this work. The minimum cost mold design consists of a minimum number of mold pieces. The chosen cavity transfer method in this study resulted in a minimum number of two mold pieces for each of the molding stages.

The process sequence developed to manufacture a multi-material compliant MAV drive mechanism is presented in Figure 4.11. The first stage of the process involved molding miniature hinges for realizing articulating joints in the structure. Demolded first stage components were then transferred to the second stage mold cavity. After the mold closing, the second stage glass fiber filled polymer was injected into the multiple cavities to create the rigid links of the mechanism structure. Note, that this step automatically produces an assembly operation, which took place directly inside the mold during the second stage molding (i.e., in-mold assembly). The compliant structure was then demolded and was ready to be assembled with the remaining mechanism modules.

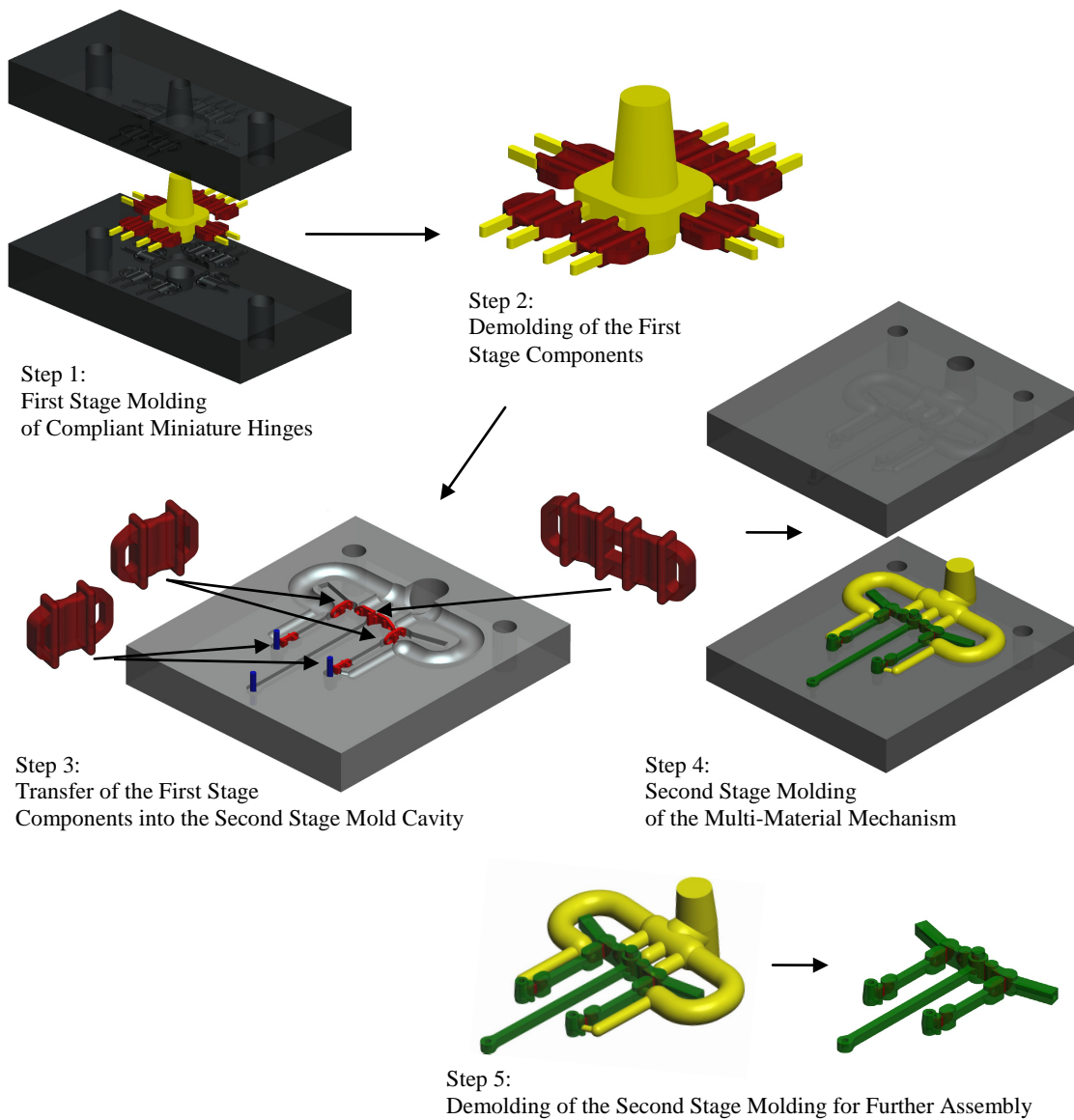


Figure 4.11 Overview of the developed in-mold assembly process

The developed process sequence order was determined by the necessity to create the 3D mechanical interlocking features on the hinge sub-moldings. Assuming a reversed order, creating negatives of these cavities inside the rigid links' sub-

moldings would require using a sacrificial core molding, which would increase the process cost significantly.

The molds were machined from aluminum blocks using a CNC milling machine. This method imposed some restriction on feature sizes and shapes, directly dependant on the milling process orientation constraints and the sizes of the available tools. In this case, the minimum tool diameter was 1/32 inch (0.79mm). The molds were additionally polished at the parting surface to prevent from flash. Molding parameters for the first stage (HIPP) and second stage (PA6,6-GF) molding operations are listed in Table 4.6.

Table 4.6 Processing parameters used to in-mold assembly the drive mechanism

Parameter	Unit	1st Stage	2nd Stage
Injection pressure	<i>MPa</i>	168	190
Injection time	<i>s</i>	2.5	6.0
Melt temperature	<i>C</i>	200	280
Flow rate	<i>cc/s</i>	12	12

4.5.2 Mold Cavity Design

The cavity layout is the first step to design the molds for manufacturing the hinges. While designing the cavities, the part orientation and the number of parts molded in one injection have to be considered. Orientation of a geometrically complex part cavity inside the mold influences the parting surface design. The mold parting surface design influences multiple process requirements, including number of mold pieces, number of side-action cores, and equivalent equipment; therefore, a minimum

number of parting surfaces and mold pieces can be used as a measure of minimized process cost. Moreover, increased outside area causes more friction during demolding. Once the orientation of the part cavity inside the mold is determined, it then constraints the allowable feature geometries of the part design to allow for the ejection from the mold. To increase the manufacturing efficiency, the number of parts to be molded in one injection cycle (number of cavities) can be increased to fill the mold envelope allowed by the injection molding machine. However, the more cavities to fill, the more complex runner design is necessary to feed all the cavities, with additional considerations to flow balancing to ensure consistent properties of the parts.

In the first stage of the in-mold assembly process described in this section, the part (hinge) was oriented such that the rotation axis would lay on the parting surface, and the parting line would be parallel to the longest dimension of the hinge. This would ensure a long life for the hinge by allowing for the perpendicular orientation of polymer chains with respect to the hinge rotation axis. The resulting part cavity orientation constrained the allowable shapes and sizes of the part features, such that the mold part count would not increase. These included the hinge geometry itself, the hinge-link interface geometry, including the embedded length and interlocking features, and hinge positioning geometries for the second stage molding. This was described in detail in Section 4.3. The molds were designed to produce a set of hinges needed for one multi-material mechanism, molded in the second stage of the in-mold assembly process.

In the second stage molds, the part cavities, corresponding to the molded mechanism links, were positioned on the parting surface to result in the minimum number of two mold pieces. This was possible due to the planar nature of the mechanism – any other orientation would increase the number of necessary parting lines and hence, complicate the process and significantly increase its cost. Additionally, this orientation allowed for the insertion of the first stage components into the second stage mold prior to the in-mold assembly operation without a risk of flashing or damaging the sub-millimeter flexing section.

Since adhesion of subsequent shots is a considerable parameter in multi-material molding, researchers have studied bonding strength for various materials [21, 37, 42, 50, 55, 54, 93]. However, the chemical bonding between subsequent shots may not be strong enough or possible at all when specific materials were chosen to obtain required functionality of the multi-material assembly. In these cases, specially designed physical interlocking features need to be developed to provide for a robust bonding between the parts molded from chemically incompatible materials. This was described in detail in Section 4.3.

Additionally, the second stage polymer melt exerts a relatively large force on the first stage component placed in the mold cavity. This can result in displacing the hinge and re-positioning it in the final multi-material assembly, leading to parts with reduced load transfer capabilities expected for each of the previously designed features. Therefore positioning features were introduced on both the hinge and the second stage mold to constrain the hinge displacement during the in-mold assembly process.

4.5.3 Gate Design

Gate type and location are always important design variables in the injection molding process, as they largely affect the cavity fill patterns. Improper choice of gate type and location induces unbalanced flow, which causes overpacking, high shear stress, excessive warpage, and may result in incomplete filling of the mold cavity. The gate position also induces the fiber orientation for the glass filled polymers, resulting in transversely isotropic properties for the molded part. Therefore gate placement is of a great importance to achieve high quality parts with required properties. Optimal gate designs ensure the required structural properties of the product and allow for easy demolding operations.

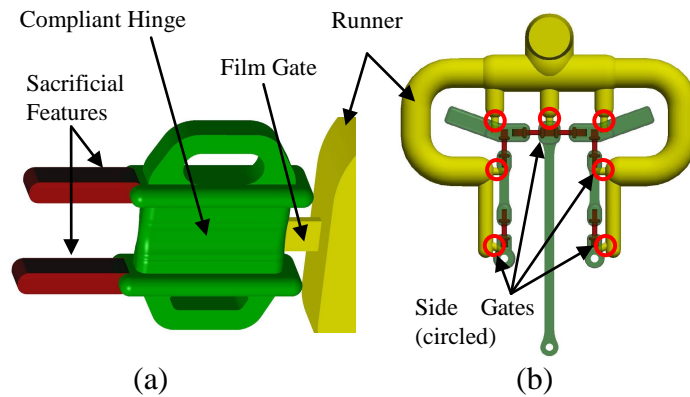


Figure 4.12 Gate designs used in the in-mold assembly process: (a) first-stage film gate, and (b) second-stage side gate layout

In the first stage of the process, compliant hinges were molded. To ensure a long life for the hinge, the polymer chains should be oriented perpendicular to the hinge as

they cross it in order to provide the greatest fatigue resistance. Therefore film gates were used to provide for a flow front progression aligned with the flexural axis of the joint. The film gate dimensions were determined to be: 0.34 mm thick, 1.27 mm wide and 1.27 mm long. Additionally, sacrificial features were added on the non-flexing parts of the hinge to allow for an easy demolding operation without the risk of damaging the miniature components. The gate and sacrificial feature of the first stage molding are shown in Figure 4.12(a).

In the second stage of the process, a multi-material mechanism frame was created by molding the rigid links over the first stage compliant hinges. Considering the functional requirements of the design, the glass fiber filled polymer composite was used to enhance the load transfer capabilities of the rigid links in the mechanism. However, as previously mentioned, the properties of the glass filled polymer moldings are highly dependent on the filler orientation across the part. Since the filling pattern inside the cavity is a strong function of the gate position, the gate positions had to be carefully designed to result in parts that orient the fibers to enhance material properties in the directions of maximum stress. Due to weight limitations in the MAV application, the volume of the drive mechanism links needed to be minimized, which resulted in several elongated cavities in the second stage mold. Since the filler particles tend to get aligned with the polymer flow during the cavity filling phase, we determined the side gate positions in these cavities to lie on one of the link ends, such that the resulting runner layout would have the minimum number of relatively long channels. Additionally, the gate directions were designed such that the second stage melt flow from the gate would not directly point at the first

stage components. The resulting gate layout was evaluated using a mold filling simulation to result in uniform orthotropic properties of the mechanism links molded from the glass fiber reinforced polymer. The gates were sized according to common injection molding guidelines [13] to be 1 mm long and 1.6 mm in diameter. The gate layout in the second stage molding is shown in Figure 4.12(b).

4.5.4 Runner Design

The primary function of the runner system in injection molds is to supply mold cavities with a molten polymer from the injection nozzle. Realizing multi-material compliant mechanisms with the in-mold assembly process requires a specific runner layout design. Molding the second stage components over the first stage parts results in the cavity separation and hence, multi-cavity molds. Each of these cavities needs a separate supplying runner. Since the cavity layout is determined by the mechanism functional design and the gate positions for each cavity are often fixed, as described in the previous sub-section, the main design objective for the runner system is to provide for a complete mold filling. Additionally, to ensure a strong encapsulation of the first stage moldings in the second stage parts, the second stage polymer flows should arrive at the pre-molded component from adjacent cavities in roughly the same time. This is required to: (1) minimize the highly directional forces which may be induced on the mold insert by an unbalanced flow pattern resulting in the insert's displacement and failed molding, and (2) to improve the strength of the weld-line formed when the second stage polymer flows around the first stage component. This is due to the fact that the weld-line strength increases with the melt temperature, as it results in higher energy and more time for the molecules to entangle during weld-line

formation [24, 74, 78]. Moreover, the polymer which solidifies inside runner cavity is treated as production waste after demolding; therefore the volume of the runner system should be minimized. All of the above leads to a complex runner optimization problem, which is described and solved in Chapter 5 of this dissertation. At this stage, however, the diameters of the long runners were increased to minimize the resistance of the flows reaching the cavities being the furthest from the sprue. Using a mold filling simulation, we scaled the remaining runner diameters to obtain a solution which satisfied all of the above constraints. The runner layout designed to realize the multi-material compliant mechanism is shown in Figure 4.13.

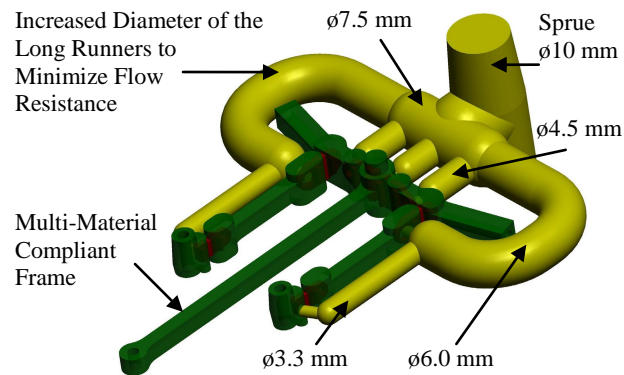


Figure 4.13 Initial runner design used in the in-mold assembly process

4.6 Case Study

As previously mentioned, the investigation in this chapter was performed on a platform for a prototype flapping wing micro air vehicle (MAV). In particular, the compliant characteristics of the hinge are very desirable for the drive mechanism of

the MAV. The main challenge in MAV applications is the weight reduction of the vehicle. This leads to more payload capacity, which enables the realization of various missions. Flapping wing MAVs present several advantages over conventional MAVs [14, 19, 40, 52, 83, 107, 111]. For example, bio-inspired flapping wing air vehicles are an attractive alternative to the traditional rotor-wing and fixed-wing air vehicles, because they are quieter and more maneuverable.

Development of a high performance MAV compliant drive mechanism is a complex problem, with many parameters and design options to be considered simultaneously. The primary objective is to minimize the weight of the drive mechanism. The mechanism shape and size have to meet the load-bearing requirements, ensuring a satisfying Factor of Safety (FoS) in terms of stresses induced on the structure by external forces. To allow for the drive mechanism design optimization, an experimental method is required to obtain input values for FEA evaluation. Furthermore, structure shape and size need to respect the molding constraints. Additionally, structure mechanical properties determine the gate and runner design of the multi-cavity molds needed for the multi-material molding of compliant structures.

4.6.1 Overview of Design Process

This section presents the main functional requirements for the drive mechanism, describes the mechanism concept, defines the optimization problem and describes the main steps in the approach for converting the concept into a detailed design. The primary functional requirement for the MAV drive mechanism is to translate the rotary motion of the motor to the flapping wing motion of the wings. The wing motions had to be synchronized to ensure the required flapping range for a successful

flight of the MAV and the overall stability of the mechanism. Based on previous findings [14], the flapping range was determined to be 65°. Preliminary tests indicated a flapping frequency of 4 to 6 Hz was required to sustain flight. The electronic components required for powering and controlling the MAV were chosen from the lightest market-available options.

Figure 4.14 shows the schematic diagram of the MAV drive mechanism concept. Based on the weight, size, and functionality constraints, a compliant mechanism was chosen as the most suitable for realizing the drive mechanism [14, 51, 76, 107, 122]. Several flexural joints were incorporated into the mechanism to provide for a localized (lumped) compliance in the structure to facilitate motion. To enforce the synchronization of wing motions, a prismatic joint was introduced.

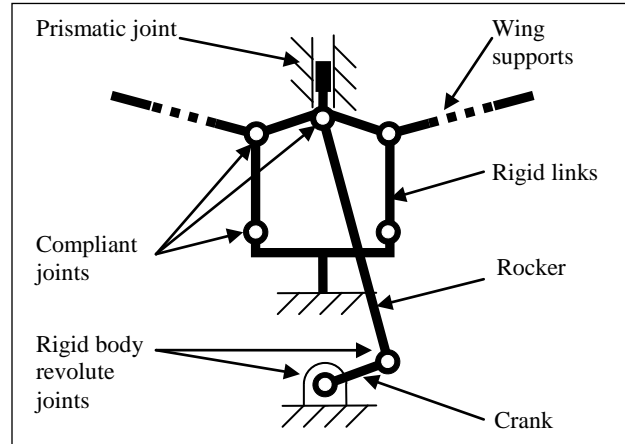


Figure 4.14 Schematic diagram of compliant mechanism for flapping wing action

The design problem for this case study was defined as follows. The main decision variables are: (1) mechanism shape and sizing, (2) miniature compliant joints' sizes and interlocking geometries, (3) wing design capable of strong lift and thrust

performance and (4) multi-material molding process to realize the drive mechanism design. The primary objective function for this problem is weight minimization. The following four constraints need to be satisfied. First, the stresses in the structure should not exceed the material limits. Second, the structure shape and size should meet molding process constraints. Third, gate positions should be chosen to allow for uniform fiber alignment during molding of filled polymers. This is required to obtain consistent orthotropic properties resulting from the fiber orientation [1, 36, 58]. Finally, the runner system design should result in fully filled moldings and have the minimum runner volume.

This problem was decomposed into four main steps. The first step was to derive the shape synthesis of the MAV drive mechanism. This included: (1) the geometry of the mechanism rigid links, and (2) miniature compliant joint features for successful interconnection with the links in multi-material structure. These steps are described in Sections 4.6.2 and 4.3, respectively. Since one of the most important factors determining the overall MAV performance is the wing design, it was necessary to develop an experimental setup to evaluate lift and thrust performance of several wing designs with varying stiffness layout of the wing structure. The developed setup was used to select a wing design with satisfactory lift and thrust generation. This step is described in Section 4.6.3. The next step was to develop a parametric model of the mechanism and perform optimization of its dimensions to minimize the part volume while meeting the required FoS and satisfying all manufacturability constraints. FEA was deployed to evaluate the designs using boundary conditions resulting from the experimental lift and thrust measurements. This step is described in Section 4.6.4.

The final step was to develop a suitable method of molding the multi-material compliant mechanism design generated by the optimization. To ensure successful molding of multi-material structures using the cavity transfer method and multi-cavity molds, the mold design parameters had to be considered. To ensure consistent structural properties of the rigid links molded from reinforced polymer composite, the gates had to be positioned carefully to result in unidirectional flow in the cavities and hence, a high level of filler alignment. Finally, the runner system volume should be kept to a minimum while ensuring a complete mold filling. The approach for designing the multi-material molding process to realize compliant structures was described in Section 4.5.

4.6.2 Elaboration of Mechanism Shape

The first step in the overall approach was to perform the shape synthesis of the MAV drive mechanism. The synthesis included the development of the basic mechanism geometry from the concept illustrated Figure 4.14, as well as identification of interlocking features on miniature compliant joints to achieve successful interconnection with the rigid links in a multi-material structure, described in Section 4.3. Towards this end, we carried out the shape synthesis of the mechanism using the following three step approach described in [14]. Here, however, some of the revolute joints were replaced by the compliant hinges.

First, to generate a basic shape of the mechanism, we detailed the design concept by adding functionality and manufacturability constraints. Second, we determined the constrained dimension of the mechanism by analyzing mating components and

motion requirements. Finally, the parametric model resulting from this approach is presented.

To achieve flapping wing motion from the rotary input of the motor, a crank-rocker mechanism based on the concept illustrated in Figure 4.14 was designed. The motor's rotational velocity was transferred to the crank through a gearbox to obtain the required flapping frequency. The crank was connected to a rocker, which displaced the symmetrically placed wing arms. These arms were pivoted on supporting members, which allowed for displacement of the pivoting point by utilizing lumped compliance. To ensure symmetry in the flapping motion, a prismatic joint was introduced at the point where rocker transferred the energy to the wing arms. This was crucial to the amount of thrust produced by the wings of the MAV.

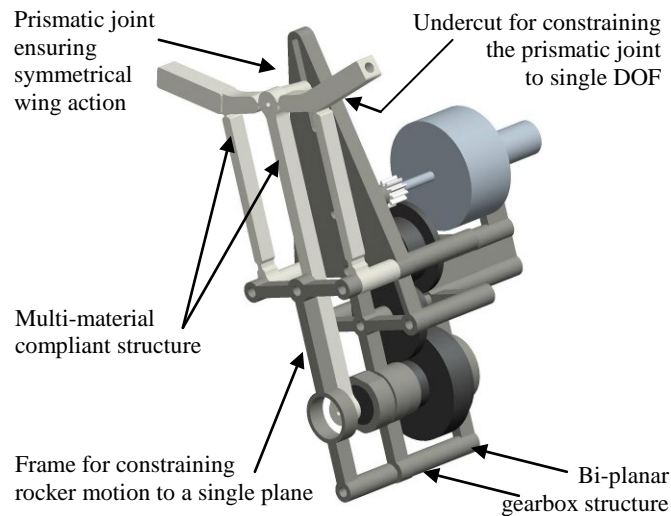


Figure 4.15 MAV drive mechanism design

The experimental results showed that disturbance forces can cause significant out of plane motion of the rocker and the wing arms. To eliminate these issues, we designed an additional frame for physical constraint of the rocker motion to a single plane, and an undercut feature on the back of the prismatic joint to constrain its motion to only one DOF. This is illustrated in Figure 4.15.

The developed drive mechanism utilized a multi-material compliant structure to transform the motor's rotational velocity to the flapping motion. This novel design combined seven rigid links connected with six compliant hinges to create a functional, single-piece mechanism. The molded structure consisted of the rocker, wing arms and their supports. It also provided for the prismatic joint attachment point and proper offset with respect to the crank.

In order to reduce the rotational velocity of the motor to match the flapping frequency requirement, a three-step gear reduction of 55.4:1 was designed. A Futaba FUTM3405 spur gear set with modules 0.3 and 0.4 was used. The gearbox was designed to match the gear bearing surfaces and it utilized a bi-planar design. This allowed for two-point support of the gears' axes and allowed for prevention of the crank wobbling effect induced by torque transmission to the rocker. To reduce the friction, machine grease was applied to the bearing surfaces and the gear teeth. The bi-planar gearbox assembled with the frame constraining the rocker created a rigid tri-planar enclosure of the mechanism, preventing it from damage during MAV landing. This is illustrated in Figure 4.15.

In order to ensure moldability of the multi-material compliant mechanism, fillets around the compliant joints had to be introduced to minimize the differences in the

cavity cross-section and allow for robust hinge encapsulation in the rigid structure. This was discussed in more detail in Section 4.3.

After identifying the basic shape of the mechanism using the functionality and moldability constraints, the next step was to determine the dimensions of the mechanism. Considering the functional requirements and constraints on the overall size of the MAV, it was important to first identify the constrained and free dimensions of the mechanism design. The constrained dimensions were identified from the functional requirements of the MAV.

The design of the mechanism required the rocker operational envelope to be placed between the wing arm supports. Therefore the minimum separation between the supporting members was constrained to 19 mm. For the required flapping range of 65° the relative angle on the wing arms was designed to be 15° and the length of the crank and the rocker to be 4.1 mm and 45.7 mm respectively. The range of flapping motion also determined the range for the prismatic joint to be at least 12 mm to account for elastic deformations of the structure in operation due to loading. The gear axis separation and the range of motion for the prismatic joint determined the minimum length of the mechanism to be 66 mm.

Moldability constraints of the compliant mechanism frame required that the main parting direction of the mold had to be perpendicular to the frame plane. Therefore the minimum thickness of the compliant joints was set to be 0.79 mm. However, this constraint can be deactivated by using partially thinned flexing section of the hinge, as described in Section 4.3. The only condition is that the hinge thickness in the

proximity of the link cavity has to be equal to the minimum one established above to prevent flashing.

The fixed dimensions of the mechanism based on the constraints described above are illustrated in Figure 4.16.

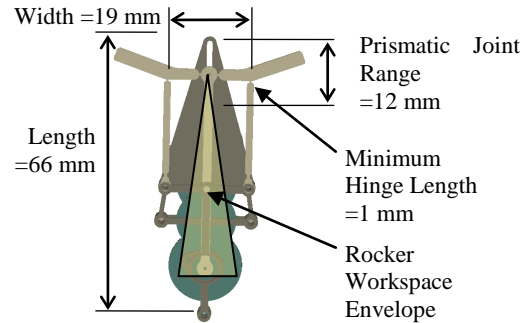


Figure 4.16 Constrained dimensions of the design

4.6.3 Wing Selection

One of the main challenges in designing a flying flapping wing MAV is the right choice of the wings. As the wings flap, thrust is generated, propelling the MAV through the air. Aerodynamic loading causes significant deformation of the wings, resulting in a large lifting surface. With appropriate wing design, the balance of lift and thrust provides good flight performance in multiple ways, including maneuverability, controllability, climbing rate, and payload capacity. Therefore the wing design is a key factor determining the overall MAV performance. In this section a test method for determining the lift and thrust performance for a wing design is presented and used to select a design with satisfactory results that can be used for the design of the compliant drive mechanism.

The MAV experiences four primary forces during flight: lift, thrust, drag, and gravity. Lift and thrust measurement is required to select a suitable wing design, as well as to quantify the aerodynamic and structural performance of the MAV. A 1-DOF test stand was developed to measure the thrust and lift of the MAV. Orientation of the MAV was reconfigurable to align with the measurement axis of the load cell both lift and thrust testing.

The vehicle was mounted in a clamp fixed to a low-friction rigid linear air bearing RAB1S from Nelson Air. Within the cavity of the bar held by the bearing, a Cooper Instruments LCFD-1KG miniature load cell was mounted to measure the dynamic load generated by the operating MAV. The air bearing and the load cell were mounted on a Newport Optics SA Series aluminum plate with elastomeric vibration dampeners. The load cell resolution is 0.0147 N@1220 Hz. Voltage data from the load cell was transformed into a digital signal using a Vishay Measurements Group P-3500 Strain Indicator. National Instruments NI USB 6009 DAQ was used to record the data at 1220 Hz. The data was filtered and scaled using LabView software to enable subsequent analysis.

During thrust testing, no moving air stream was used. However, during lift testing, moving air was required for the wings to function properly by producing aerodynamic lift. Without air flow over the wings, positive lift is exactly cancelled out by negative lift during each flap cycle. To simulate real flight conditions, we constructed a simple wind tunnel. The tunnel was comprised of 5 interlocking axial sections, measuring a total of 20 feet in length and 3 by 3 feet in the test cross-section. Air flow was generated by a Marley Industrial Products 30ACHA fan head with variable speed

control. By adjusting the wind tunnel flow velocity and wing angle of attack, the wind tunnel lift results were tuned to match real world payload test results.

Using the test equipment described, we performed lift and thrust measurements on a variety of wing configurations. The tested wings were constructed of carbon fiber rod stiffeners with a Mylar foil skin. Each of the tested wing designs used varying stiffness layout of the carbon fiber rods' structure to investigate the effect on force generation.

The wing design having strong performance characteristic in both lift and thrust outputs was chosen for subsequent flight testing and mechanism modeling. The top view of the wings is shown in Figure 4.17 and the weight and performance characteristics are summarized in Table 4.7.

Table 4.7 MAV wings characteristics

Parameter	Unit	Value
Wing weight	<i>g</i>	8.2
Measured lift	<i>g</i>	60.3
Measured thrust	<i>g</i>	39.2



Figure 4.17 Final MAV wing design

4.6.4 Modeling and Optimization of Mechanism

The next step in the approach undertaken in this case study was to develop models to allow for design optimization of the multi-material compliant drive mechanism of the MAV based on the lift and thrust measurements for the wing design. To this end, the parametric models of the mechanism resulting from unconstrained dimensions developed in Section 4.6.2 were employed and the experimental data from lift and thrust measurements of the wings developed in Section 4.6.3 were used as the boundary conditions in the design evaluation.

Since the overall functionality of the MAV depends on its payload capabilities, the weight of the drive mechanism should be minimized with constraints set on the load transfer capabilities required by a specific application. The design variables included sizing of the mechanism rigid links, critical for the drive functionality, as well as sizing dimensions of the miniature compliant joint cross-section. The experimental results of lift and thrust forces generated by MAV wings were inserted into a dynamic simulation model as input boundary conditions. The simulation was used to estimate propagation of the wing forces through the mechanism structure. The results were then inputted into Pro/Mechanica FEA module to calculate stresses and strains on the structure. To minimize the weight of the mechanism without risking its failure, parts were sized to achieve the required FoS. The overview of the optimization process is shown in Figure 4.18.

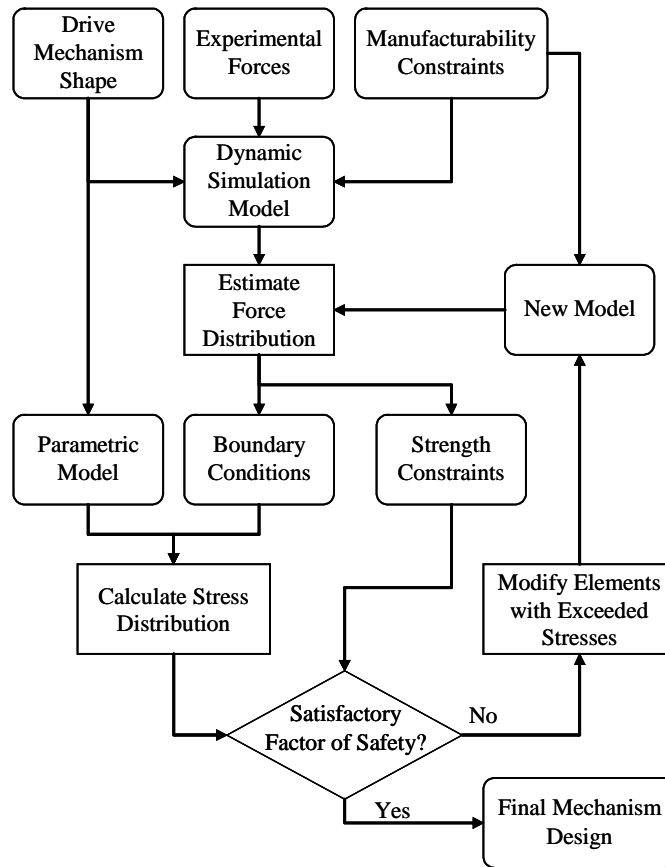


Figure 4.18 Optimization process flowchart

Design optimization of the mechanism required knowledge of the forces acting on links and joints. Using the load cell setup described in Section 4.6.3, lift and thrust forces generated by the wings were collected. The measured average thrust was 39.2 grams, with peak amplitude of 175.8 grams. Thrust values were recorded using a stationary platform with non-moving airstream. The measured average lift was 60.3 grams, with peak amplitude of 189.9 grams. Lift values were recorded using our wind tunnel with a moving airstream to simulate flight conditions.

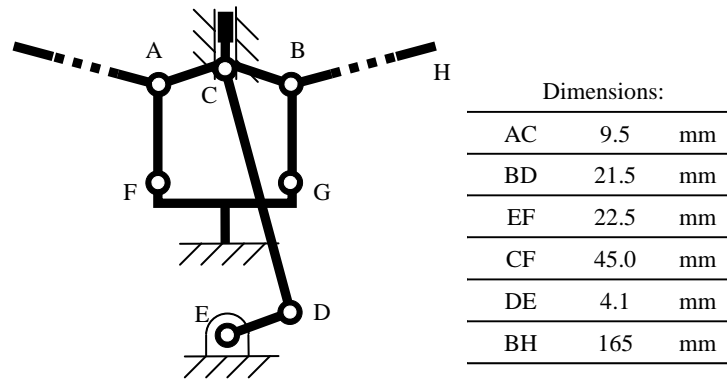


Figure 4.19 Kinematic representation of the model

The simulation of wing forces' propagation onto the mechanism parts was performed using a planar dynamics model. The mechanism forces resulting from the flapping wings were modeled as a sinusoidal loading applied in the direction normal to the wing spars. The force was applied to the mid-span point of the spars. Constant rotary motion $\Omega = 338$ Hz was applied to the gearbox output shaft. A kinematic representation of the model with the key dimensions is shown in Figure 4.19.

Weights of the mechanism components were first included in the model; however, they were considered to be negligible, due to the low operating frequency of the mechanism, and a relatively low mass of the moving components. Therefore the inertial effects of the mechanism were ignored.

The mechanism was modeled using MSC Adams View R3 software. The model synthesized in Figure 4.20 was then used to analyze the distribution of reaction forces. Static equilibrium simulation for two full wing flap cycles was performed. Since this was a time-dependant problem, we had to find the cases where the combined load on the structure induced the highest von Mises stresses. The most

demanding and prone to failure mechanism components were identified as the rocker element (at point C) and the wing arms (at points A and B). The most demanding hinges were present also in point C, therefore the reaction forces in this point were plotted with a resolution of 1 millisecond. The data points with the greatest magnitude of combined loading during the flapping cycle were chosen as inputs to the FEA, such that the FoS would correspond to the worst case scenario loading of the design.

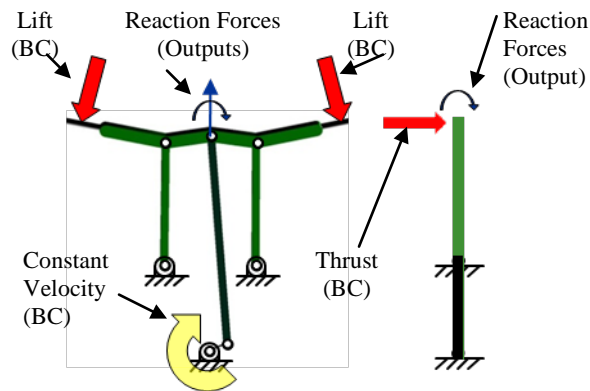


Figure 4.20 Model synthesis with input boundary conditions (BC) and estimated reaction forces

After constraining the dimensional parameters of the mechanism to accommodate mechanical and electronic components required for the functionality of the MAV, the remaining mechanism dimensions had to be determined, namely rocker (CD) thickness, wing arms' (AC) thickness, and the compliant hinge cross-section. These were assigned by FEA-based design optimization.

The goal of optimization was to minimize the weight of the mechanism, while satisfying the manufacturability and maximum allowable stresses constraints. The cases with maximum combined loading magnitude were selected to reduce the

number of FEA iterations. The von Mises stresses in the mechanism were found from these worst case loading scenarios. The loading conditions found to induce the largest stresses in the mechanism are listed in Table 4.8. These loads were applied to the corresponding points on the 3D mechanism model. Since forces resulting from the weight of motor and gears were an order of magnitude smaller than the forces resulting from the motion, these forces were excluded from the FEA. The rigid links of the mechanism were modeled using the material properties of PA6,6F (density=1230 kg/m³, Poisson's ratio=0.3, Young's Modulus=5.5 GPa).

Table 4.8 FEA load components

Component	Applied to	Unit	Value
X	A	<i>N</i>	-1.159
Y	A	<i>N</i>	-32.767
Z	A	<i>N</i>	-1.559
X	C	<i>N</i>	0.026
Y	C	<i>N</i>	31.141

Finite element analysis was performed using the Pro/Mechanica module of Pro/Engineer Wildfire 4.0 software. We performed the FEA of the worst case loading scenario and plotted the maximum von Mises stresses across the structure. The yield strength of the PA6,6F material (110 MPa) was then divided by the peak stress to determine the resulting FoS. The rocker and wing arms were designed to have a FoS of 2. This was identified as the average recommended value for known materials with certification under constant environmental conditions, subject to stresses that can be determined using qualified design procedures. Therefore the

required cross-sectional dimensions of the rocker were found to be 2.1 x 2.5 mm and of the wing arms to be 2.5 x 5.1 mm. Similarly, the hinge cross-sectional dimensions were obtained, which was discussed in greater detail in Section 4.4.

4.6.5 Results

Solving the design optimization problem as described in the above sub-section resulted in a complete set of dimensional parameters for the design of the flapping wing drive mechanism. The design of a suitable multi-material molding process developed to manufacture the drive mechanism, which utilized miniature compliant hinges, was described in Section 4.5. Multi-material compliant frame for MAV drive mechanism was molded on a Milacron Babyplast injection molding machine. The following materials used to manufacture the drive mechanism. HIPP was used in molding the first stage components – compliant joint inserts. Short glass fiber-filled Nylon 6,6 (PA66F) was used in the second stage molding to create the rigid links of a multi-material compliant structure. Delrin was used for manufacturing the crank, motor holder and the gearbox frame for the mechanism. Since the feasibility of creating similar gearbox frames using multi-piece, single-material molding was demonstrated previously [14] and lies outside the scope of this work, CNC-machined components were used for prototyping flexibility.

Figure 4.21 shows the photograph of the multi-material molding of the compliant MAV drive frame molded using a cavity transfer method developed in this section. Careful visual inspection of the demolded part revealed no molding defects such as deep weld-lines, excessive warpage or displaced compliant joints. The differential shrinkage of the part could not be completely eliminated. Nevertheless, since it did

not affect the functionality of the mechanism, we concluded that the maximum shrinkage in the structure, 0.41% for the longest rocker element, was functionally acceptable.

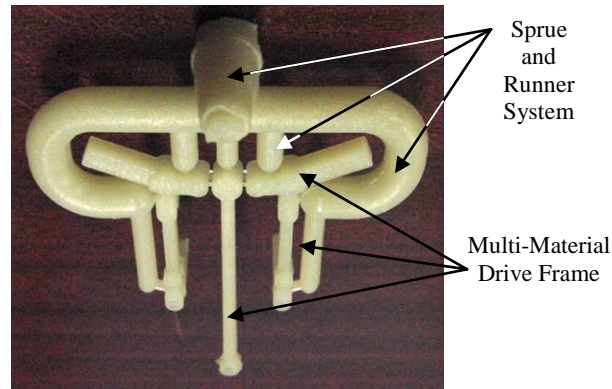


Figure 4.21 Multi-material molding of MAV drive frame

After successfully accomplishing the molding of the multi-material compliant drive frame, the mechanism was assembled using the molded and machined parts along with off-shelf components, including gears, rods, and motor. The body of the MAV consisted of the drive mechanism with wings attached on the front and the tail servomotor at the back, both connected with two carbon fiber rods and a foam body. The foam body served as housing for the motor speed controller and remote control receiver, as well as the rear anchoring point for the wings. The assembly of the MAV is shown in Figure 4.22.

The MAV designed and developed in the Advanced Manufacturing Laboratory at the University of Maryland was capable of: (1) a remote launch from a four-wheel RC vehicle, (2) holding a sustained outdoor flight with controlled ascent, descent, and steering, and (3) controlled landing in a safe area. The main performance

specifications are listed in Table 4.9. Video of the successful indoor and outdoor flights can be found at the project website [47].

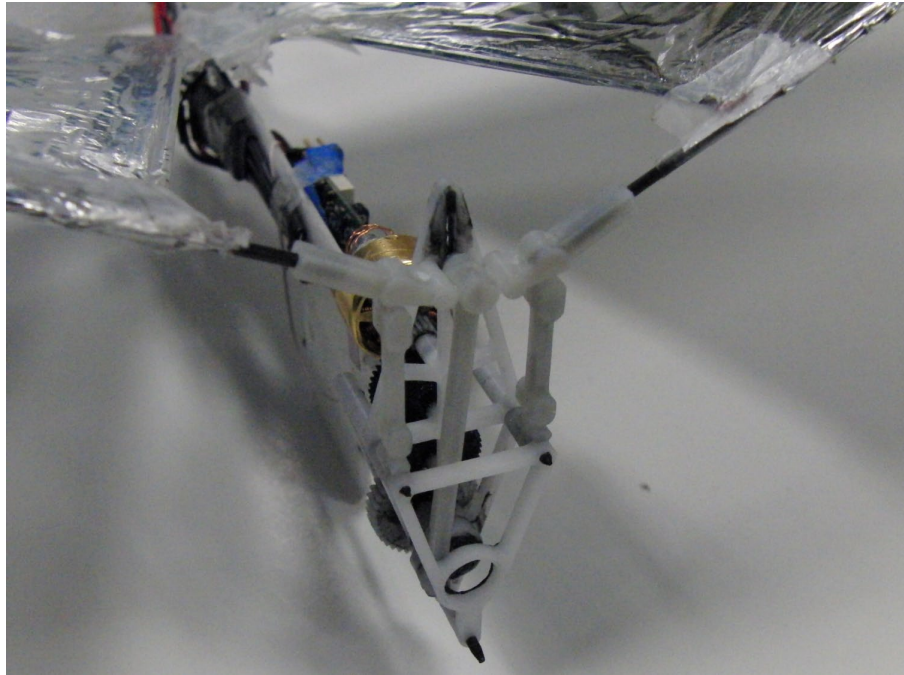


Figure 4.22 MAV assembly

Table 4.9 MAV test flight results

Parameter	Unit	Value
Overall Max. Weight	<i>g</i>	72.5
Payload Capacity	<i>g</i>	31.0
Flapping Frequency	<i>Hz</i>	5.2
Wing Area	<i>cm²</i>	920.2
Wing Span	<i>cm</i>	63.5
Flight Duration	<i>min</i>	15
Flight Velocity	<i>m/s</i>	3.0

4.7 Summary

This chapter presented the approach for design and fabrication of miniature compliant hinges in multi-material compliant mechanisms. The methodology described in this chapter allows for concurrent design of the part and the manufacturing process.

The following new results were reported in this chapter. First, a method to design miniature hinges in multi-material structures was presented, subjected to demanding loading conditions and large deflections. The shape synthesis of the hinge geometry involved incorporation of in-mold assembly process-specific features. These included the hinge geometry itself, the hinge-link interface geometry, including the embedded length and interlocking features, and hinge positioning geometries for the second stage molding. Second, an optimization model of the hinge was presented, involving functional and manufacturing constraints. Third, a new manufacturing method was described for creating multi-material compliant structures using injection molding processes. This included the in-mold assembly process sequence, the mold cavity design, gate selection, and runner system development. Finally, a case study of a multi-material compliant mechanism used as the drive mechanism in a MAV prototype was presented. The technical feasibility of our mechanism design was demonstrated through successful test flights of our MAV. The MAV was capable of repeatable flights with a 31 gram payload, which represents 75% of the total unloaded MAV weight. While airborne, the MAV was highly stable and controllable in both indoor and outdoor flights

Miniature hinges utilized to achieve selective, localized compliance in the multi-material structure resulted in an efficient and compact design of the MAV drive mechanism. Additionally, the multi-material compliant mechanism resulted in a reduced number of parts in the drive assembly by eliminating several rigid body articulating joints. Methods described in this chapter are applicable to any lightweight, load-bearing compliant mechanism with miniature hinges manufactured using in-mold assembly process. The specific shapes generated in this work are applicable only to the in-mold assembly process involving miniature components. However, the shape synthesis process developed in this dissertation is applicable to a wide variety of manufacturing processes.

5 Runner Optimization for In-mold Assembly of Multi-Material Compliant Mechanisms

The runner system in injection molding process is used to supply the polymer melt from injection nozzle to the gates of final part cavities. Runner system should be designed to achieve balanced flow, resulting in minimum variations in pressure and temperature gradients in all cavities at the end of filling phase [13, 61]. If the flow inside the mold is not balanced, overpacking, high shear stress, and excessive warpage may occur, resulting in inconsistent and/or low quality products. Realizing multi-functional complex mechanisms by in-mold assembly process requires special runner layout design considerations, including the interface geometry, the existence of the first stage components, and fiber orientation of the second stage moldings.

This chapter presents the development of an optimization approach for runner systems in the in-mold assembly process of multi-material compliant mechanisms. First, the issues specific to the process are identified and analyzed. Next, the general optimization problem is formulated, followed by identification of all parameters, design variables (DV), objective functions (OF) and constraints. Next, the implementation of the optimization problem in Matlab[®] environment is described based on a case study of a runner system for an in-mold assembly of a MAV drive mechanism. This multi-material compliant mechanism consists of seven rigid links interconnected by six compliant hinges. Finally, several optimization approaches are analyzed to study their performance in solving the formulated problem. This includes the analysis of results from each of the methods, their relative ranking and the

selection of the most robust and efficient optimization approach. The case study showed the applicability of the developed optimization approach to runner systems for complex in-mold assembled multi-material mechanisms.

5.1 Motivation and Challenges

The main function of the runner system in any injection molding process is to supply the mold cavities with a molten polymer from injection point. Once the mold is filled and the polymer solidifies, the molding¹ is ejected and the runner system is detached from the part. A common practice in the injection molding community is to minimize the runner volume, since it is a production waste, and influences not only the process cost, but also the amount of total energy from the sustainability point of view. This objective was used by many researches in different runner optimization problems [13, 12, 57, 60, 79, 117, 120, 121]. However, in-mold assembly of multi-material multi-component structures such as compliant mechanisms entails certain design considerations specific to the nature of both the assembly design, as well as to the manufacturing process.

The details of mechanism design optimization were described in Chapter 4 of this dissertation. One important outcome of this optimization was the process sequence. Due to the various requirements and constraints associated with the final multi-material mechanism assembly, the first stage of the process involved molding of the compliant joints (hinges), and the second stage involved molding of the rigid links. Using pre-molded inserts (compliant joints) results in cavity separation and hence

¹ The ejected solidified part with the runner system is referred to as a molding (noun) in this chapter.

multi-cavity molds. Multi-cavity molds require a complex, multi-branch runner system to supply all the cavities with the molten polymer in order to fill the mold. Therefore the mechanism kinematic design mirrored in the cavity layout determines the molding system complexity. In general, more cavities require more complex runner segment configurations to fill the entire mold with the molten plastic.

Another important consideration is related to the functionality of the design obtained by a carefully chosen injection-moldable material. The wide variety of polymeric compounds available on the market allows the designer to select a grade with required functional properties for virtually any application. In case of molding mechanism links, their rigidity can be obtained with a glass fiber filled polymer composite. However, the required structural properties result from the filler alignment, which is a function of the cavity filling flow pattern, and is controlled by the gate type and position. To obtain uniform properties of components such as mechanism links, the gate position needs to be set during mechanism design stage. The level of filler alignment has to be evaluated by means of mold filling simulations.

All of the above design constraints lead to a complex runner design. This design additionally needs to comply with general empirical rules involving dimension relationships between the supplying channel and the sub-segments being fed by it. These include the minimum runner cross-section required for sufficient cavity feed and runner branching rules.

Next important consideration is connected with the positioning of the first stage components inside the second stage mold for the in-mold assembly. As described in Chapter 4, these first stage components need specially designed positioning features

to enable correct placement inside the second-stage mold. The size of these features however needed to be minimized, as it directly influences the main objective, namely minimum weight. Additionally, due to the compliant nature of the first stage component material, these features were capable of elastic deformation during the second stage molding, which allows for the component displacement and resulted in failed assembly.

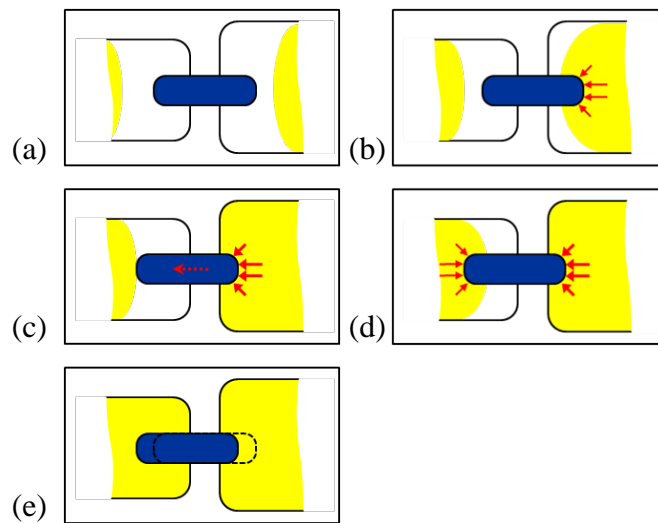


Figure 5.1 Schematic of differential pressure exerted on the first stage component

The reason for such displacement is the separation of link cavities by the hinge insert in the second stage molding. Consider the schematic animation shown in Figure 5.1. Since the cavities are separated, they fill with the molten plastic independently (a), and the filling pattern and timing is dependent on the design of the gate and runner supplying the cavity. If one of the cavities adjacent to the hinge insert fills faster than the other, the molten polymer starts exerting pressure on the insert (b), causing the deformation of positioning features mentioned before. This

results in hinge directional displacement inside the mold cavity (c) until the pressure on the hinge insert is compensated by the flow in the second cavity (d). This results in failed multi-material assembly (e), as the carefully designed features on the hinge insert are not capable of playing their original role when misplaced and not fully encapsulated inside the second stage molding. This failure mode observed during exploratory experiments is shown in Figure 5.2.

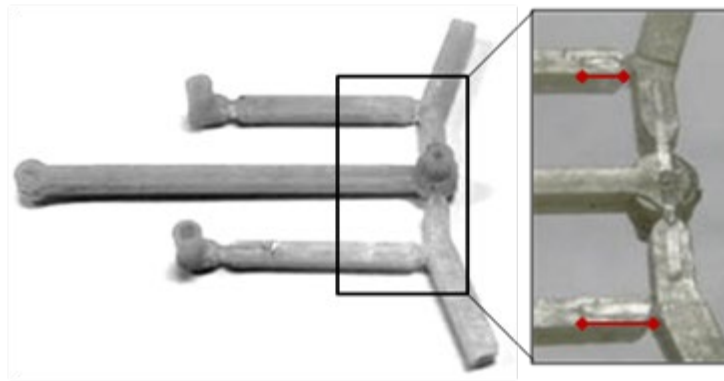


Figure 5.2 Displaced in-mold assembled hinges in a multi-material mechanism
(embedded hinge section lengths marked)

Therefore it is highly desired for the flows to meet on the opposite sides of the compliant insert with the minimum possible time difference to avoid excessive directional force exerted on the insert. This however is an objective dependent on the already complex runner layout, sizing, processing parameters and material properties; therefore it requires a mold filling simulation to calculate the time difference between the flows arriving at the pre-molded components.

The need of mold filling simulation being involved in the runner optimization routine poses additional challenges concerning the software integration. Autodesk®

MoldFlow[®] simulation software, commonly used in the research community and commercial industry to simulate the injection molding process, does not allow for posing the arrival time difference objective, as well as it requires runner lengths to be fixed. On the other hand, interfacing MoldFlow[®] simulation with an external optimizer is tedious. In this study, a custom mold filling simulation was developed, based on a pressure meta-model built from results of MoldFlow[®] simulations. This allowed for exploration of variety of optimization methods to obtain optimal solutions.

5.2 Overview of the Approach

This section describes the overall approach to design optimization of runner systems for in-mold assembly of multi-material compliant mechanisms. The goal of the approach is two-fold: (1) to define the optimization problem specific to the in-mold assembly of multi-material compliant mechanisms, and (2) to select the best method to solve the problem. The in-mold assembly process-specific constraints include the relative layout of multiple mold cavities and the gate locations for fiber-filled moldings. The injection molding process constraints include empirical formulations for minimum runner diameter to allow for sufficient feed of melt to mold cavity and runner branching rules. In order to evaluate the solution methods, a case study of a multi-material MAV drive mechanism is defined and encoded into calculation environment. This includes the development of computationally fast mold filling simulation based on a pressure meta-model. The case study runner system is then optimized using several different optimization approaches. Next, the optimization methods are ranked in terms of the solution quality, calculation time,

robustness and scalability. Finally, the best approach to the runner optimization problem is selected. The overall approach is outlined in Figure 5.3.

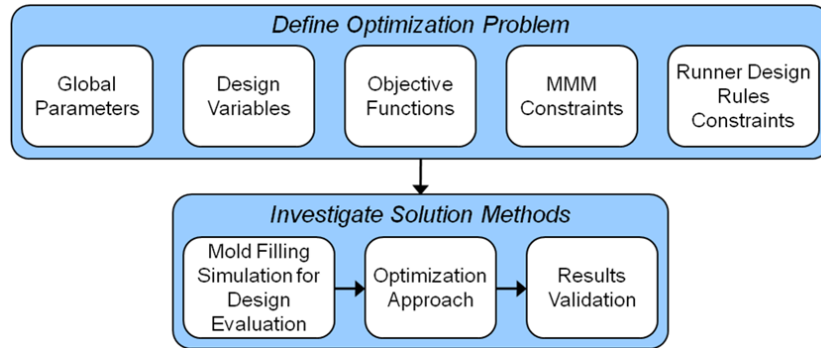


Figure 5.3 Runner system optimization approach

5.3 Development of Optimization Problem

This section describes the details of optimization problem formulation for runner systems used in in-mold assembly of multi-material compliant mechanisms.

5.3.1 General Formulation

The runner optimization problem considered in this study is defined as follows. The first objective is to minimize runner volume, which is a production waste. The second objective is to minimize the difference in arrival times of the molten polymer from adjacent cavities to the first stage components. The design variables are the dimensions of the runner channels. The design variables are subject to three main constraints: (1) geometric layout resulting from the molded assembly design and gate positions, (2) mold filling necessary condition, which can be imposed by empirical classical injection molding rules for runner system design, such as minimum runner

diameter as a function of supplying cavity and/or runner branching rules, and (3) parameters depending of the available manufacturing resources, such as injection nozzle diameter, tooling sizes for mold manufacturing etc. The global optimization parameters include the molding system representation (excluding values of runner dimensions represented by the design variables), definition of locations for which the flow arrival time difference is compared and minimized, the second stage molding material properties for the flow viscosity model in the mold filling simulation, and injection molding processing parameters, such as injection rate, melt temperature, velocity/pressure switch-over value etc. Once the problem is fully defined, the next step is to encode it in mathematical representation for an automated design optimization step.

5.3.2 Mathematical Formulation

This sub-section presents the mathematical formulation of the runner optimization problem described and stated above.

Parameters

To develop the mathematical formulation of the problem, all relevant information needs to be gathered, such as material properties, performance requirements, resource limits, costs etc. Also, all assumptions about the problem necessary to formulate and solve it have to be made [8]. The following parameters are necessary for the optimization problem defined in Section 5.3.1:

1. Molding system representation, including
 - a. Number of the runner segments within the molding, N

- b. Set of the first stage components being in-mold assembled with the second stage molding, M
 - c. Lengths and diameters of both the runner segments and the in-mold assembly cavities to be filled, L and R
2. Second stage molding material properties, including
- a. Recommended processing parameters
 - Mold temperature range
 - Melt temperature range
 - Ejection temperature
 - Maximum shear stress and rate
 - b. Rheological properties
 - Glass transition temperature
 - Viscosity model with coefficients (for example Cross-WLF¹ for viscosity as a function of temperature and shear rate)
 - c. Thermal properties
 - Specific heat capacity
 - Thermal conductivity
 - d. Specific volume properties
 - Melt and solid density
 - Specific volume as a function of temperature and pressure
 - e. Filler properties, if any

¹ Williams-Landel-Ferry

3. Manufacturing resources available and their control parameters
 - a. Injection molding machines with V/P switch
 - Injection volumetric flow rate (constant)
 - Maximum pressure for Velocity/Pressure switch-over
 - Maximum injection volume
 - b. Injection molding machines with other control strategies have to incorporate the adequate parameters.

Design Variables

The design variable vector X consists of the values of runner channels'

$$\text{dimensions: } \forall i \in N : X_i = L_i \cup R_i \quad \text{EQ. 5.1}$$

where:

N is the number of runner segments, and

L_i is the length of i^{th} runner segment.

Due to many different constraints outlined in the motivation section of this chapter, most of the runner channel lengths are fixed before the optimization, therefore the design variables mainly represent the runner cross-section dimensions (radius or diameter), and the feasibility of incorporation of runner length depends on a particular design case.

Objective Functions

The first objective to be minimized is defined as the runner system volume, calculated as the sum of volumes of all runner channels:

$$\text{OF\#1: Minimize } V = \sum_{i=1}^N (L_i \cdot A_i) \quad \text{EQ. 5.2}$$

where:

A_i is the cross-section of i^{th} runner segment as a function of its radius R_i :

$$A_i = \pi \cdot R_i^2 \quad \text{EQ. 5.3}$$

The second objective to be minimized is defined as the maximum of the flow arrival time difference defined for points where the second stage flow meets the first stage component:

$$\text{OF\#2: } \forall j \in M : \text{Minimize } T = \max(\Delta t_j) \quad \text{EQ. 5.4}$$

where:

M is the set of the first stage components being in-mold assembled with the second stage molding, and

Δt_j is the j^{th} flow arrival time difference to each of the M first stage components defined as:

$$\forall j \in M : \Delta t_j = t_{j,1} - t_{j,2} \quad \text{EQ. 5.5}$$

where:

$\Delta t_{j,1}$ and $\Delta t_{j,2}$ are the flow arrival times to the j^{th} first stage component from adjacent cavities.

Constraints

As outlined in the general problem formulation, the design variables are subject to three main types of constraints. The first constraint type, the geometric layout resulting from the molded assembly design and gate positions, determines the fixed lengths of runner channels.

The second constraint type considers the necessary condition for any injection molding process – complete mold filling. The satisfaction of this condition should be checked by a mold filling simulation. However, to minimize occurrence of molding defects such as air traps or racing effect, several empirical design relationships for runners have been established and commonly used by mold designers [13, 12, 60, 65, 79, 110]. The first important relationship constrains the minimum runner cross-section for sufficient cavity feed, according to Equation 5.6.

$$d_{feed} \geq s \cdot d_{part_cavity} \quad \text{EQ. 5.6}$$

where s is an empirical coefficient. Using $s = 1.0$ is reported as acceptable in most design cases. Therefore the latter value was selected in this approach, as it directly and largely influences the first optimization objective – runner volume. It is also worth noticing that this constraint is used as the lower boundary of the design variable corresponding to all the runner channels connected directly to the molding cavities. The second important empirical relationship for the runner design is the branching rule, expressed by Equation 5.7.

$$d_{feed} \geq d_{branch} \cdot B^{1/3} \quad \text{EQ. 5.7}$$

where B is the number of branches.

The above empirical dimensional runner design rules can be easily encoded as a set of linear inequalities and/or lower bounds for the design variables. The upper boundaries should be set with regard to the geometrical layout constraints; they are, however, not expected to be active, due to the minimum volume objective.

The final constraint type considers the parameters of manufacturing resources available to the optimized design. This includes the minimum sprue diameter, determined by the size of the injection nozzle, or minimum runner diameters due to the tooling sizes available for mold manufacturing without increasing its cost.

5.4 Computational Experiment

In order to investigate the optimization solution methods, the developed model was applied to a case study of an in-mod assembly of a MAV multi-material drive mechanism. This section presents the implementation of the optimization approach, which in many dimensions is highly dependent of the particular design case. First, the computational framework is shortly described. Next, the details of the case study are introduced, followed by the design representation details. Finally, the details of optimization approach applied to the case study are described. This includes the development of a custom mold filling simulation based on a pressure meta-model for the second objective evaluation, as well as the details of constraints formulation.

5.4.1 Computational Framework

The main computation environment utilized in this study was the MathWorks[®] Matlab[®] R2010a software. The optimization routines were performed using Matlab[®] Optimization Toolbox. The custom mold filling simulation was also developed using

Matlab[®]. Autodesk[™] MoldFlow[®] Insight software was used to develop the pressure meta-model and validate the custom simulation results. All calculations were performed on personal computers with Intel[®] Core[™]2 Duo processors with minimum clocking frequency of 2.2 GHz. All computers used Microsoft[®] Windows[®] XP SP3 32-bit operating systems.

5.4.2 Case Study: Multi-Material MAV Drive Frame

This sub-section introduces the details of the case study and the design representation. The multi-material compliant mechanism used as a drive mechanism on a MAV platform was considered as a representative case study. The mechanism consisted of six compliant joints molded in the first stage of the process and seven rigid links molded during the second stage. Link cavities were separated by the pre-molded hinges, which resulted in a complex molding system. The design of the in-mold assembled mechanism was described in great detail in Chapter 4 of this dissertation.

The mold cavity (sprue, runners, gates and cavities) was represented as a tree structure. The tree edges represent channels of constant diameter and specified length, and the nodes carry the information about the node type. The mold cavity CAD model with marked nodes and the corresponding tree structure are shown in Figure 5.4. Node types are defined in a vector $\mathbf{N_TYP}$, where i -th element is a node type of the i -th node. The values of $\mathbf{N_TYP}$ vector corresponding to node types are as follows: (1) injection point; (2) node where flows split; (4) intermediate node, where flow is entering a cavity of a different size, or the node is required for determination of the time when the flow reaches a certain point of a cavity for

constraint satisfaction in the optimization routine; and (0) terminal node, where flow reaches the end of the channel. The edges of the tree are defined in matrices of diameters and lengths in [inch], **Dia_inch** and **Length_inch** respectively. These matrices have nN columns, where nN is the total number of nodes, and $nParNmax$ rows, where $nParNmax$ is the highest parent node number in the tree. The matrices corresponding to the tree structure from Figure 5.4 are shown in Figure 5.5.

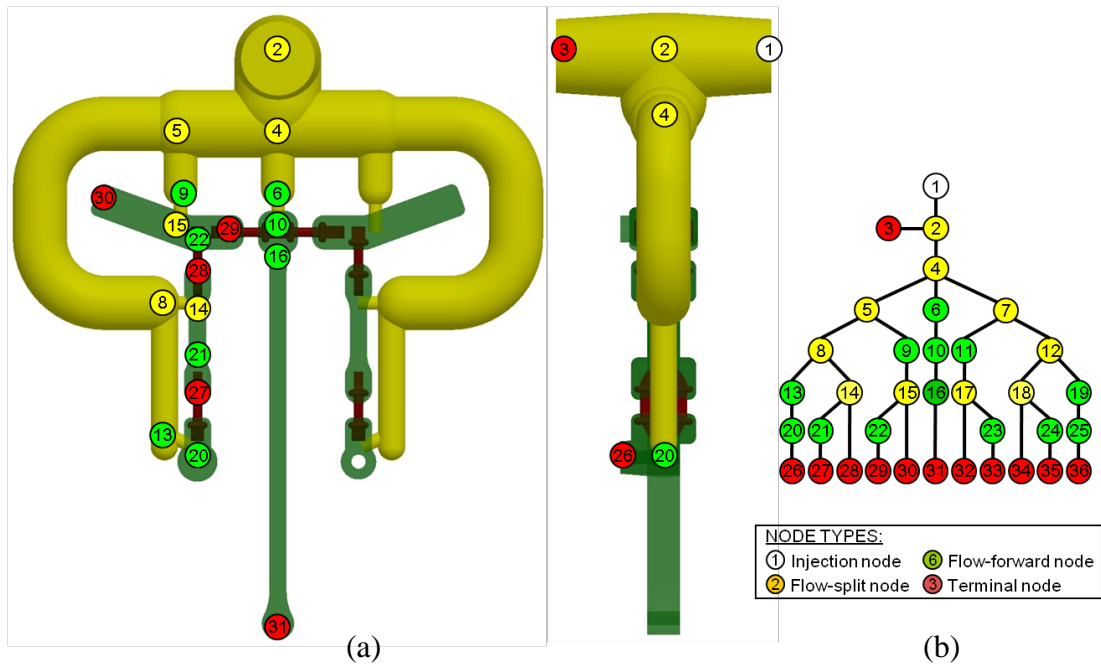
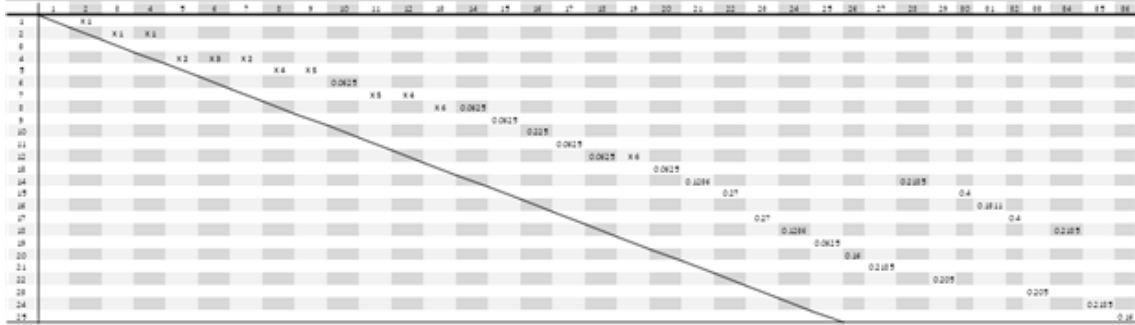
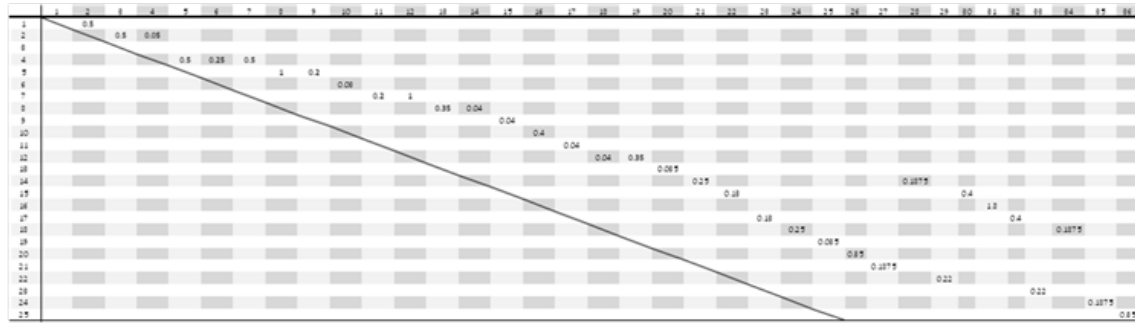


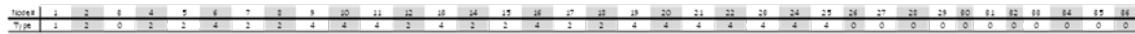
Figure 5.4 Molding system for In-mold assembly of MAV drive frame: (a) CAD model with marked nodes and (b) corresponding tree structure



(a)



(b)



(c)

Figure 5.5 Matrix representation of the molding system: (a) edge diameter in inches, (b) edge length in inches, and (c) nodal type

5.4.3 Implementation of Design Optimization Approach

This sub-section presents the detailed implementation of the runner optimization mathematical formulation presented in Section 5.3 on the case study presented in Section 5.4.2.

Parameters

The global optimization parameters of the presented case study contained all the fixed values used throughout the optimization process. This included the molding

representation, described in Section 5.4.2, with the values of runner dimensions represented by the design variables set to zero. The node sets for flow arrival time comparison objective were defined as (10, 22), (14, 22) and (20, 21). The material properties for the mold filling simulation were stored in a pressure meta-model, described in more detail in Section 5.4.4. Finally, the injection molding processing parameters corresponding to the available equipment have been defined to match the characteristics of Babyplast® injection molding machine used for the in-mold assembly of the case study. These parameters are listed in Table 5.1.

Table 5.1 Injection molding processing parameters used in the case study

Parameter	Unit	Value
Injection flow rate (constant)	m^3/s	1.19e-5
Injection temperature	C	285
Velocity/pressure switch-over	MPa	150
Maximum injection volume	cm^3	6.786

Design Variables

The design variable vector X consists of the values of runner channels' diameters. Due to the layout constraints, the runner channel lengths are fixed before the optimization as global parameters. The assignment of the design variables to the runner radiuses according to Equation 5.1 is defined by Equations 5.8 to 5.13 and visually shown in Figure 5.6.

$$x_1 = R_{(1,2)} \quad \text{EQ. 5.8}$$

$$x_2 = R_{(4,5)} \quad \text{EQ. 5.9}$$

$$x_3 = R_{(4,6)} \quad \text{EQ. 5.10}$$

$$x_4 = R_{(5,8)} \quad \text{EQ. 5.11}$$

$$x_5 = R_{(5,9)} \quad \text{EQ. 5.12}$$

$$x_6 = R_{(8,13)} \quad \text{EQ. 5.13}$$

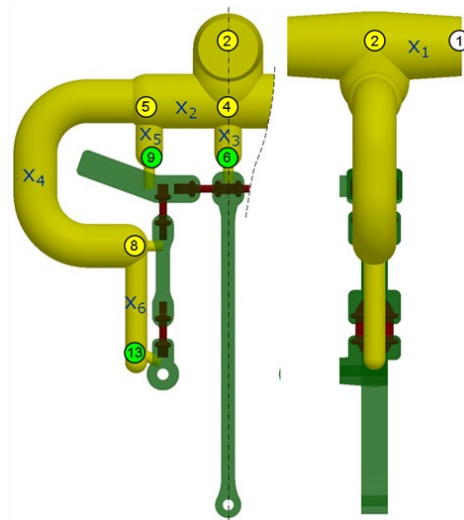


Figure 5.6 Case study design variables' assignment

Objective Functions

The first objective to be minimized was defined as the runner system volume by Equation 5.2 as the sum of volumes of all runner channels. This objective function is defined for the case study as:

$$\text{Min. } V = V_{(1,2)} + V_{(2,3)} + V_{(2,4)} + V_{(4,6)} + 2 \cdot (V_{(4,5)} + V_{(5,8)} + R_{(5,9)} + R_{(8,13)}) \quad \text{EQ. 5.14}$$

where:

$$V_{(1,2)} = \pi \cdot x_1^2 \cdot L_{(1,2)} \quad \text{EQ. 5.15}$$

$$V_{(2,3)} = \pi \cdot x_1^2 \cdot L_{(2,3)} \quad \text{EQ. 5.16}$$

$$V_{(2,4)} = \pi \cdot x_1^2 \cdot L_{(2,4)} \quad \text{EQ. 5.17}$$

$$V_{(4,5)} = \pi \cdot x_2^2 \cdot L_{(4,5)} \quad \text{EQ. 5.18}$$

$$V_{(4,6)} = \pi \cdot x_3^2 \cdot L_{(4,6)} \quad \text{EQ. 5.19}$$

$$V_{(5,8)} = \pi \cdot x_4^2 \cdot L_{(5,8)} \quad \text{EQ. 5.20}$$

$$V_{(5,9)} = \pi \cdot x_5^2 \cdot L_{(5,9)} \quad \text{EQ. 5.21}$$

$$V_{(8,13)} = \pi \cdot x_6^2 \cdot L_{(8,13)} \quad \text{EQ. 5.22}$$

The second objective to be minimized was defined using Equation 5.4 as the maximum of the flow arrival time difference defined for points where the second stage flow meets the first stage component. Polymer's resistance to flow in the channel is a coupled function of viscosity, flow rate, temperature distribution (frozen layer), and channel size. Therefore, analytical calculation methods are not suitable for evaluation of this objective, and therefore mold filling simulation has to be used to estimate the times of flow arriving to the pre-molded components. In the investigated case study, the flow arrival time differences corresponding to Equation 5.5 are:

$$\Delta t_1 = t_{(10)} - t_{(22)} \quad \text{EQ. 5.23}$$

$$\Delta t_1 = t_{(14)} - t_{(22)} \quad \text{EQ. 5.24}$$

$$\Delta t_1 = t_{(20)} - t_{(21)} \quad \text{EQ. 5.25}$$

The second objective to be minimized is therefore the maximum absolute value of the time differences represented by Equations 5.23 to 5.25.

Constraints

To satisfy the complete mold filling necessary condition for any injection molding process, mold filling simulation needs to be performed. Satisfaction of this constraint was checked by the custom mold filling simulation described in Section 5.4.5 and verified by a 3D MoldFlow[®] simulation.

To further ensure the mold filling on the design variable level and minimize the occurrence of molding defects such as air traps or racing effect, the empirical design relationships for runners have been incorporated as both linear inequality constraints, as well as lower bounds for the design variables.

The first empirical relationship represented by Equation 5.6 constrains the minimum runner cross-section for sufficient cavity feed. In the considered case study, this equation has to be applied to all the design variables related to runners directly connected to the final part cavities:

$$x_3 \geq R_{(10,16)} \quad \text{EQ. 5.26}$$

$$x_4 \geq R_{(14,28)} \quad \text{EQ. 5.27}$$

$$x_5 \geq R_{(15,30)} \quad \text{EQ. 5.28}$$

$$x_6 \geq R_{(20,26)} \quad \text{EQ. 5.29}$$

The second empirical relationship, represented by Equation 5.7, considers the channel branching rules. In the considered case study, this equation was applied to all the design variables related to runner branches connected to a supplying channel:

$$x_1 \geq 3^{1/3} \cdot \frac{2 \cdot x_2 + x_3}{3} \quad \text{EQ. 5.30}$$

$$x_2 \geq 2^{1/3} \cdot \frac{x_4 + x_5}{2} \quad \text{EQ. 5.31}$$

$$x_4 \geq 2^{1/3} \cdot \frac{R_{(14,28)} + x_6}{2} \quad \text{EQ. 5.32}$$

$$x_5 \geq 2^{1/3} \cdot R_{(15,22)} \quad \text{EQ. 5.33}$$

It is important to note here, that Equation 5.33 is superior to Equation 5.29, meaning that the latter can be omitted, as it can never be active. This is due to the runner layout design, where the gate is positioned in the middle of the cavity, and hence the runner supplies “split” cavities.

Next, the direct geometric layout constraints between the design variables were modeled. This concerned the diameters of runners (4, 6) and (5, 9) in Figure 5.4, as their relative axis distance was fixed by the gate layout design to be 0.45 [inch]. The minimum distance between the runners was set to be 0.1 [inch], hence the inter-relationships becomes:

$$x_3 + x_5 + 0.1 \leq 0.45 \quad \text{EQ. 5.34}$$

The minimum sprue diameter (x_1) was constrained by the injection nozzle diameter to be 0.2 [inch]. The remaining otherwise directly unbounded design variable (x_2) was constrained by the tooling sizes available for mold manufacturing without increasing its cost to be 1/32 [inch].

The upper boundaries in this case study were set to be all with regard to the geometrical layout constraints; they are, however, not expected to be active, due to the minimum volume objective.

The final linear inequality constraints are simplified to Equations 5.35-38, and the upper and lower boundaries are listed in Table 5.2.

$$g_1 : -x_1 + (2 \cdot C_3) \cdot x_2 + C_3 \cdot x_3 \leq 0 \quad \text{EQ. 5.35}$$

$$g_2 : -x_2 + C_2 \cdot x_4 + C_2 \cdot x_5 \leq 0 \quad \text{EQ. 5.36}$$

$$g_3 : -x_4 + C_2 \cdot x_6 - C_2 \cdot D_{28}^{14} \leq 0 \quad \text{EQ. 5.37}$$

$$g_4 : x_3 + x_5 - 0.35 \leq 0 \quad \text{EQ. 5.38}$$

where the C's are constants: $C_2 = 2^{1/3}/2$ and $C_3 = 3^{1/3}/3$

Table 5.2 Case study design variables upper and lower boundaries (in inches)

Boundary	x_1	x_2	x_3	x_4	x_5	x_6
Upper	0.49	0.49	0.49	0.49	0.49	0.49
Lower	0.2	0.033	0.225	0.2185	0.3402	0.16

5.4.4 Development of Pressure Meta-Model

The material properties required for the mold filling simulation were stored as global parameters in form of the pressure meta-model. The pressure building up in the filled channel is a function not only of the polymer properties affecting its viscosity, but also external variables, including the constant flow rate, channel cross-section and the flow elapsed length. The meta-model was built based on the measurements of pressure increase from 1D MoldFlow[®] simulations. The simulations were done for a range of flow rate values and channel diameters, and in all cases the channel length was defined to be 100 mm. Due to the fact that the runner system is considered as the production waste and its volume should be in general minimized, this value was assumed sufficient to cover maximum length of a

single runner. A series of simulations were performed in MoldFlow[®], each consisting of 400 beam elements (0.25 mm). The meta-model has to be built for each material used. In this study, pressure meta-models for two materials were developed: Lanxess Lustran ABS 680 and 15% glass fiber filled PA6,6 (DuPont EP Zytel DMX 61G15H BK407 MoldFlow verified material). Simulation parameters are listed in Table 5.3.

Table 5.3 Simulation parameters used for building the meta model

Parameter	Unit	Value(s)	
Injection flow rates	cm^3/s	1, 2, 4, 8, 12	
Runner entity diameters	<i>inch</i>	1/32, 1/16, 1/8, 1/4, 3/8, 1/2	
Material	-	ABS	GF-PA6,6
Melt temperature	<i>C</i>	260	285
Mold temperature	<i>C</i>	25	25
V/P switch-over	<i>MPa</i>	150	150

After running the simulations, the “Pressure” results were read manually into a separate spreadsheet for each of standard 24 frames offered by MoldFlow[®], along with corresponding flow front progression measured by the closest node coordinates. Since these results contained non-uniform values for flow front progression, they had to be normalized before placing them into the meta-model. This was performed using linear interpolation in Matlab[®] to result in uniformly spaced flow front progression values. Finally, the 3D array $\mathbf{MM_PRESS}_{[21 \times 6 \times 6]}$ of pressure drop values in [Pa] was composed, along with the axis labeling vectors $\mathbf{MM_X}_{[1 \times 21]}$, $\mathbf{MM_Y}_{[1 \times 6]}$ and $\mathbf{MM_Z}_{[1 \times 6]}$, corresponding to flow front progression in [m], flow rate in [m^3/s] and channel diameter in [m], respectively. To ensure proper interpolation results, $\mathbf{MM_X}$

and **MM_Y** vectors and the **MM_PRESS** array had additional zero values added. All the units inside the meta-model were converted into SI units. The meta-model building flowchart is presented in Figure 5.7. The meta-model arrays were defined as global variables during the simulation to allow fast accessibility by the interpolation function described in Section 5.4.5.

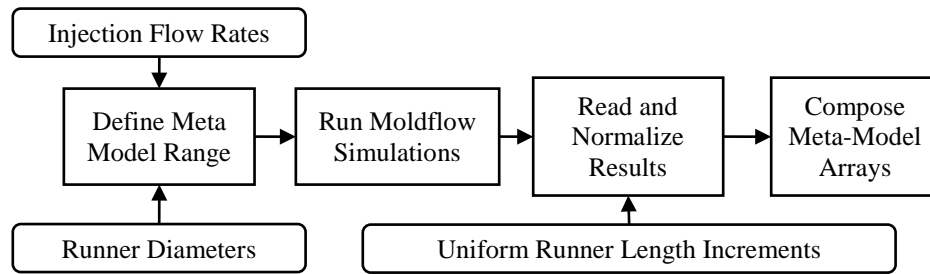


Figure 5.7 Meta model building flowchart

5.4.5 Development of Custom Mold Filling Simulation

To evaluate the second objective of the optimization problem developed in Section 5.3, a mold filling simulation had to be used to estimate the time difference of flows arriving at the first stage component from adjacent cavities during the second stage molding. In order to overcome the limitations of MoldFlow[®] simulation software, mainly the calculation time and issues concerning integration with external optimizers, a custom mold filling simulation was developed in Matlab[®] environment. The simulation was constructed as a function, operating on the tree representation of the molding system described in Section 5.4.2. The simulation function inputs were the runner design variables and a structure of global parameters, described in Section 5.4.3. This structure included the pressure meta-model described in

Section 5.4.4. The general output of the function was a vector of flow arrival times to all the nodes in the tree representation. From these values, the time differences of flow arrivals to the pre-molded component were calculated and transformed to their absolute values. Finally, the maximum of these values was returned as the function output. The simulation flowchart is presented in Figure 5.8.

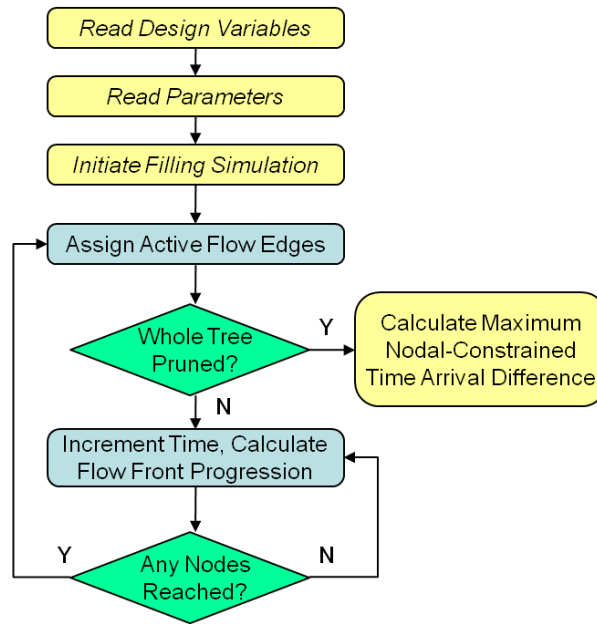


Figure 5.8 Flowchart for estimation of nodal flow arrival times

The function begins with reading the current design variables, supplied by the optimizer for evaluation. These variables are assigned to the corresponding entries in the molding representation. For faster computation, the constant parameters are kept in the memory as global variables throughout the whole optimization procedure. The simulation begins with calculation of sprue filling time, as it is always a single channel, connected directly to the injection nozzle.

The mold filling simulation principals are as follows. The flow fronts are advanced in the channels with active flows in a time-step manner, and measured by the flow elapsed length. The flow advancement calculation is based on: (1) the total pressure build-up at the injection point as a result of the flow resistance in all of the channels with active flows, and (2) the conservation of a constant flow rate supplied by the machine. In each time step, for all the channels with active flows, the current pressure increase is interpolated linearly from the meta-model array. Then, the new flow rates are calculated, and the procedure is repeated until any of the active-flow channels are fully filled. Once any node is reached, the global filling time is assigned to the general output vector, and the node type is checked to determine the next action. There are three node types defined for the molding system representation, and the procedures undertaken based on the node type are as follows:

Flow-forward node – assigned to the points where the channel diameter changes. This is used for runner-gate and gate-mold cavity interfaces, as well as the change of effective diameter within the mold cavity itself. If this node is reached, the channel with just initiated flow advancement is assigned as active, and the procedure continues to check if this was the only node reached in the current time step. After all the reached nodes are checked, the time is incremented and the flow front advancement procedure is continued for the active tree edges.

Flow-split node – assigned to the points where the channel splits into two (or more) channels. This is used mainly for runner-runner interfaces, as well as the layout of the mold cavity itself. If this node is reached, the channels with just initiated flow advancement are assigned as active, and the flow rates for these channels are

determined. Due to the fact that the initial flow rate in the split channels is unknown, the simulation uses the initial resistance coefficients' matrix to assign the estimated flow rates. Since these initial coefficients are estimated based only on the channel radius (power four), they are inaccurate and hence, a convergence loop for the pressure drops was developed before advancing the flows. The convergence loop artificially advances the flow fronts for ten-times the simulation resolution time, and interpolates the resulting pressure build-up. Then, the statistics for convergence criterion evaluation are calculated: the mean and standard deviation of the interpolated pressures and the difference between them. If the convergence criterion is still violated, the flow rates are changed and the convergence procedure is repeated. All convergence parameters are adjustable. Finally, the procedure checks if this was the only node reached in the current time step, the time is incremented and the flow front advancement procedure is continued for the active tree edges.

Terminal node – assigned to the points where the channel ends. The procedure deactivates the flows in the filled edge and checks if there are any active edges down the stream from the parent node. If this is not the case, the tree is “pruned” until there is an active edge found. If the “pruning” reaches the injection node, the simulation stops and the outputs are calculated.

The simulation code was benchmarked on several mold cavity designs as described below. First, the procedure was tested on several designs composed of runners only. The comparison of these results with respect to MoldFlow[®] 1D simulations is presented. After obtaining satisfactory error in the nodal arrival times predicted by the simulation, it was then engaged to estimate the nodal arrival times in a complex

in-mold assembly molding system. The results were benchmarked against MoldFlow[®] 3D simulation. Common MoldFlow[®] simulation parameters are listed in Table 5.4.

Table 5.4. Common MoldFlow[®] simulation parameters used in validation studies

Parameter	Unit	Value(s)
Material	-	Lanxess Lustran ABS 680
Melt temperature	C	260
Mold temperature	C	25
V/P switch-over	MPa	150
Injection flow rate	cm ³ /s	12

Case Study I: Two-Runner System

In order to validate the developed simulation and determine the error in nodal flow front arrival times predictions, simple runner system geometry was initially used. The geometry consisted of a cold sprue and two runners of the same length, but with different diameters. This system was modeled in MoldFlow[®] using 1D beam elements with appropriate diameters, each 0.25 mm long. The parameterized molding system tree is shown in Figure 5.9 (a) and the corresponding MoldFlow[®] study geometry is presented in Figure 5.9 (b).

MoldFlow[®] filling simulation was performed and the nodal arrival times were manually read from the “Fill time” result set. For this study, MoldFlow[®] filling simulation took 70.5 seconds, including mesh generation.

The developed custom mold filling simulation with time increment set to be 0.0005 seconds took 3.1 seconds of calculation time. The nodal arrival times resulting from both approaches are listed in Table 5.5.

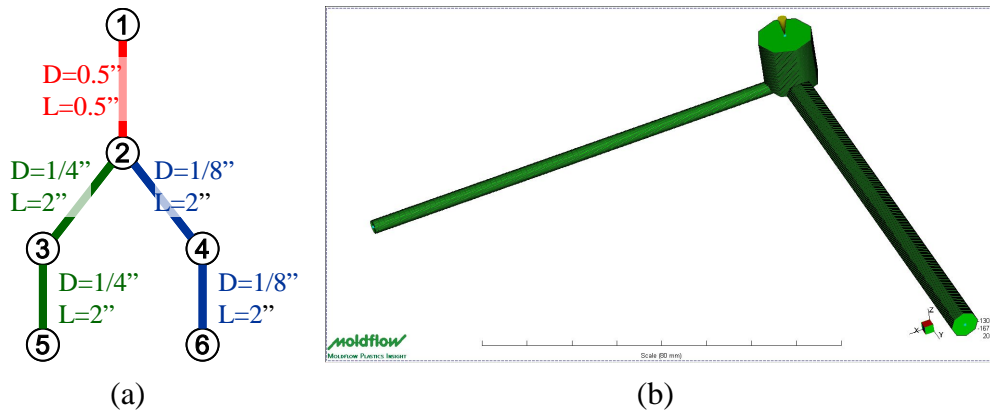


Figure 5.9 Molding system of case study I: (a) tree representation with dimensions and (b) corresponding MoldFlow[®] 1D filling study

Table 5.5 Case study I results comparison with MoldFlow[®] 1D simulation

Node #	Nodal Flow Arrival Times [s]		% diff.
	Custom code	MoldFlow [®] 1D	
1	0	0	-
2	0.1341	0.1339	0.1
3	0.2791	0.2885	-3.3
4	0.4291	0.4506	-4.8
5	0.4241	0.4415	-3.9
6	0.4591	0.4913	-6.6

This case study showed the applicability of the developed simulator to runner geometries with split channels. The acceptable accuracy (<7%) of evaluated arrival

times was obtained in roughly twenty-times less calculation effort than the 1D MoldFlow[®] simulation time.

Case Study II: Three-Runner System with Non-uniform Diameters

After successful application of the developed simulation to runner geometries with split channels, more complex runner system geometry was used to evaluate the error in nodal flow front arrival times prediction. The new geometry consisted of a cold sprue, a cold-slug-well, three runners of the same length, but with different diameters, each supplying a cavity of the same length and circular cross-section. This system was also modeled in MoldFlow[®] using 1D beam elements with appropriate diameters, each 0.25 mm long. The parameterized molding system tree is shown in Figure 5.10 (a) and the corresponding MoldFlow[®] study geometry is presented in Figure 5.10 (b).

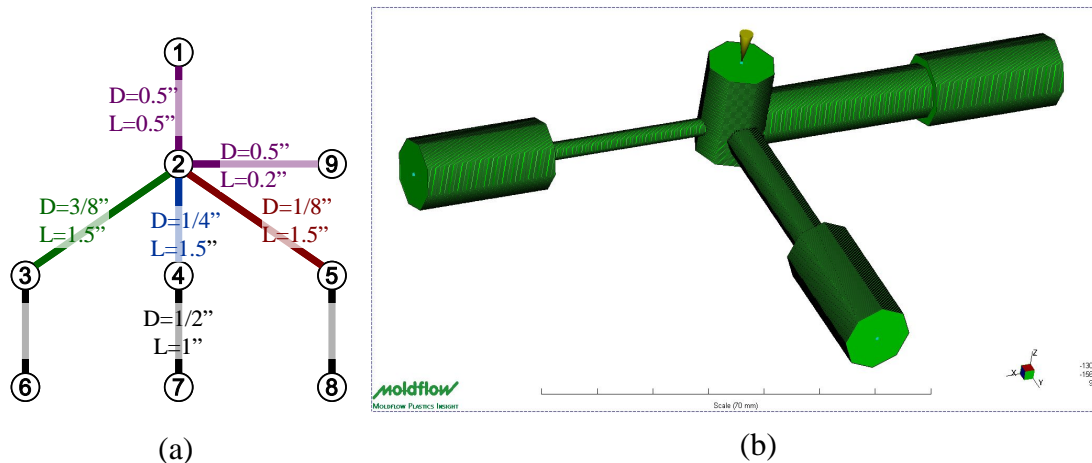


Figure 5.10 Molding system of case study II: (a) tree representation with dimensions and (b) corresponding MoldFlow[®] 1D filling study

MoldFlow[®] filling simulation was performed and the nodal arrival times were manually read from the “Fill time” result set. For this study, MoldFlow[®] filling simulation took 73.4 seconds, including mesh generation.

The developed custom mold filling simulation with time increment set to be 0.0005 seconds took 5.6 seconds of calculation time. The nodal arrival times resulting from both approaches are listed in Table 5.6.

Table 5.6 Case study II results comparison with MoldFlow[®] 1D simulation

Node #	Nodal Flow Arrival Times [s]		% diff.
	Custom code	MoldFlow [®] 1D	
1	0	0	-
2	0.1341	0.1348	-0.5
3	0.4896	0.4920	-0.5
4	0.7891	0.7625	3.5
5	1.0286	1.1210	-8.2
6	0.8026	0.8185	-1.9
7	1.0791	1.0915	-1.1
8	1.3466	1.3920	-3.3
9	0.2186	0.2145	1.9

This case study showed applicability of the developed simulator to runner geometries with multiple channels of varying diameters. Still acceptable accuracy (<9%) of evaluated arrival times was obtained in roughly twenty-times smaller calculation time when compared to MoldFlow[®] 1D filling simulation result.

Case Study III: In-mold Assembly of MAV Frame Molding System

After successful validation of the developed simulation, it was finally used to predict flow front arrival times on a complex in-mold assembly molding system. The tree representing the molding system consisted of 31 nodes, with the maximum parent node number equal to 22. This system was also imported into MoldFlow[®] 3D study using IGES file exported from a Pro/Engineer[™] 4 solid CAD model. The part meshing resulted in 47533 tetrahedral elements. The molding system tree is shown in Figure 5.11 (b) and the corresponding solid model is presented in Figure 5.11 (a).

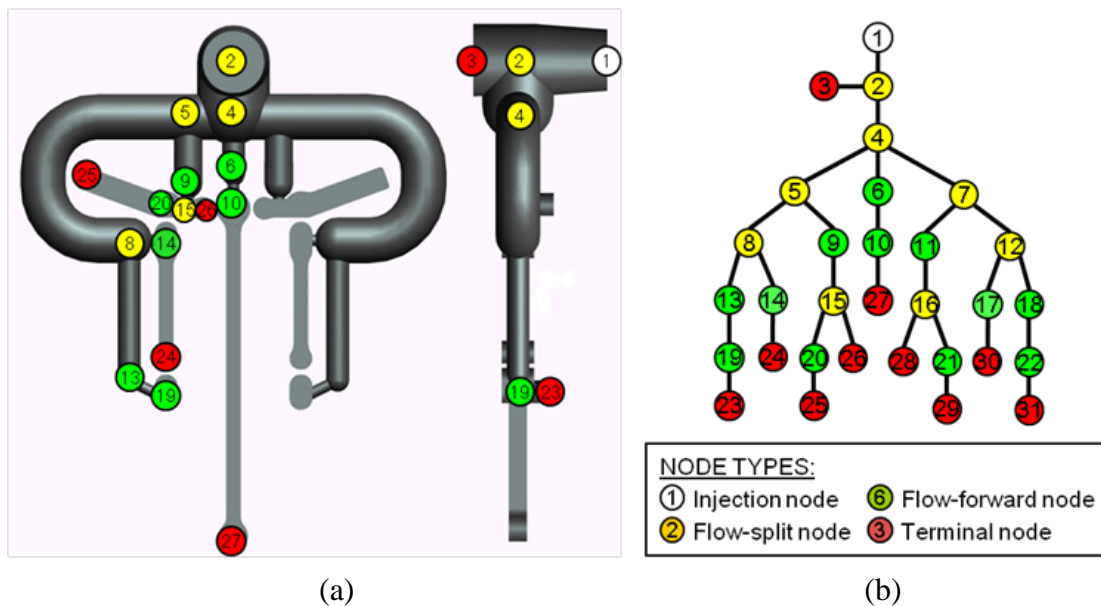


Figure 5.11 Molding system for In-mold assembly of MAV drive frame: (a) CAD model with marked nodes and (b) corresponding tree structure

MoldFlow[®] filling simulation was performed and the nodal arrival times were manually read from the “Fill time” result set. For this study, MoldFlow[®] filling simulation took 317 seconds, and mesh generation took additional 26 seconds.

The developed custom mold filling simulation with time increment set to be 0.0005 seconds took 98 seconds of calculation time. The nodal arrival times resulting from both approaches are listed in Table 5.7.

Table 5.7 Case study III results comparison with MoldFlow[®] 3D simulation

Node #	Nodal Flow Arrival Times [s]		% diff.
	Custom code	MoldFlow [®] 3D	
1	0	0	-
2	0.086	0.0938	9
3	0.172	0.16	-7
4	0.181	0.17	-6
5	0.203	0.19	-7
6	0.267	0.25	-11
8	0.490	0.45	-9
9	0.288	0.28	-3
10	0.281	0.305	8
13	0.591	0.508	-16
14	0.497	0.47	-6
15	0.289	0.3	4
19	0.592	0.52	-14
20	0.370	0.43	14
23	0.601	0.565	-6
24	0.609	0.565	-8
25	0.470	0.51	8
26	0.370	0.44	16
27	0.619	0.58	-7

This case study showed the applicability of the developed simulator to complex runner geometries, supplying multiple cavities for in-mold assembly process. Even

for a fairly complex runner layout design the developed simulator's calculation time was three times faster than the MoldFlow[®] 3D filling simulation. The accuracy of nodal arrival time estimation was within 16% of error range.

The simulator was shown to be sufficiently accurate in evaluation of the range of filling times between distinct points of the molding system. This provided valuable information on the nodal flow arrival times for the multi-material molding system evaluation in runner system optimization.

5.5 Evaluation of Potential Solution Methods

This section presents the analysis of optimization methods pre-selected to solve the runner optimization problem presented in Section 5.3 based on the case study presented in Section 5.4.2. First, the in-mold assembly specific runner optimization considerations are described, along with identification of the rationale for selecting candidate solution methods. Next, the optimization methods are compared based on a relative ranking. The considered performance measures include the solution quality, calculation time, robustness, and scalability. Based on the ranking, the best approach to the runner optimization problem is selected. Finally, the results from the selected approach are presented and discussed.

5.5.1 Identification of Optimization Approaches

In order to select the candidate design optimization methods to solve the runner optimization problem described in Section 5.3, several issues specific to the nature of the defined problem had to be considered.

The first important consideration comes from the fact, that the second objective function (Equation 5.4) requires involvement of a mold filling simulation to estimate the times of flow arriving to the pre-molded components. This objective returns the maximum of time differences recorded for flows arriving at multiple pre-molded components (or nodal pairs) residing in the second stage mold. Since the objective does not differentiate between the constrained node pairs and their assignment to the pre-molded component, only returns the maximum of recorded differences, the solution space for this objective becomes discontinuous. The discontinuity of the design space creates a concern about the globality of the obtained result, as many of the optimization methods can obtain local minima only.

The second important consideration is the objective space dimension. The first objective, minimization of the runner volume, is intuitive and logical for any of the runner optimization approach, as its goal is to minimize the production waste. The economical and environmental importance of this objective was described in Section 5.1. The second objective, on the other hand, is very specific to the in-mold assembly process of multi-material mechanisms. As mentioned in the above paragraph, this objective does not consider the actual location of the maximum flow arrival time difference, or in other words, a specific pre-molded component experiencing the directional force filed during unbalanced mold filling. Such constructed objective is suitable for cases where the first stage components are dimensionally similar and their positioning features are comparable. However, if there is a rational justification for minimizing the flow arrival differences for particular pre-molded components separately, the problem becomes multi-objective,

with the number of objectives equal to the number of separately minimized flow arrival time differences, plus one, the minimum volume objective. Then, however, the multi-dimensionality of the objectives poses its additional implementation challenges, such as relative weighting of these objectives, or selection criteria for the optimal solution with respect to all the objectives considered.

Therefore, the general formulation of the second objective function developed in Section 5.3 results in only one value, the maximum of absolute values of the flow arrival time differences to all of the pre-molded components to maintain the generality of the formulated problem by keeping the number of joints to be in-mold assembled into the multi-material compliant mechanism unconstrained. Additionally, treating the first stage components of the in-mold assembled mechanism equally in terms of flow arrival times allows for the component's design unification, and hence, reduces the level of the first stage component identification prior to positioning inside the second stage mold. This concern applies only to cavity transfer methods. The alternative are morphing cavity methods, which are fully automated, however they require very complex and expensive mold designs and auxiliary equipment. In the presented case study, the load transfer capabilities required for the hinges were similar; therefore a uniform hinge design was used in multiple positions of the mechanism.

The final optimization consideration is due to the complexity of the runner system, which requires special runner design rules to be incorporated into the optimization. Since these rules can be easily defined as a set of linear inequalities, as described in Section 5.4.3, it is desirable for the optimization method to handle such constraints.

Therefore, in order to solve the complete problem, only constrained optimization approaches were considered as candidates.

In summary, the solution approaches for the developed runner optimization model need to satisfy the requirements: (1) ensure the globality of solutions for the discontinuous simulation-evaluated objective space, (2) allow for minimization of at least two objectives without their relative weighting, and (3) allow for linear inequality constraints to be incorporated as the result of design rules for complex runner systems.

Multiple optimization methods readily offered by the Matlab[®] Optimization Toolbox were examined for their compliance with the above requirements.

All gradient-based optimization approaches were identified as not suitable for solving the considered problem for two main reasons. First, the solutions obtained by these methods are only locally optimal and sensitive to the provided initial solution. If the optimizer is initialized in one of the discontinuous solution space regions, it is not able to explore the remaining solution spaces, and hence, its solution is only as good as the guess about the starting point. This issue can be theoretically addressed by supplying the optimizer with large enough number of starting points. However, due to the non-linear nature of the second objective, the globality of the obtained result is never guaranteed and can be only assumed based on the coverage of the design space by the resolution of design variables and their combinations at the starting points. This, however, makes the calculation efforts highly inefficient, as the majority of the feasible design solution space would have to be explored in order to claim the global optimality of results. The second important reason against gradient-

based methods is the internal gradient calculation. Since the second objective value has to be evaluated by simulation, the gradients cannot be determined and modeled as equations upfront. This results in additional calculation effort from the optimization method to estimate the gradient using numerical techniques. Additionally, multi-objective optimization problem needs to be converted to a single-objective model in order to be solved using gradient-based methods. One example of such conversion is the weighted-sum method, where multiple objectives are combined into a single fitness value by weighting coefficients. The quality of such obtained solution is however sensitive to the values of fitness coefficients assigned to the objectives and carries the risk of decreasing the importance of design points resulting in the minimum of each of the separate objectives. Therefore, the gradient-based methods are not preferred solution approaches for the developed runner optimization problem.

To overcome the limitations of the gradient-based methods, the genetic algorithm (GA)-based optimization methods were considered. The main advantage of these methods is the near-global optimality of the obtained solutions. GA can easily operate on the discontinuous design space by evaluation of all the design points within the generation with respect to the objectives, selecting and storing the best solutions between the generations, and changing the ‘non-optimal’ design points for design space exploration. The ‘changing’ is performed by a selected mutation and/or crossover functions with appropriate parameters.

Since the defined optimization problem needs to consider two objectives, multi-objective genetic algorithm (*MOGA*) optimization approach was expected to be the most suitable for obtaining optimal solutions. The main advantage of *MOGA* when

compared to the single-objective GA's is its simultaneous relative fitness function comparison, where the candidate optimal solutions (Pareto-solutions) are selected based on gain in one objective without increasing the other. As a result, multiple Pareto points are returned, and the optimal solution has to be chosen based on the rational criteria concerning the nature of the particular design problem. The Pareto front also provides useful information about the solution space, which is different for every design case, namely the actual trade-off between the objectives for the feasible solutions. It is also worth to note here, that the built-in Matlab[®] *MOGA* function (*gamultiobj*) does not handle non-linear constraints; therefore the ability to write the runner design rules as linear inequalities is an important factor terms of possible solution method selection. Additionally, *MOGA* has slightly different stopping criteria than the single objective GA, namely the spread of Pareto-solutions, and not the average change in the single objective over a pre-defined number of stall generations. This difference requires the objectives to be properly scaled, and the exit parameters adjusted to the absolute fitness function values.

In order to rationalize the results obtained by *MOGA*, a combinatory of single objective GA optimizations were also considered. This involved minimizing one of the objectives with the second either omitted or constrained to a certain value or a value range.

The methods for minimizing only a single objective were employed to investigate the minimum feasible values for each of the objectives independently, and the ones with one of the objectives treated as a constraint were envisioned to explore the feasible solution space.

In case of minimizing the runner volume, it is logical to constrain the maximum nodal arrival time difference to one fixed value. This ensures that the cumulative directional force exerted on the first stage component does not cause its positioning features to deform elastically and the pre-molded insert does not displace during the second stage mold filling. On the other hand, constraining the volume to minimize the flow arrival times requires more complex approach, as fixing only the maximum runner volume is very probable to result in sub-optimal solutions with respect to the production waste. To overcome this issue, ϵ -constrained method can be used with the approach to explore the feasible design space by minimizing the flow arrival times for certain ranges of runner volume. This can be realized by setting the ϵ -constrained volumes and ϵ values to form intervals for which the flow arrival time is minimized. The intervals, centered at the constrained values and 2ϵ wide, should cover the feasible solution space for the exploration of possible OF#2 minima. Since the runner volume is a monotonic function of the particular design variables, the minimum and maximum values can be obtained using the upper and lower DV boundaries. This, however, does not consider the feasibility of solutions with respect to the linear constraints, which can result redundant exploration of infeasible design space. Additionally, depending on the value of the upper DV boundaries set, some ϵ -constrained intervals can be also redundant, as they can explore sub-optimal runner volumes. Therefore some additional calculation effort is required to set the ϵ -constrained intervals to the feasible and acceptable runner volume range.

The optimization approaches considered in this investigation are listed in Table 5.8.

Table 5.8 Notation for optimization methods' exploration

Method	Objective Function		Matlab[®]	Comments
	Symbol	Volume	MaxNATD	
<i>GA_Vu</i>	OF	-	ga	
<i>GA_VcT</i>	OF	Constrained	ga	<i>MaxNATD</i> value constrained
<i>GA_Tu</i>	-	OF	ga	
<i>GA_TcV</i>	Constrained	OF	ga	Epsilon-Constrained Method
<i>MOGA</i>	OF	OF	gamultiobj	
<i>GB_Vu</i>	OF		fmincon	
<i>GB_Tu</i>		OF	fmincon	

5.5.2 Performance Metrics Identification

In order to compare the relative performance of methods in terms of solving the runner optimization of multi-cavity molds, a rank table was constructed and the approaches were assigned a grade for each of the performance measures. The considered performance metrics were divided into two categories – primary and secondary. The primary performance metrics considered the quality of the obtained solution and the calculation effort required to arrive at these solutions. The secondary performance metrics considered the optimization method scalability to more complex runner system designs and the robustness of the approaches, measured by the repeatability of results. The range of ranking values assigned to the each of the methods was defined as a set of integers {0, 1, 2}. The symbolic assignment of the performance metrics along is presented in Table 5.9.

Table 5.9 Performance metrics of the optimization approaches

Importance	Performance Metric	Symbol
Primary	1. Solution quality	PPM1
	2. Computation time	PPM2
Secondary	3. Scalability	SPM1
	4. Robustness	SPM2

PPM1: Solution Quality

The first primary performance metric was the solution quality. The quality measures being considered included the following: (1) the absolute and relative significance of attained objective function value(s), (2) the level of constraint satisfaction, and (3) handling of both objectives.

Gradient-based optimization approaches obtain a solution by changing the values of design variables and calculating the gradient of the objective to find the search directions until the objective cannot be further minimized without violation of constraints. Due to this fact, the resulting solution is only a local optimum, highly dependent on the starting point. As mentioned before, the design space can be explored by invoking the optimization process from many different starting points. This, however, poses serious concerns about right selection of these starting points, their amount, resolution, and the actual globality of results achieved. Additionally, handling more than one objective requires the definition of their relative importance before the optimization is initiated, which is not desired in the runner optimization described in this chapter. Due to the above reasons, along with the discontinuity of the design space resulting from the simulation-evaluated objective, the quality of

gradient-based optimization solutions (GB_Vu and GB_Tu) was ranked the smallest possible, {0}.

The investigated GA-based approaches for minimizing only one of the objectives without considering the other, namely GA_Vu and GA_Tu , were also low-ranked {0} in terms of the results quality. This assignment was dictated by the dual nature of the optimization and the concern about approach generality. The objectives may or may not be conflicting, depending on the specific in-mold assembly design, for which the runner system is optimized. If the objectives are not conflicting, the single objective runner volume minimization (OF#1) can be performed without utilization of computationally expensive mold-filling simulation (OF#2). However, the assessment whether the objectives are conflicting or not has to be rationalized. This can be achieved by separately minimizing both OF#1 and OF#2 and comparison of results. As an effect, both GA_Vu and GA_Tu methods have to be engaged anyway just to justify using one of them. Then, if the objectives are found to be in fact conflicting, other methods concerning both OF's have to be additionally used to verify the possible trade-offs. It is however necessary to note that the single objective optimization approaches (GA_Vu , GA_Tu) arrive to the absolute recorded minimum the most efficient manner. This is possible due to the elimination of one of the objectives from being evaluated, as well as the fact that no relative comparison between the OF values is being performed.

The GA-based approaches for minimizing one of the objectives with the second one being treated as a constraint, namely GA_VcT and GA_TcV , were ranked in terms of the results quality the middle of the scale, {1}. In these methods, both of the

objectives were considered which is required for the defined runner optimization problem. However, setting the values of the OF to be treated as a constraint requires engagement of additional design solution space exploration methods before initializing the optimization, for example using both *GA_Vu* and *GA_Tu* approaches in parallel. This is needed to avoid constraining the OF to an infeasible or sub-optimal solution space, which would cause the optimizer's efforts to find a feasible solution to be respectively either pointless or redundant.

MOGA, the multi-objective GA-based approach for minimizing simultaneously both of the OF's was awarded the highest rank {2} in terms of the quality of solutions. The main reason behind this decision is the ability of unbiased minimization of both objectives simultaneously, which is highly required in the optimization of runner systems for the in-mold assembly process. *MOGA* returns the results in form of a set of multiple, non-dominated solutions, which can be plotted as a Pareto frontier to visualize the trade-offs between the objectives. The trade-offs can be then analyzed to select the optimal solution with respect to the specific character of the runner design being considered. Also, *MOGA* handles any discontinuities of the solution space, as it does not calculate gradients between the solutions. Due to the fact that individual solutions undertake mutation and crossover transformations between the generations, the exploration of the design space can be performed efficiently in the automated manner. Provided that the active optimization termination conditions are the ones concerning the required solution quality, *MOGA* guarantees the globality of the obtained results.

Several GA stopping criteria allow for controlling the quality of solutions. Provided no other termination criteria are defined or reached earlier, GA applies evolutionary algorithms on the intermediate solutions over consequent generations until the required solution quality is achieved. *MOGA* termination parameters concerning the solution quality include the maximum average change in value of the spread of Pareto set over consequent stall generations, and the number of stall generations.

On the other hand, optimization termination conditions which do not consider the solution quality include the maximum number of generations and the maximum allowed computation time. These however have to be used with extreme care. Depending on the complexity of the optimized design, as well as the type and resolution of the simulation engaged to evaluate the timing objective, the optimization routine may not be able to reach solutions of the desired quality within the constrained time or generation limit. Allowing these conditions to be the active stopping criteria requires detailed analysis of relative improvement in objective functions over the generations with respect to the required accuracy of the design variables and the physical and economical significance of the gain in the optimized runner system design.

PPM2: Computation Time

In GA-based optimization methods, the solution quality is coupled with the calculation effort required to arrive at the optimal solutions. This coupling is directly proportional to the complexity of the problem, as the number of design variables dictates the necessary number of individuals in the population to ensure the globality

of solutions and sufficient exploration of the design space. This coupling is additionally amplified by the need to involve a mold filling simulation to evaluate one of the objectives. Regardless of the simulation type, its execution time is directly proportional to the simulation resolution (linearly) and the complexity of the optimized problem (non-linearly). Therefore the computation time needed to arrive at the solution with prescribed optimization parameters was chosen as the second of the primary performance metrics used to evaluate the optimization solution methods.

The highest rank {2} was assigned to the runner system optimization approaches considering only the volume objective: the gradient-based *GB_Vu*, and GA-based *GA_Vu*. Since the OF#2 was not considered, the time-consuming simulation to evaluate it was not engaged in the optimization process. The runner volume (OF#1) is a monotonic quadratic function of the design variables and can be evaluated within small fractions of a second, which makes the optimization method to be the fastest of all considered in this study.

Several considered optimization methods had to be penalized with respect to their calculation time performance. These included *GA_VcT*, *GA_Tu*, *GB_Tu*, and *MOGA*, which all were assigned the middle ranking {1}. This was primarily due to involvement of simulation to evaluate the flow arrival times in each of the individuals, either as an objective or constraint.

The lowest rank {0} in terms of computation time was assigned to the *GA_TcV* method. This penalty is due to the fact, that a separate optimization routine needs to be invoked for each of the ε -constrained volumes. Hence, the total calculation time is a linear function of the number of intervals. Additionally, setting the ε -constrained

volumes and ε values forming the intervals for which the flow arrival time has to be minimized is not obvious and requires additional design solution space exploration before initializing the optimization. This is necessary to avoid ε -constrained volume intervals which do not contain feasible solutions or concern volume ranges which are sub-optimal from the manufacturing (waste) cost point of view.

SPM1: Scalability

The first secondary performance metric considered the scalability of the optimization methods to handle complex runner system designs. The main role of the runner system is to fill all the cavities with molten polymer supplied to the mold from usually one injection location, the nozzle. The runner system is designed for a particular part cavity layout; hence its complexity depends on the number of cavities to be filled during the second stage molding.

Considering the in-mold assembly of multi-material compliant mechanisms, where the layout is fixed and the number of cavities is equal to the number of links in the mechanism, the runner system complexity depends on the kinematic design of the final mechanism. This design also determines the mold design. As described in detail in Chapter 4 of this dissertation, it is always desired to minimize the number of mold pieces. The minimum number of two mold pieces is always required to allow for the solidified molding ejection. Therefore, runner systems are always designed to lie on the parting plane to reduce the number of mold pieces. If the extension of the runner system to the third dimension is necessary, it is always realized with channels perpendicular to one of the parting surfaces they connect. On the parting surface, runner channels can be laid out freely, constrained only by the final part design.

Due to the above, none of the considered runner optimization approaches were awarded the highest rank {2}, as their scalability is primarily dependent on the ability to incorporate all necessary runner design rules as constraints, specific to the optimized design case.

The middle rank {1} was assigned to all the methods involving the mold filling simulation, as the number of flow arrival times for the objective calculation is unconstrained. The optimization problem outlined in Section 5.3.1 defines the maximum of absolute values of differences in flow arrival to all of the pre-molded components as an objective to be minimized. This formulation can be therefore scaled to virtually any level of molding complexity, provided all time differences are treated equally. However, if there is a rational justification for minimizing the flow arrival differences for particular pre-molded components separately, the number of objectives increases. The multi-dimensionality of timing objectives requires development of additional methods for their relative weighting, or selection criteria for the optimal solution with respect to all the objectives considered, which is not addressed in this consideration.

The lowest rank {0} was assigned to the remaining methods, which did not include the timing objective (OF#2) in their formulation, namely *GB_Vu* and *GA_Vu*, as they serve only as supporting methods in the optimization problem outlined in Section 5.3.1.

SPM2: Robustness

The final performance metric used to evaluate runner optimization approaches considered their robustness measured by repeatability of results. The repeatability

was obtained by invoking the particular method for at least six times and comparing the results of each trial between each other.

The highest rank {2} was awarded primarily to the *GA_Vu* method. This is due to simplicity of OF#1 evaluation, which allows for orienting the optimization stopping criteria towards the best possible quality without noticeable increase in the calculation time.

The highest rank {2} was also assigned to the representative gradient-based methods (*GB_Vu*, *GB_Tu*), as their local optimum solutions were highly repeatable for the same starting points.

The middle rank {1} was assigned to the following methods: *GA_VcT*, *GA_Tu*, and *MOGA*, as their results were repeatable between the trials within the range defined by the optimization stopping criteria concerning solution quality. The observed differences between trials in *GA_VcT*, *GA_Tu* were insignificant with respect to the absolute values of the objectives. In *MOGA*, the final solution had to be chosen from the Pareto set. The number of solutions in the Pareto set was observed to slightly differ between trials. However, the distances between the Pareto frontiers of the repeated trials were insignificant with respect to the absolute values of the objectives.

The lowest rank {0} was assigned to the *GA_TcV* method. This ranking was dictated by the purpose of the approach, which was considered mainly as exploration of the feasible design space. Therefore, the repeatability of solutions was considered inadequate and reflected in the ranking with the assigned lowest value.

Rank Table

The final ranking of the methods was combined as the sum of all the particular rankings described above. The rankings of the investigated optimization approaches are listed in Table 5.10.

Table 5.10 Rank table of the optimization approaches

Method	PPM 1	PPM 2	SPM 1	SPM 2
<i>GA_Vu</i>	0	2	0	2
<i>GA_VcT</i>	1	1	1	1
<i>GA_Tu</i>	0	1	1	1
<i>GA_TcV</i>	1	0	1	0
<i>MOGA</i>	2	1	1	1
<i>GB_Vu</i>	0	2	0	2
<i>GB_Tu</i>	0	1	1	2

5.5.3 Results and Discussion

Based on the relative ranking of the relative performance of solution methods presented above, multi-objective genetic algorithm (*MOGA*) was selected as the best approach to solve the runner optimization of multi-cavity molds used for in-mold assembly of multi-material structures. There are two important factors to this decision. First, all the methods with {0} ranks have been identified as not suitable or even incapable of solving the proposed optimization in a comprehensive manner, and hence were eliminated from the set of possible best methods. Second, the two remaining approaches (*GA_VcT* and *MOGA*) were compared to select the better one. Due to the fact that the nature of the optimized design cannot be predicted upfront in

terms of relative objectives' behavior, *MOGA* was identified to be the more comprehensive optimization approach, which minimizes both of the required objectives simultaneously.

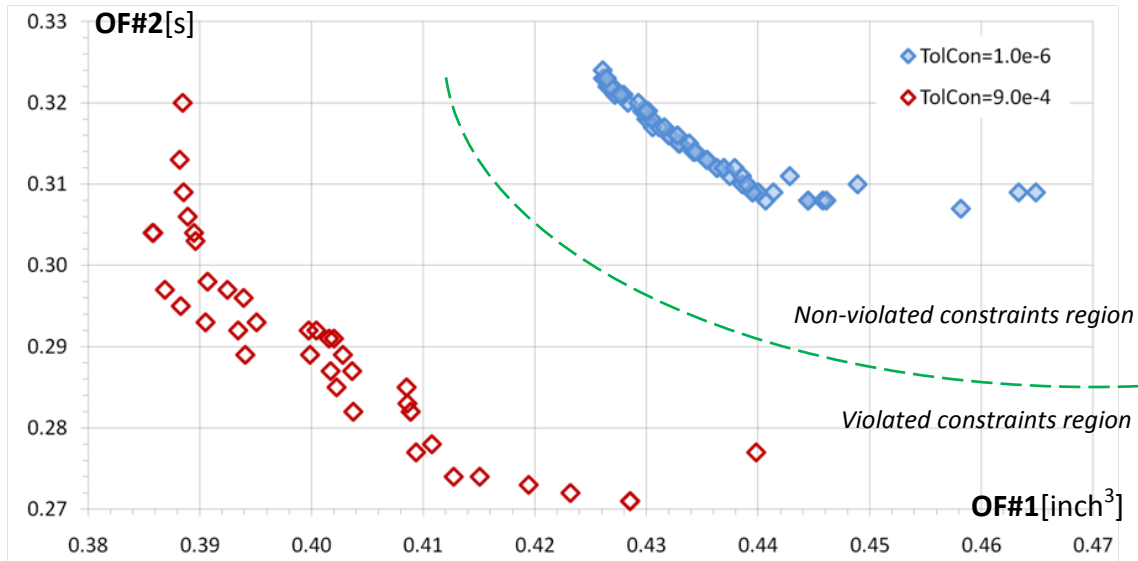


Figure 5.12 Constraint violation influence on optimization results

Next, the influence of constraint violation on the quality of results was analyzed. The allowable constraint violation is controlled in Matlab[®] by the *TolCon* parameter, where the actual constraint violation allowed is the square root of the number stored in *TolCon*. Note, that this relationship is not included in the Matlab[®] documentation and had to be determined separately during the computational experiment. The *MOGA* results with an allowed constraint violation of less than 0.03 (*TolCon*=0.0009) are overlaid with the results for non-violated constraints (*TolCon*=1.0e-6) in Figure 5.12. This figure shows the influence of the active linear constraint (Equation 5.30) in the considered case study on the feasible solution space. The

violation of this constraint by 0.03 resulted in reduction of x_l by 0.02-0.03 inches, which is within a 1 mm range. In the considered case study, allowing for active constraint violation resulted in significant improvement of the objectives, but also less repeatable solutions for methods concerning the arrival time objective (OF#2). Therefore the constraint violation should be allowed only to the extent that can be justified for the specific design case by the nature of the active constraint being violated and the effect it causes on the obtained results.

Based on the cumulative ranking of the investigated optimization methods presented in Table 5.10, multi-objective GA-based optimization (*MOGA*) was found to be the superior method to solve the general optimization problem of the runner system for the in-mold assembly of multi-material compliant mechanisms. Due to the nature of the objectives, where OF#1 is the production waste, and OF#2 a product's possible failure source, both of them were considered equally important. *MOGA* offered unbiased and automated minimization of both of the objectives, returning a set of solutions with their relative trade-offs rather than a single solution, and at the same time was comparable with other methods in terms of calculation time, scalability, and robustness. The common GA parameters used in the investigated optimization methods are listed in Table 5.11.

Table 5.11 Final parameters used in the investigated GA optimizations

Optimization Parameter	Used Value	Matlab [®] Default	Range
<i>PopulationSize</i>	180	#DV*15	1-∞
<i>TolFun (MOGA)</i>	1.0E-2	1.0E-6	0-∞
<i>TolFun (all other)</i>	1.0E-4		
<i>TolCon</i>	1.0E-6	1.0E-6	0-∞
<i>TolCon (violated region)</i>	9.0E-4		
<i>StallGenLimit</i>	15	20	1-∞
<i>CrossoverFraction</i>	0.7	0.8	0-1
<i>ParetoFraction</i>	0.5	0.35	0-1
<i>EliteCount</i>	18	2	integer ⁺
<i>MutationFcn (mutationadaptfeasible)</i>	0.05	-	0-1

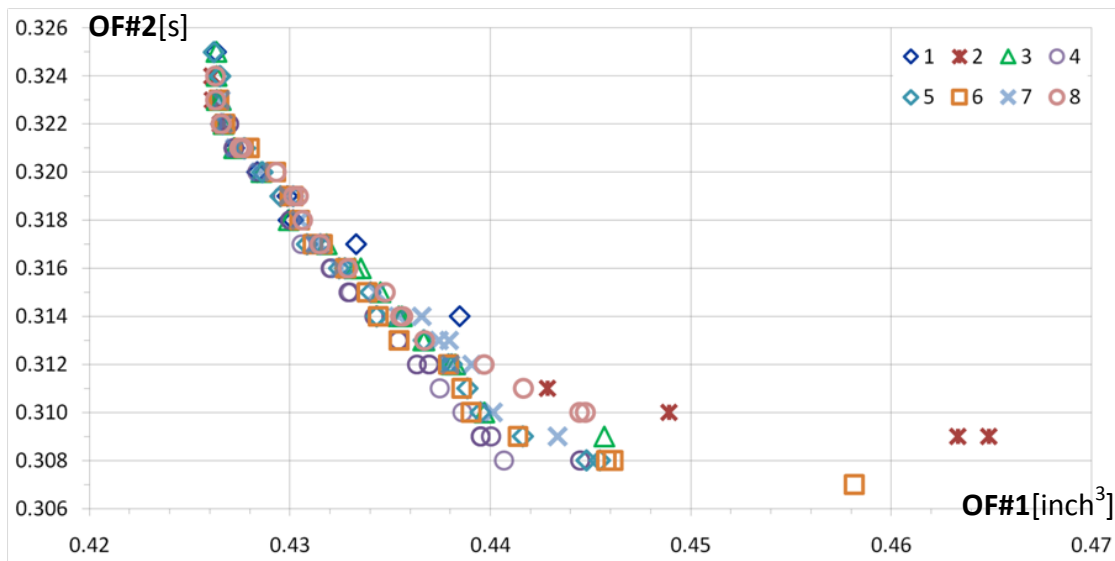


Figure 5.13 *MOGA* optimization result – Pareto sets from eight trials

The Pareto set of solutions from the representative *MOGA* optimization of runner system defined in Section 5.4 is plotted for eight repeated trials in Figure 5.13. The Pareto set visually shows the trade-offs between the runner volume and the maximum difference in flow arrivals to the pre-molded components. Since the two objectives

have different physical and economical meaning, the actual gains in OF#2 were observed to be much less significant to the problem than the gains in OF#1. This is due to the fact that the differences between OF#2 values in the Pareto set were comparable to the resolution of simulation used to evaluate it, and were also insignificant with respect to the actual ability of the flows arriving at the first stage component to displace it. This however cannot be treated as a general remark, as the results highly depend on the optimized problem complexity and implementation.

On the other hand, gains in OF#1 can always be translated into real savings in production cost according to the following equation:

$$\Delta C_{\text{prod}} [\text{\$}] = \Delta V_{\text{R}} \cdot \rho_{\text{mat}} \cdot C_{\text{mat}} \cdot P \quad \text{EQ. 5.35}$$

where:

ΔV_{R} is the gain in runner volume [in unit volume],

ρ_{mat} is the material density [unit weight per unit volume],

C_{mat} is the material cost [\$ per unit weight], and

P is the total number of parts to be manufactured.

In the case study presented in Section 5.4.2, the total runner volume optimized by *MOGA* ranged between 0.42 to 0.47 cubic inches. The material density was $\rho_{\text{CF-PA6,6}}=1610$ [kg/m³] and the material price was $C_{\text{CF-PA6,6}}=5$ [\$/lb]. The total number of parts (multi-material compliant mechanisms) to be manufactured was assumed to be $P=5,000,000$, which is a rational value for the mass production injection molding process. After substituting these values into Equation 5.35, the gain of 0.01 [inch³] in a single molding translates into \$14,541 for the total batch. Considering the range of results, the possible material cost savings are \$72,705. This

does not include the energy needed to process the additional material and the carbon footprint connected with it; hence the final savings resulting from this optimization are much greater. However, the actual energy usage impact was not evaluated here, since the estimation of the sustainability gains is not within the scope of this research.

Due to the above considerations, the optimal solution was chosen with the primary emphasis on the runner volume, and not on the maximum arrival time objective. However, please note, that this was the case in the optimized design only and cannot be treated as a general remark towards selection of final optimal solution. The selected optimal design point is presented in Table 5.12.

Table 5.12 Final optimal solution

X [inch]	OF#1 [inch ³]	OF#2 [s]	Δt [s]
x_1 0.4576	0.4261	0.323	(10,22) -0.323
x_2 0.3641			
x_3 0.2252			(14,22) -0.104
x_4 0.2378			
x_5 0.3404			(20,21) -0.112
x_6 0.1602			

The optimal solution's design variables were then incorporated into a Pro/Engineer CAD model and exported to MoldFlow[®] via IGS format to verify the mold filling criteria and the flow arrival times. The model mesh and "Fill time" results are shown in Figure 5.14.

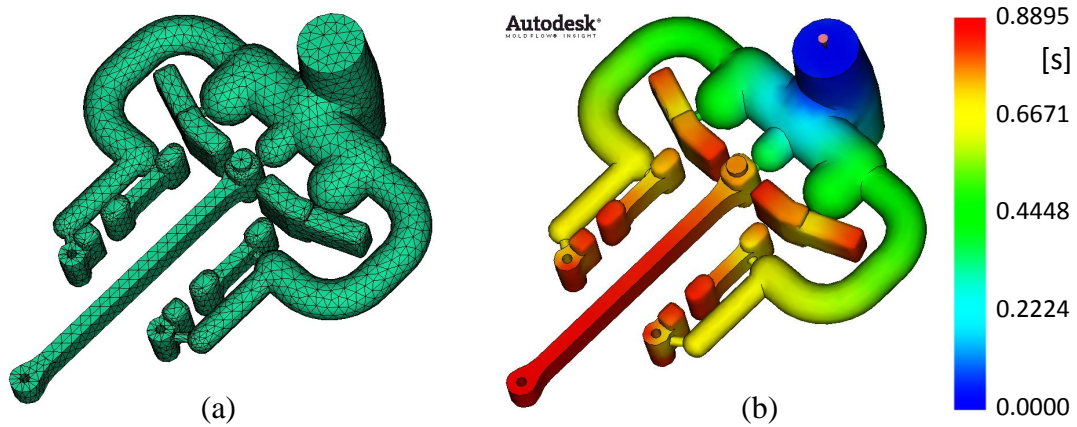


Figure 5.14 MoldFlow® optimal solution validation: (a) mesh, (b) fill time plot

The model was meshed in MoldFlow® into 92260 tetrahedral elements with 17512 nodes. The meshing CPU time was 158 s. The injection point was selected at the middle node of the sprue. The material properties listed in Table 5.3 were assigned to the model. Fill analysis CPU time was 676 s. From the fill time result animated over the period of the mold filling, the times of flow arriving to the points corresponding to the constrained pairs were recorded. The comparison of these results with the custom simulation described in Section 5.4.5 is presented in Table 5.13. The maximum error of all arrival times in the custom simulation with 0.001 s resolution was observed to be 25% for node #22. The error percentage for time differences were calculated with respect to the MoldFlow® absolute arrival time to the second of compared nodes.

Table 5.13 Validation of flow arrival times obtained by the custom simulation

Node#	MoldFlow[®] [s]	Custom [s]	Error [%]
10	0.3666	0.405	-11
14	0.5740	0.624	-9
20	0.6234	0.688	-10
21	0.7419	0.800	-8
22	0.5839	0.728	-25
10-22	-0.217	-0.323	-18
14-22	-0.010	-0.104	-16
20-21	-0.119	-0.112	1

Once the optimal design was validated, the second stage mold was manufactured from 3x4x0.5 [inch] aluminum blocks on the Boxford XT milling machine. Finally, the molds were pre-loaded with the first stage components and the in-mold assembly process was performed. The resulting multi-material molding was incorporated into a flapping wing robot as a drive mechanism. The mechanism was inspected and it was observed that all of the hinges were in the correct positions, which validated the applicability of the OF#2 to the optimization of runner systems for in-mold assembly.

5.6 Summary

This chapter described the approach for design optimization of a runner system for the in-mold assembly of multi-material compliant mechanisms with miniature hinges. The novel aspects of this work include: (1) development of a complete optimization model and (2) determination of the most reliable and efficient method to perform the formulated optimization.

The formulations and methods described in this chapter are applicable to any runner system designed to supply multiple cavities for in mold assemblies of multi-material structures. The mold cavities are separated with the pre-molded components, which due to their size scale are sensitive to the effects caused by the polymer melt during the mold filling. This is especially important for miniaturization of devices.

The developed runner optimization was defined as a concurrent minimization of the production waste and the in-mold assembly failure factors, with runner geometric dimensions as design variables, subject to the runner design. The mathematical formulation of the general optimization model was also presented.

In order to enable evaluation of solution methods, the developed optimization model was implemented on a case study of an in-mold assembly of a MAV multi-material drive mechanism. The computational environments were described, followed by the details of the case study design and its representation. The details of optimization model application to the case study were also described. This included the development of custom mold filling simulation based on a pressure meta-model for the second objective evaluation, as well as the details of constraints formulation.

With all the optimization components in place, the selected solution methods were investigated in terms of applicability and efficiency. First, the in-mold assembly-specific runner optimization considerations were described, along with identification of the rationale for selecting the candidate solution methods. Next, the optimization methods were executed and compared based on a relative ranking of the results. The performance measures considered included the solution quality, calculation time, robustness, and scalability. Based on the final ranking, the best method to solve the

runner optimization problem was identified as the multi-objective genetic algorithm (*MOGA*).

6 Conclusions

This chapter describes the intellectual contributions and the anticipated benefits resulting from the contributions reported as part of this dissertation. Also, the possible future extensions of this research are presented.

6.1 *Intellectual Contributions*

This dissertation is envisioned to yield several contributions in the in-mold assembly field by providing an integrated approach to create novel multi-functional polymeric structures for miniaturization of devices. This section describes the three main contributions of this dissertation.

6.1.1 Development of Methods for Embedding Actuators using In-Mold Assembly Process

As a part of this effort, a systematic approach for embedding actuators in multi-functional polymer structures using in-mold assembly process has been developed. Embedded actuators generate heat during operation, which must be dissipated for proper functioning of the device. The heat dissipation can be enhanced by using thermally conductive fillers (fibers, tubes, beads) inside the polymer matrix.

To dissipate the required amount of heat generated by the embedded small scale actuators, the minimum required thermal conductivity of the material for the structure was identified. The influence of the fiber orientation on the heat dissipation performance was found to be insignificant, and therefore modeling of complex orthotropic thermal properties resulting from the fiber orientation was shown to be

not necessary for the functionality assessment. A simplified thermal conductivity model was sufficiently accurate in predicting the thermal performance enhancement of the structure.

The modeling approach that has been developed allows for selection of optimal design parameters for thermally conductive polymer structures with embedded actuators using in-mold assembly for miniaturization of devices.

Also, as part of this effort, an understanding of influence of injection molding process on the survivability of the embedded actuator was developed. Using highly filled thermally conductive polymers requires more demanding processing parameters, which were shown to be capable of destroying the miniature actuator during the embedding process. The model concerning the part geometrical dimensions and the injection pressure of the polymer was developed. This model allows for concurrent optimization of both the structure and the injection molding process to ensure the functionality of the actuator embedded using in-mold assembly methods for miniaturization of devices.

6.1.2 Development of Design Solutions and Models for realizing Multi-Material Compliant Mechanisms with Miniature Hinges using In-Mold Assembly

As part of this effort, methods to design and fabricate multi-material compliant mechanisms with miniature hinges were developed. Failure modes which are specific to the size and functionality requirements of multi-material mechanisms have been experimentally investigated. To prevent the observed failure modes, the necessary hinge and link design features have been identified. Shapes and orientations of these

features were analyzed with respect to their functionality, mutual dependencies, and the process cost. A parametric model of the compliant hinge design consisted of the hinge geometry, hinge-link interface geometry, including the embedded length and the interlocking features, and hinge positioning geometries for the second stage molding. The hinge design optimization model was presented, which involved both functional and manufacturing constraints.

The developed parametric model of the hinge and the hinge-link interface allows for design optimization of any lightweight, load-bearing compliant mechanism with miniature hinges manufactured using multi-material injection molding.

6.1.3 Development of Methods to Optimize Runner Systems for Multi-Cavity Molds used in In-Mold Assembly

Another significant contribution is in the area of design optimization of a runner system used in multi-cavity molds for in-mold assembly of multi-material mechanisms. The novel aspects of this work include: (1) development of a complete optimization model and (2) determination of the most reliable and efficient method to perform the formulated optimization.

The developed general optimization model was defined as a concurrent minimization of the production waste and the in-mold assembly failure factors as a function of the runner geometrical dimensions, subject to the runner design rules and the fiber orientation of filled polymers as the design constraints. Details of the general optimization model implementation to a specific design case were described.

Based on the relative ranking of several optimization approaches with respect to their applicability and performance measures, the best method to solve the runner

optimization problem was identified as the multi-objective genetic algorithm (*MOGA*). This method offered an unbiased and automated minimization of both of the objectives with the best overall solution quality and the remaining performance measures comparable to other methods.

The developed optimization approach is applicable to any runner system design supplying multiple cavities separated with pre-molded components, which are sensitive to the effects caused by the polymer melt during the mold filling. This is especially useful for in-mold assembly of multi-material mechanisms with compliant hinges, which enable an important step towards miniaturization of devices.

6.2 *Anticipated Benefits*

The focus of this dissertation is on the development of methods to design and manufacture multi-functional structures using in-mold assembly to facilitate miniaturization of robotic devices. The enhancement of structural functionality can be obtained by utilization of novel polymer composites with the appropriate fillers. In multi-material mechanisms utilizing selective compliance, glass fiber filled polymers are utilized for molding the rigid links, and highly compliant and impact resistant unfilled polymers are used to mold the mechanism joints (hinges). Current manufacturing methods for production of multi-material compliant mechanisms include a variety of prototyping techniques, which, along with some material and geometry constraints, are suitable only for a small batch production due to expensive processing equipment resources required. Injection molding, on the other hand, is a fully automated high throughput process which is capable of creating geometrically complex heterogeneous structures. Hence the methods developed as part of this

dissertation enable fully automated large scale production of multi-material compliant mechanisms with miniature hinges. This is expected to significantly reduce the cost of such mechanisms, and hence the area of their application in popular customer devices.

Another benefit of using in-mold assembly is the potential of reduced part weight. This is due to the polymer being used as the raw material in the injection molding. Polymers are significantly lighter than their metallic counterparts. The novel filled polymer composites allow for realization of virtually any functional capability through the material selection, including heat dissipation or stiffness requirements previously reserved only for metals. Polymers are also usually less expensive and require much fewer post-processing operations when compared to metals. Due to these advantages, in-mold assembled parts are expected to obtain the required levels of functionality and therefore eliminate the metallic components from the assembly.

Multi-material molding can also reduce the part count of the multi-functional structure or assembly. In case of complex mechanisms, using in-mold assembled compliant hinges allows for elimination of articulated revolute joints. In case of embedded actuators, the thermally conductive polymer anchoring structure allows for elimination of additional components serving as a heat sink. Reduction of components within a multi-functional assembly is particularly beneficial in miniaturization of devices for three reasons. First, in-mold assembly significantly reduces the number of post-processing and assembly operations, which leads to reduced manufacturing costs and improved product quality consistency, resulting in relatively inexpensive and reliable products. Second, replacing articulated revolute

joints with compliant in-mold assembled hinges allows for improvement of the overall mechanism efficiency. The slightest misalignment resulting from the manual assembly and/or the dimensional tolerances of the assembled components results in increased friction between the articulating surfaces, and therefore requires more powerful actuation source to overcome the additional resistance. Finally, combining the novel polymer composites with the advances in multi-material molding allows for creating new product possibilities.

6.3 *Future Directions*

This dissertation is a step towards the in-mold assembly of miniature multi-functional structures. It shows the feasibility of manufacturing in-mold assembled miniature actuators and compliant mechanisms using filled polymer materials. However, the advances reported as part of this dissertation open several new research directions. This section defines possible extensions of the work presented in this dissertation.

6.3.1 Modeling of Thermally Conductive Filled Polymer Structures with Embedded Actuators

In this dissertation a new modeling approach is developed to characterize the heat dissipation performance of the thermally conductive polymer structures with embedded small scale actuators. The models and their experimental validation methods are described in Section 3.3. However, the convection coefficients obtained using these methods are considered only for specific structure geometries and the heat source power density. The model deals only with very few geometries and a limited

range of the heat generated by the embedded actuator. The functionality of different classes of structure shapes and the relative positioning of the heat source needs to be characterized with respect to the energy density of the embedded actuator and other dimensional size scales. Furthermore, new experimental methods have to be developed to validate the models and obtain the coefficients needed for heat dissipation functionality assessment. Additionally, the process design variables influencing the fiber orientation can be incorporated into the models to extend functionality of the structure not only in terms of the thermal, but also structural performance.

6.3.2 Characterization of Design Features to Facilitate Other Classes of Miniature Compliant Joints

This dissertation characterizes the design and fabrication methods for in-mold assembly of miniature compliant hinges. These hinges, capable of load transfer, represent one of the main general classes of compliant joints. Hence methods developed for compliant hinges can be extended to be applied to other classes of compliant joints, such as ball joints. However, allowing for additional degrees of freedom will impose several challenges during the in-mold assembly of other classes of miniature compliant joints. Therefore, a direct extension of the methods developed for miniature hinges with only 1 DOF will not be possible. Experimental investigation needs to be conducted to identify the design features necessary for other classes of compliant joints. Appropriate parametric models have to be developed to enable the shape and size optimization with respect to their functionality and process cost for new types of in-mold assembled small scale multi-material kinematic pairs.

6.3.3 Multi-Material Interface Optimization

A new optimization approach for multi-material interfaces with miniature features is presented in this dissertation. These interfaces are especially important if the in-mold assembled structure has to perform tasks such as load and motion transfer. The interface features and their shapes identified in Chapter 4 consider the most general design case where the materials are assumed chemically incompatible and will not bond during the in-mold assembly process. This assumption is conservative and valid for many material combinations with respect to the level of bonding on the molecular level and the actual interface strength under loading. However, the reported compatibility results cover only a small fraction of all possible combinations between available polymer grades. Therefore, future findings from the material compatibility studies have a strong potential of revealing chemically compatible polymer pairs which will satisfy the multi-functionality requirements defined for the multi-material assembly. This will allow for elimination of features responsible for the physical interlocking and create an opportunity to further minimize the overall weight of the assembly for miniaturization of devices. However, new interface geometry will have to be synthesized to account for the load transfer requirement as a function of the molecular bonding level, interface surface area, and the effects of dynamic loading during operation.

6.3.4 Runner System Layout Optimization

This dissertation presents a new approach to the optimization of runner systems supplying multi-cavity molds for the in-mold assembly of multi-material compliant mechanisms. The optimization approach developed in Chapter 5 is directly

applicable to any class of planar multi-material assemblies with fixed geometric layout. This layout is a function of the gate locations for each of the cavities, which is required to obtain the desired properties of the part as a result from the filler orientation. Therefore, the extension of the developed approach to mold designs with unconstrained or only partially constrained gate locations will pose additional challenges. Variable shapes, sizes and positions of the gates result in an additional layout problem, which needs to be incorporated into the runner optimization. The layout feasibility has to be accounted for during the design evaluation with respect to the connectivity constraints between the runner segments and cavity relative positions, including elimination of self intersections. Additionally, in case of parts molded using filled polymers, the mechanical properties of the structure will have to be incorporated into the optimization in order to characterize the functionality of the final assembly.

Bibliography

1. S.G. Advani and C.L. Tucker III, "The use of tensors to describe and predict fiber orientation in short fiber composites," *Journal of Rheology*, **31** (8): pp. 751-784, 1987
2. K. Alam and M.R. Kamal, "Runner balancing by a direct genetic optimization of shrinkage," *Polymer Engineering and Science*, **44** (10): pp. 1949-1959, 2004
3. K. Alam and M.R. Kamal, "A robust optimization of injection molding runner balancing," *Computers & Chemical Engineering*, **29** (9): pp. 1934-1944, 2005
4. E.M. Alawadhi and C.H. Amon, "PCM thermal control unit for portable electronic devices: experimental and numerical studies," *IEEE Transactions on Components and Packaging Technologies*, **26** (1): pp. 116-125, 2003
5. A. Ananthanarayanan, W. Bejgerowski, D. Mueller and S.K. Gupta, "Development of a multi-piece multi-gate mold for manufacturing a flapping wing drive-mechanism," In Proceedings of the *North American Manufacturing Research Conference*, Monterrey, Mexico, May, 2008
6. A. Ananthanarayanan, S.K. Gupta and H.A. Bruck, "Mechanical characterization of cold weld-lines and meld lines in mesoscopic revolute joints for bioinspired structures," In Proceedings of the *Society of Experimental Mechanics XI International Congress & Exposition on Experimental and Applied Mechanics*, Orlando, FL, 2008
7. A. Ananthanarayanan, S.K. Gupta and H.A. Bruck, "Characterization and control of plastic deformation in mesoscale premolded components to realize in-mold assembled mesoscale revolute joints," *Polymer Engineering Science*, **49** (2): pp. 293-304, 2009
8. J.S. Arora, "Introduction to optimum design, 2nd Edition," *Elsevier Academic Press*, 2004
9. R. Bahadur, "Characterization, modeling and optimization of polymer composite pin fins," *Ph.D. Dissertation*, Mechanical Engineering Department, University of Maryland, College Park, MD, 2005
10. R. Bahadur and A. Bar-Cohen, "Thermal performance limits of polymer composite pin fin heat sinks," In Proceedings of the *55th Electronic Components and Technology Conference*, Vol. 2, pp. 1720-1727, 2005
11. A.G. Banerjee, X.J. Li, G. Fowler and S.K. Gupta, "Incorporating manufacturability considerations during design of injection molded multi-material objects," *Research in Engineering Design*, **17** (4): pp. 207-231, 2007

12. J.P. Beaumont, R. Nagel and R. Sherman, "Successful injection molding: Process, design, and simulation, 1st Edition," *Hanser Gardner Publications*, 2002
13. J.P. Beaumont, "Runner and gating design handbook: Tools for successful injection molding," *Hanser Gardner Publications*, 2004
14. W. Bejgerowski, A. Ananthanarayanan, D. Mueller and S.K. Gupta, "Integrated product and process design for a flapping wing drive mechanism," *Journal of Mechanical Design*, **131** (6): pp. 061006, 2009
15. W. Bejgerowski, H.A. Bruck and S.K. Gupta, "A modeling approach for simulating heat dissipation from actuators and electronic components embedded in thermally conducting polymers," In Proceedings of the *ASME Computers and Information in Engineering Conference*, San Diego, CA, August 30-September 2, 2009
16. W. Bejgerowski, S.K. Gupta and H.A. Bruck, "Multifunctional highly-filled polymer composites for embedding electronic components," In Proceedings of the *SEM Annual Conference & Exposition on Experimental and Applied Mechanics*, Vol. 1:22, pp. #85, Albuquerque, New Mexico, June 1-4, 2009
17. W. Bejgerowski, S.K. Gupta and H.A. Bruck, "A systematic approach for designing multifunctional thermally conducting polymer structures with embedded actuators," *Journal of Mechanical Design*, **131** (11): pp. 111009, 2009
18. W. Bejgerowski, J.W. Gerdes, S.K. Gupta, H.A. Bruck and S. Wilkerson, "Design and fabrication of a multi-material compliant flapping wing drive mechanism for miniature air vehicles," In Proceedings of the *ASME Mechanism and Robotics Conference*, Montreal, Canada, August, 2010
19. F. Breugel, Z.E. Teoh and H. Lipson, "Flying insects and robots," *Springer Berlin Heidelberg*, 2009
20. H.A. Bruck, "A one-dimensional model for designing functionally graded materials to attenuate stress waves," *International Journal of Solids and Structures*, **37**, pp. 6383-6395, 2000
21. H.A. Bruck, G. Fowler, S.K. Gupta and T. Valentine, "Using geometric complexity to enhance the interfacial strength of heterogeneous structures fabricated in a multi-stage, multi-piece molding process," *Experimental Mechanics*, **44** (3): pp. 261-271, Jun 2004
22. J.R. Cannon and L.L. Howell, "A compliant contact-aided revolute joint," *Mechanism and Machine Theory*, **40** (11): pp. 1273-1293, 2005

23. R.Y. Chang, Y.H. Peng, D.C. Hsu and W.H. Yang, "Three-dimensional insert molding simulation in injection molding," In Proceedings of the *62nd ANTEC Conference*, Vol. 1, pp. 496-500, Chicago, IL, 2004
24. C.S. Chen, T.J. Chen, R.D. Chien and S.C. Chen, "Investigation on the weldline strength of thin-wall injection molded ABS parts," *International Communications in Heat and Mass Transfer*, **34** (4): pp. 448-455, Apr 2007
25. C.H. Chien and H.M. Yu, "Using the hot embossing technology to fabricate the movable component on polymer material," chapter in "Progress on Advanced Manufacture for Micro/Nano Technology 2005, Pt 1 and 2", *Trans Tech Publications Ltd*, pp. 103-108, 2006
26. J.S. Cintra Jr and C.L. Tucker, "Orthotropic closure approximations for flow-induced fiber orientation," *Journal of Rheology*, **39** (6): pp. 1095-1122, 1995
27. N.B. Crane, L.L. Howell, B.L. Weight and S.P. Magleby, "Compliant floating-opposing-arm (FOA) centrifugal clutch," *Journal of Mechanical Design*, **126** (1): pp. 169-177, Jan 2004
28. M.R. Cutkosky and S. Kim, "Design and fabrication of multi-material structures for bioinspired robots," *Royal Society of London Philosophical Transactions Series A*, **367**, pp. 1799-1813, 2009
29. Y.M. Deng, D. Zheng and X.J. Lu, "Injection moulding optimisation of multi-class design variables using a PSO algorithm," *International Journal of Advanced Manufacturing Technology*, **39** (7-8): pp. 690-698, Nov 2008
30. S.S. Dimov, C.W. Matthews, A. Glanfield and P. Dorrington, "A roadmapping study in multi-material micro manufacture," In Proceedings of the *2nd Int. Conf. on Multi-Material Micro Manufacture - 4M*, pp. xi-xxv, Grenoble, 20-22 Sept., 2006
31. M.B. Dogruoz and M. Arik, "An investigation on the conduction and convection heat transfer from advanced heat sinks," In Proceedings of the *11th Intersociety Conference on Thermal and Thermomechanical Phenomena in Electronic Systems*, pp. 367-373, Orlando, FL, 2008
32. T.C. Duc, G.K. Lau and P.M. Sarro, "Polymeric thermal microactuator with embedded silicon skeleton: Part II: Fabrication, characterization, and application for 2-DOF microgripper," *Journal of Microelectromechanical Systems*, **17** (4): pp. 823-831, 2008
33. E. Egan and C.H. Amon, "Measuring thermal conductivity enhancement of polymer composites: Application to embedded electronics thermal design," *Journal of Enhanced Heat Transfer*, **8** (2): pp. 119-135, 2001

34. S. Egelkraut, C. Heinle, B. Eckardt, P. Kramer, Z. Brocka, M. Marz, H. Ryssel and G.W. Ehrenstein, "Highly filled polymers for power passives packaging," In Proceedings of the *2nd Electronics System Integration Technology Conference*, pp. 403-410, London, UK, 2008
35. J. Fjelstad, "MIDs in our midst " *Global SMT & Packaging Magazine*, Vol. 7 (6), 2007, <http://www.globalsmt.net/content/view/2605/106/> (accessed 12/14/2009)
36. F.P. Folgar and C.L. Tucker, "Orientation behaviour of fibers in concentrated suspensions," *Reinforced Plastic Composites*, **3** (2): pp. 98-119, 1984
37. G.T. Fowler, "Cost and performance evaluation models for comparing multi-shot and traditional injection molding," *Master of Science Thesis*, Mechanical Engineering, University of Maryland, College Park, 2004
38. J.Y.H. Fuh, Y.F. Zhang, A.Y.C. Nee and M.W. Fu, "Computer aided injection mold design," *Marcel Dekker Inc.*, 2004
39. C.P. Fung, J.R. Hwang and C.C. Hsu, "The effect of injection molding process parameters on the tensile properties of short glass fiber-reinforced PBT," *Polymer-Plastics Technology and Engineering*, **42** (1): pp. 45-63, 2003
40. J.W. Gerdes, S.K. Gupta, H.A. Bruck and S. Wilkerson, "A review of bird-inspired flapping wing miniature air vehicle designs," In Proceedings of the *ASME Mechanism and Robotics Conference*, Montreal, Canada, August, 2010
41. R.J. Goldstein, E.R.G. Eckert, W.E. Ibele, S.V. Patankar, T.W. Simon, T.H. Kuehn, P.J. Strykowski, K.K. Tamma, J.V.R. Heberlein, J.H. Davidson, J. Bischof, F.A. Kulacki, U. Kortshagen and S. Garrick, "Heat transfer - a review of 2001 literature," *International Journal of Heat and Mass Transfer*, **46** (11): pp. 1887-1992, May 2003
42. R.M. Gouker, S.K. Gupta, H.A. Bruck and T. Holzschuh, "Manufacturing of multi-material compliant mechanisms using multi-material molding," *International Journal of Advanced Manufacturing Technology*, **30** (11-12): pp. 1049-1075, Oct 2006
43. C.A. Griffiths, S.S. Dimov and E.B. Brousseau, "Microinjection moulding: the influence of runner systems on flow behaviour and melt fill of multiple microcavities," *Proceedings of the Institution of Mechanical Engineers Part B- Journal of Engineering Manufacture*, **222** (9): pp. 1119-1130, 2008
44. M. Grujcic, V. Sellappan, M.A. Omar, N. Seyr, A. Obieglo, M. Erdmann and J. Holzleitner, "An overview of the polymer-to-metal direct-adhesion hybrid technologies for load-bearing automotive components," *Journal of Materials Processing Technology*, **197** (1-3): pp. 363-373, 2008

45. M. Grujicic, V. Sellappan, B. Pandurangan, G. Li, A. Vahidi, N. Seyr, M. Erdmann and J. Holzleitner, "Computational analysis of injection-molding residual-stress development in direct-adhesion polymer-to-metal hybrid body-in-white components," *Journal of Materials Processing Technology*, **203** (1-3): pp. 19-36, 2008
46. M. Grujicic, V. Sellappan, G. Arakere, N. Seyr, A. Obieglo, M. Erdmann and J. Holzleitner, "The potential of a clinch-lock polymer metal hybrid technology for use in load-bearing automotive components," *Journal of Materials Engineering and Performance*, **18** (7): pp. 893-902, 2009
47. S.K. Gupta, "Flapping wing micro air vehicle designs by SK Gupta's group," <http://terpconnect.umd.edu/~skgupta/UMdBird>, accessed on: 10/28/2010
48. L.S. Gyger Jr., B.W. Spranklin, S.K. Gupta and H.A. Bruck, "Bio-inspired, modular, and multifunctional Thermal and Impact Protected (TIPed) Embedded Sensing Controls Actuation Power Element (ESCAPE) structures," In Proceedings of the *SEM Annual Conference & Exposition*, St. Louis, MO, June 4-7, 2006
49. J.A. Heiser and J.A. King, "Thermally conductive carbon filled nylon 6,6," *Polymer Composites*, **25** (2): pp. 186-193, 2004
50. A. Housden and J. Gould, "Moulded interconnect devices," *PRIME Technology Watch*, Loughborough, 2002
51. L.L. Howell, "Compliant mechanisms," *Wiley-Interscience*, 2001
52. C.K. Hsu, J. Evans, S. Vytla and P.G. Huang, "Development of flapping wing micro air vehicles - Design, CFD, experiment and actual flight," In Proceedings of the *48th AIAA Aerospace Sciences Meeting Including the New Horizons Forum and Aerospace Exposition*, Vol. AIAA 2010-1018, Orlando, Florida, 2010
53. C.-T. Huang, M.-C. Chen, W.-L. Yang, K.-J. Chang and S.-C. Tseng, "Investigation on warpage and its behavior in sequential overmolding," In Proceedings of the *65th ANTEC Conference*, Vol. 2, pp. 760-764 Cincinnati, OH May, 2007
54. A. Islam, H.N. Hansen, P.T. Tang and E.M. Kjær, "Bond strength of two-component injection moulded MIDs," In Proceedings of the *7th International Congress on Moulded Interconnect Devices*, pp. 245-254, Fuerth, Germany, Sept., 2006
55. A. Islam, "Two component micro injection moulding for moulded interconnect devices," *Ph.D. Dissertation*, Mechanical Engineering, Technical University of Denmark, 2008

56. B. Iverson and S. Garimella, "Recent advances in microscale pumping technologies: a review and evaluation," *Microfluidics and Nanofluidics*, **5** (2): pp. 145-174, 2008
57. C. Javierre, A. Fernandez, J. Aisa and I. Claveria, "Criteria on feeding system design: conventional and sequential injection moulding," *Material Processing Technology*, **171** (3): pp. 373-384, 2006
58. G.B. Jeffery, "The motion of ellipsoidal particles immersed in viscous fluid," In Proceedings of the *Royal Society of London*, Vol. A102, pp. 161, 1922
59. K.K. Kabanemi, J.F. Hetu and A. Derdouri, "Design sensitivity analysis applied to injection molding for optimization of gate location and injection pressure," *International Polymer Processing*, **17** (3): pp. 254-264, Sep 2002
60. D.O. Kazmer, "Injection mold design engineering, " *Hanser Gardner Publications*, 2007
61. P. Kennedy, "Flow analysis of injection molds, " *Hanser Gardner Publications*, 1995
62. H.S. Kim, J.S. Son and Y.T. Im, "Gate location design in injection molding of an automobile junction box with integral hinges," *Journal of Materials Processing Technology*, **140**, pp. 110-115, 2003
63. J.W. Kim and D.G. Lee, "Fiber orientation state depending on the injection mold gate variations during FRP injection molding," *Key Engineering Materials*, **321-323**, pp. 938-941, 2006
64. K.J. Kim and S. Tadokoro, "Electroactive polymers for robotic applications, " *Springer*, 2007
65. P.C. Knepper, "The effect of runner diameter on packing of a plastic part with injection molding," In Proceedings of the *SPE Annual Technical Conference*, Chicago, 2004
66. M. Kumar and S.K. Gupta, "Automated design of multi-stage molds for manufacturing multi-material objects," *Journal of Mechanical Design*, **124** (3): pp. 399-407, 2002
67. Y.C. Lam and S. Jin, "Optimization of gate location for plastic injection molding," *Journal of Injection Molding Technology*, **5** (3): pp. 180-192, 2001
68. B.H. Lee and B.H. Kim, "Automated selection of gate location based on desired quality of injection-molded part," *Polymer-Plastics Technology and Engineering*, **35** (2): pp. 253-269, 1996

69. B.H. Lee and B.H. Kim, "Automated design for the runner system of injection molds based on packing simulation," *Polymer-Plastics Technology and Engineering*, **35** (1): pp. 147-168, 1996
70. J. Lee and J. Kim, "Micro genetic algorithm based optimal gate positioning in injection molding design," *Journal of Mechanical Science and Technology*, **21** (5): pp. 789-798, May 2007
71. K.S. Lee and J.C. Lin, "Design of the runner and gating system parameters for a multi-cavity injection mould using FEM and neural network," *International Journal of Advanced Manufacturing Technology*, **27** (11-12): pp. 1089-1096, 2006
72. C.S. Li and Y.K. Shen, "Optimum design of runner system balancing in injection molding," *International Communications in Heat and Mass Transfer*, **22** (2): pp. 179-188, 1995
73. X.J. Li and S.K. Gupta, "Geometric algorithms for automated design of rotary-platen multi-shot molds," *Computer-Aided Design*, **36** (12): pp. 1171-1187, Oct 2004
74. S.J. Liu, J.Y. Wu, J.H. Chang and S.W. Hung, "An experimental matrix design to optimize the weldline strength in injection molded parts," *Polymer Engineering and Science*, **40** (5): pp. 1256-1262, May 2000
75. R.A. Malloy, "Part design for injection molding, " *Hanser Gardner Publications*, 1994
76. N.D. Mankame and G.K. Ananthasuresh, "A novel compliant mechanism for converting reciprocating translation into enclosing curved paths," *Journal of Mechanical Design*, **126** (4): pp. 667-672, 2004
77. N.D. Mankame and G.K. Ananthasuresh, "Synthesis of contact-aided compliant mechanisms for non-smooth path generation," *International Journal for Numerical Methods in Engineering*, **69** (12): pp. 2564-2605, 2007
78. N. Mekhilef, A. Aitkadi and A. Ajji, "Weld lines in injection-molded immiscible blends - Model predictions and experimental results," *Polymer*, **36** (10): pp. 2033-2042, May 1995
79. G. Menges, W. Michaeli and P. Mohren, "How to make injection molds, 3rd Edition," *Hanser Gardner Publications*, 2001
80. W. Michaeli, A. Rogalla and C. Ziegmann, "Micro assembly injection moulding of hybrid microsystems," *Journal of Polymer Engineering*, **21** (2-3): pp. 99-109, 2001

81. W. Michaeli, D. Opfermann and T. Kamps, "Advances in micro assembly injection moulding for use in medical systems," *International Journal of Advanced Manufacturing Technology*, **33** (1-2): pp. 206-211, 2007
82. S.I. Moon, L.L. Monson and C.W. Extrand, "Insert-molded poly(ether imide)/carbon fiber poly(ether ether ketone) bimaterial composites: Fracture and interfacial analysis," *Journal of Applied Polymer Science*, **102** (3): pp. 2362-2371, 2006
83. D. Mueller, J. Gerdes and S.K. Gupta, "Incorporation of passive wing folding in flapping wing miniature air vehicles," In Proceedings of the *ASME Mechanism and Robotics Conference*, pp. 87543, San Diego, CA, 2009
84. I. Pandelidis and Q. Zou, "Optimization of injection molding design. Part I: Gate location optimization," *Polymer Engineering & Science*, **30** (15): pp. 873-882, 1990
85. N. Pappafotis, W. Bejgerowski, R. Gullapalli, J.M. Simard, S.K. Gupta and J.P. Desai, "Towards design and fabrication of a miniature MRI-compatible robot for applications in neurosurgery," In Proceedings of the *ASME 2008 International Design Engineering Technical Conferences & Computers and Information in Engineering Conference IDETC/CIE*, New York, NY, 2008
86. B. Paul, "Prediction of elastic constants of multiphase material," *Transactions of the Metallurgical Society of AIME*, **218**, pp. 36-41, 1960
87. T.M. Pendleton and B.D. Jensen, "Compliant wireform mechanisms," *Journal of Mechanical Design*, **130** (12): pp. 6, Dec 2008
88. D. Pessey, N. Bahlouli, C. Raveyre, J. Guillet, S. Ahzi, J.M. Hiver and A. Dahoun, "Characterization of contamination effects for two polypropylene-based materials," *Polymer Engineering & Science*, **50** (1): pp. 1-9, 2010
89. A.K. Priyadarshi, S.K. Gupta, R. Gouker, F. Krebs, M. Shroeder and S. Warth, "Manufacturing multi-material articulated plastic products using in-mold assembly," *International Journal of Advanced Manufacturing Technology*, **32** (3-4): pp. 350-365, Mar 2007
90. B.H. Rabin, R.L. Williamson, H.A. Bruck, X.-L. Wang, T.R. Watkins and D.R. Clarke, "Residual strains in an Al₂O₃-Ni joint bonded with a composite interlayer: Experimental measurements and FEM analysis," *Journal of the American Ceramic Society*, **81**, pp. 1541-1549, 1998
91. G. Regnier, D. Dray, E. Jourdain, S. Le Roux and F.M. Schmidt, "A simplified method to determine the 3D orientation of an injection molded fiber-filled polymer," *Polymer Engineering and Science*, **48** (11): pp. 2159-2168, Nov 2008

92. J.B. Rosmarin and H.H. Asada, "Synergistic design of a humanoid hand with hybrid dc motor – SMA array actuators embedded in the palm," In Proceedings of the *IEEE International Conference on Robotics and Automation*, pp. 773-778, Pasadena, CA, 2008
93. J. Rotheiser, "Joining of plastics - Handbook for designers and engineers, " *Hanser Gardner*, 2004
94. Z. Rutkauskas and A. Bargelis, "Knowledge-based method for gate and cold runner definition in injection mold design," *Mechanika*, **4**, pp. 49-54, 2007
95. H. Sadabadi and M. Ghasemi, "Effects of some injection molding process parameters on fiber orientation tensor of short glass fiber polystyrene composites (SGF/PS)," *Journal of Reinforced Plastics and Composites*, **26** (17): pp. 1729-1741, Nov 2007
96. A. Saxena, "Topology design of large displacement compliant mechanisms with multiple materials and multiple output ports," *Structural and Multidisciplinary Optimization*, **30** (6): pp. 477-490, 2005
97. Y.M. Shabana, M.L. Pines and H.A. Bruck, "Modeling the evolution of stress due to differential shrinkage in powder-processed functionally graded metal-ceramic composites during pressureless sintering," *International Journal of Solids and Structures*, **43**, pp. 7852-7868, 2006
98. C.Y. Shen, X.R. Yu, Q. Li and H.M. Li, "Gate location optimization in injection molding by using modified hill-climbing algorithm," *Polymer-Plastics Technology and Engineering*, **43** (3): pp. 649-659, 2004
99. Y.-K. Shen, C.-W. Wu, Y.-F. Yu and H.-W. Chung, "Analysis for optimal gate design of thin-walled injection molding," *International Communications in Heat and Mass Transfer*, **35** (6): pp. 728-734, 2008
100. Y.K. Shen and W.Y. Wu, "An analysis of the three-dimensional micro-injection molding," *International Communications in Heat and Mass Transfer*, **29** (3): pp. 423-431, 2002
101. J. Shoemaker, "Moldflow design guide: A resource for plastics engineers, " *Hanser Publishers*, 2005
102. P. Shokri and N. Bhatnagar, "Effect of packing pressure on fiber orientation in injection molding of fiber-reinforced thermoplastics," *Polymer Composites*, **28** (2): pp. 214-223, Apr 2007
103. R. Shokri and N. Bhatnagar, "Effect of melt and mold temperature on fiber orientation during flow in injection molding of reinforced plastics," *International Polymer Processing*, **21** (5): pp. 480-486, Nov 2006

104. D.E. Smith, D.A. Tortorelli and C.L. Tucker, "Analysis and sensitivity analysis for polymer injection and compression molding," *Computer Methods in Applied Mechanics and Engineering*, **167** (3-4): pp. 325-344, 1998
105. R. Stewart, "Multicomponent molding - In-mold techniques eliminate downstream operations to cut costs and boost quality," *Plastics Engineering*, **64** (6): pp. 16, 2008
106. T. Tantanawat, "Optimal design of compliant systems for dynamic applications," *Ph.D. Dissertation*, Mechanical Engineering, University of Michigan, Michigan, 2007
107. T. Tantanawat and S. Kota, "Design of compliant mechanisms in minimizing input power in dynamic applications," *Journal of Mechanical Design*, **129** (10): pp. 1064-1075, 2007
108. N.J. Teh, P.P. Conway, P.J. Palmer, S. Prosser and A. Kioul, "Statistical optimisation of thermoplastic injection moulding process for the encapsulation of electronic subassembly," *Journal of Electronics Manufacturing*, **10**, pp. 171, 2000
109. Y. Tian, B. Shirinzadeh, D. Zhang and Y. Zhong, "Three flexure hinges for compliant mechanism designs based on dimensionless graph analysis," *Precision Engineering*, **34** (1): pp. 92-100, 2009
110. P.A. Tres, "Designing plastic parts for assembly, 2nd Edition, " *Hanser Gardner Publications*, 2004
111. B.J. Tsai and Y.C. Fu, "Design and aerodynamic analysis of a flapping-wing micro aerial vehicle," *Aerospace Science and Technology*, **13** (7): pp. 383-392, 2009
112. M. Vincent, T. Giroud, A. Clarke and C. Eberhardt, "Description and modeling of fiber orientation in injection molding of fiber reinforced thermoplastics," *Polymer*, **46** (17): pp. 6719-6725, 2005
113. D.P. Webb, D.A. Hutt, N. Hopkinson, P.P. Conway and P.J. Palmer, "Packaging of microfluidic devices for fluid interconnection using thermoplastics," *Journal of Microelectromechanical Systems*, **18** (2): pp. 354-362, Apr 2009
114. E.H. Weber, M.L. Clingerman and J.A. King, "Thermally conductive nylon 6,6 and polycarbonate based resins. I. Synergistic effects of carbon fillers," *Journal of Applied Polymer Science*, **88** (1): pp. 112-122, 2002
115. C.M. Yen, J.C. Lin, W.J. Li and M.F. Huang, "An abductive neural network approach to the design of runner dimensions for the minimization of warpage in injection mouldings," *Journal of Materials Processing Technology*, **174** (1-3): pp. 22-28, 2006

116. S. Zelenika, M.G. Munteanu and F. De Bona, "Optimized flexural hinge shapes for microsystems and high-precision applications," *Mechanism and Machine Theory*, **44** (10): pp. 1826-1839, 2009
117. M. Zhai, Y.C. Lam and C.K. Au, "Algorithms for two gate optimization in injection molding," *International Polymer Processing*, **20** (1): pp. 14-18, Mar 2005
118. M. Zhai, Y.C. Lam, C.K. Au and D.S. Liu, "Automated selection of gate location for plastic injection molding processing," *Polymer-Plastics Technology and Engineering*, **44** (2): pp. 229-242, 2005
119. M. Zhai and C.Y. Shen, "An optimization scheme based on flow resistance to locate optimum gate of complex part," *Journal of Reinforced Plastics and Composites*, **24** (15): pp. 1559-1566, 2005
120. M. Zhai, Y.C. Lam and C.K. Au, "Runner sizing and weld line positioning for plastics injection moulding with multiple gates," *Engineering with Computers*, **21** (3): pp. 218-224, 2006
121. M. Zhai, Y.C. Lam and C.K. Au, "Runner sizing in multiple cavity injection mould by non-dominated sorting genetic algorithm," *Engineering with Computers*, **25**, pp. 237-245, 2009
122. H. Zhou and K. Ting, "Shape and size synthesis of compliant mechanisms using wide curve theory," *Journal of Mechanical Design*, **28**, pp. 551-558, 2006